Synthesis of a Hydrogel-Based Vaccine to Mimic Dendritic Cell Responses to Pathogens

By

Siddhartha Jain

5-Year Integrated Masters of Technology, Biochemical Engineering and Biotechnology,
Indian Institute of Technology (Delhi), 2001

Submitted to the Biological Engineering Division in partial fulfillment of the requirements for the degree of

Doctor of Philosophy

At the

Massachusetts Institute of Technology

June, 2006

Signature of author: _____

Biological Engineering Department

Certified by: _____

Darrell J. Irvine
Eugene Bell Associate Professor of Tissue Engineering
Thesis Advisor

Accepted by: _____

Alan Grodzinsky
Professor, Director for Center for Biomedical Engineering

Synthesis of a Hydrogel-Based Vaccine to Mimic Dendritic Cell Responses to Pathogens

By

Siddhartha Jain

5-Year Integrated Masters of Technology, Biochemical Engineering and Biotechnology,
Indian Institute of Technology (Delhi), 2001

Submitted to the Biological Engineering Division in partial fulfillment of the requirements for the degree of

Doctor of Philosophy

At the

Massachusetts Institute of Technology

June, 2006

Thesis Committee:

Prof. D.A. Lauffenburger, Biological Engineering Department
Prof. K.D. Wittrup, Chemical and Biological Engineering
Prof. J. Chen, Biology
Prof. D.J. Irvine, Biological Engineering, Material Science & Engineering

कर्मण्येवाधिकारस्ते मा फलेषु कदाचन ।
मा कर्मफलहेतुर्भूर्मा ते सङ्गोऽस्त्वकर्मणि ॥२७॥

You have control over action alone, never over its fruits. Live not for the fruits of action, nor attach yourself to inaction.

— **Lord Krishna**

(Srimad Bhagavad Gita)

Synthesis of a Hydrogel-Based Vaccine to Mimic Dendritic Cell Responses to Pathogens

Siddhartha Jain (Thesis Advisor: Prof. D.J. Irvine)

Submitted to the Biological Engineering Division on May 25, 2006 in Partial Fulfilment of the Requirements for the Degree of Doctorate of Philosophy in Bioengineering

Abstract

Live or attenuated pathogens are the basis of many successful vaccines due in part to the orchestrated response of dendritic cells (DCs) triggered by these immunizations, which includes (1) DC and DC precursor attraction to the immunization site, (2) efficient antigen delivery to class I and class II MHC loading pathways coincident with maturation of DCs, and (3) emigration to draining lymph nodes for T cell activation. We have developed a model immunization system designed to allow these steps in the DC life cycle to be controlled in the context of a subunit vaccine. The system is comprised of microspheres encapsulating chemokines and hydrogel nanoparticles; each nanoparticle contains antigen and DC maturation signals (e.g., TLR ligands). The nanoparticles remain sequestered within the carrier microspheres but the chemokine is released at a controllable rate, creating a local chemoattractant gradient centered on each microsphere. DCs are attracted to individual microspheres where nanoparticles are concentrated; attracted DCs extract nanoparticles from the carrier microspheres, and receive maturation signals coincident with the delivery of antigen into both class I and class II MHC processing pathways. In addition, the nanoparticles may be labeled to allow subsequent tracking of particle-carrying DCs *in vivo*. These components allow the attraction (or if desired, emigration) of dendritic cells and their precursors to be selectively modulated at an immunization site, and the activation signals received by these cells when they encounter antigen to be tailored. *In vitro* experiments indicate that chemokine-releasing microspheres effectively attract DCs and monocytes over significant distances, and that the gel nanoparticles efficiently trigger DC maturation and lead to both $CD4^+$ and $CD8^+$ T cell activation *in vitro* and *in vivo*. This system provides both a platform for rational immunotherapy as well as a powerful set of tools by which the function of dendritic cells can be manipulated and dissected to improve our understanding of how DC trafficking and functional state impacts immune responses.

ACKNOWLEDGMENTS

I would like to express my sincere acknowledgments to my PhD thesis advisor, Prof. Darrell Irvine who was the guiding force behind the project. At the start of the project, Darrell personally taught me basic techniques in polymer synthesis, microscopy, and tissue culturing and later was always available to help me troubleshoot any issues I had from time to time. At every point of the project, Darrell not only provided me constructive suggestions but also helped me think critically.

My thesis committee comprising of Prof. D.A. Lauffenburger, Prof. K.D. Wittrup, and Prof. J.Chen gave me valuable suggestions at different phases of my thesis work, which helped me design the course of project and certain experiments especially *in vivo* experiments accordingly, and also prompted me to quantitate my observations more, which helped me move the project forward by leaps and bounds. Acknowledgments are also due to various faculty at MIT who through the courses strengthened my background in Bioengineering. I would also like to mention the help I received from Glenn Paradis, Flow Cytometry facility at MIT for assistance with FACS experiments, animal technicians at Department of Comparative Medicine, MIT – Jennifer Statile and Elizabeth Horrigan for help with maintenance of animal colonies and *in vivo* experiments, collaborators – Dr. Nir Hacohen and Dr. Eddie Adams for insightful discussions, protocols, and transgenic mice I received from them. I also had various UROPs who worked with me on my project at different times – Woon Teck Yap, Sandra Gonzalez, Nick Chun, Teresa Wang, Clarisse Tsang, Ying-Ying Wang, and Ben Navot – always trying to add a new functionality to the vaccine components and making it into an effective vaccine. Special thanks are due to Prof. Linda Griffith for providing me lab space to carry out my research work, and to Megan Whittmore, Dan Darling, Aran Parillo, Laura Vineyard, and Emily Larsen for help in different ways while I worked in BPEC space for nearly two years.

I would also like to thank my greatest friends that I made at MIT in the course of my PhD. Anoop Rao and Ajit Dash were the first friends I found at MIT and we remain close friends to date. Nate Tedford and Maxine Jonas were great classmates and wonderful friends. I also truly enjoyed the company of my lab members especially Junsang Doh,

Vinay Mahajan, John Greenland, Sheree Beane, and Agnieszka Stachowiak, and friends – John Reed, Taro Muso, Murtaza Zafer, Adeem Usman, Alireza Khademhosseini, Grace Kim, Zeeshan Syed, Sudeep Lahiri, and Kyoung-Hee Yu. I would also like to mention the constant encouragement I received from my undergraduate advisors – Prof. G.P. Agarwal and Prof. S. Nath, and from my friend from IIT, Dr. Dhiraj Vettam. Sidney-Pacific and Graduate Student Council (Academic, Research, and Careers), Emmi Snyder, Ashfaque Khandekar, and Hector Hernandez require a special mention as they helped me work with and for the student community at MIT in different positions and at different times, and also contributed to my all-round development at MIT.

In the end, I would like to express my heartiest and deepest acknowledgments to my family because of who I am at this stage of life. If it were not for the hard work and constant encouragement of my family, I would have never reached this far. In my good and bad times, my family never let me feel I was all alone even thousands of miles away. Thank you, mom, dad, Madhavi, and Brownie – I love you all very much.

Sincerest Thanks,

Siddhartha Jain

TABLE OF CONTENTS

Abstract **4**
1. Introduction and Background **13**
1.1 Adaptive immunity and the role of dendritic cell *13*
1.2 Role of chemokines in immune response *16*
1.3 Dendritic cell activation *17*
1.4 Vaccines in practice and study *18*
1.5 Significance and design of the proposed vaccine *19*
1.6 Overall objectives and specific aims *21*
2. Reverse Targeting of Dendritic Cells by Chemotaxis **24**
2.1 Introduction *24*
2.2 Materials and Methods *27*
2.2.1 Dendritic cell migration through a membrane filter in Boyden Chamber 27
2.2.2 Encapsulation of fN'LFN'YK in PLGA Microspheres 27
2.2.3 Encapsulation of CCL20 in PLGA microspheres 28
2.2.4 Microsphere Characterization 28
2.2.5 Monocyte and monocyte-derived dendritic cell culture 29
2.2.6 Collagen gel direct visualization migration assay 30
2.2.7 Analysis of cell migration data 31
2.3 Results *32*
2.3.1 Dendritic cell migration in response to formyl peptide and CCL20 in a modified Boyden chamber 32
2.3.2 Encapsulation and release of formyl peptides from PLGA microspheres 33
2.3.3 Chemoattraction of human monocytes and DCs toward formyl peptide-releasing microspheres *in vitro* 35
2.3.4 Encapsulation and release of CCL20 chemokine from PLGA microspheres. 39
2.3.5 Phenotyping of murine BMDCs for kinetics of CCR6 expression on cell surface 41
2.3.6 Chemoattraction of murine BMDCs toward CCL20 -releasing microspheres 42
2.3.7 Modeling spatio-temporal chemokine concentration profiles in collagen 46
2.4 Discussion *53*
2.5 Conclusions *56*
3. Delivery of antigen and maturation factor by hydrogel nanoparticles **58**
3.1 Introduction *58*
3.2 Materials and Methods *63*
3.2.1 Hydrogel particle synthesis 63
3.2.2 Electrostatic assembly of CpG oligonucleotide on hydrogel particles 64
3.2.3 Hydrogel particle characterization 64
3.2.4 Hydrogel particle uptake by bone marrow-derived dendritic cells 66
3.2.5 Assesment of dendritic cell maturation/activation by hydrogel nanoparticles 67
3.2.6 *In vitro* antigen presentation to T cells by dendritic cells 68
3.2.7 *In vivo* activation of lymphocytes by hydrogel particles in C57Bl/6 mice 69
3.3 Results *71*
3.3.1 Hydrogel particle synthesis and characterization 71
3.3.2 Functionalization of hydrogel particles with CpG oligonucleotide 76

3.3.3 Encapsulated antigen release by protease digestion of hydrogel particles ... 79
3.3.4 Accessibility of native protein epitopes at the surface of hydrogel particles .. 81
3.3.6 Dendritic cell maturation by CpG-coated hydrogel particles ... 89
3.3.7 *In vitro* T cell activation by activated dendritic cells ... 93
3.3.8 *In vivo* activation of lymphocytes by hydrogel particles ... 96
3.4 Discussion ... 103
3.5 Conclusions ... 107
4. Co-delivery of Chemokine and Antigen/Activation Signals to Dendritic Cells 109
4.1 Introduction ... 109
4.2 Materials and Methods ... 112
4.2.1 Synthesis of alginate microparticles for co-encapsulation of CCL20 and ova-loaded hydrogel nanoparticles ... 112
4.2.2 Characterization of alginate microparticles ... 113
4.2.3 Analysis of antigen uptake by dendritic cells by flow cytometry ... 114
4.2.4 Time-lapse videomicroscopy analysis dendritic cell attraction to alginate microparticles ... 115
4.2.5 Bone marrow-derived macrophage cell culture ... 115
4.3 Results ... 115
4.3.1 Synthesis of alginate microparticles and characterization ... 115
4.3.2 Chemoattraction of dendritic cells to alginate microparticles ... 122
4.3.3 Enhanced antigen delivery to dendritic cells by 'reverse-targeting' ... 127
4.3.4 Selective delivery of antigen to dendritic cells by 'reverse-targeting' ... 129
4.4 Discussion ... 132
4.5 Conclusions ... 135
5. Summary and Future Work ... 137
5.1 Summary of results ... 137
5.2 List of Research Publications and Conference Presentations ... 141
5.2.1 Research Publications ... 141
5.2.2 Conference Presentations ... 141
6. References ... 143
APPENDIX 1 – CellI Culture Medium and Buffers ... 161
APPENDIX 2 – Murine bone marrow-derived dendritic cell culture ... 163
APPENDIX 3 – Preparation of collagen gel for migration studie ... 164
APPENDIX 4 – Magnetic-Assisted Cell Sorting for T cell purification ... 165
APPENDIX 5 – Enzyme Linked Immunosorbant Assay (ELISA) ... 167
APPENDIX 6 – Cell labeling with fluorescent dyes ... 169
APPENDIX 7 – Protein/peptide modification: Labeling with a fluorescent dye or PEGylation/ acrylation ... 170
APPENDIX 8 – Cell staining and Flow-Assisted Cell Sorting (FACS) ... 171
APPENDIX 9 – Epifluorescence microscopy ... 173
APPENDIX 10 – Synthesis of end-acrylated triblock copolymer for hydrogel synthesis ... 174
APPENDIX 11- T cell blasts from ova-specific $CD4^+$ and $CD8^+$ transgenic mice . 176

LIST OF FIGURES

Figure 1.1. Schematic Diagram of Innate Immunity and Adaptive Immunity linked through Antigen Presenting Cells 14
Figure 1.2. Activation of CD4+ and CD8+ T cells in cell-mediated adaptive immune response 15
Figure 1.3. Mechanisms of antigen presentation on MHC class I and class II molecules 16
Figure 1.4. Schematic diagram depicting the mechanism of action of the proposed vaccine. 20
Figure 1.5. Schematic diagram of the proposed vaccine depicting function of individual components. 22
Figure 2.1. Schematic of two-well (A) and single-well (B) time-lapse videomicroscopy migration assays. 31
Figure 2.2. Chemotactic index for murine BMDC migration to different doses of formyl peptide and CCL20 as measured in a modified Boyden chamber assay. 33
Figure 2.3. Kinetics of fN'LFN'YK chemoattractant release from PLGA microspheres in vitro 35
Figure 2.4. Formyl peptide chemoattractants released from PLGA microspheres induce directed migration of human monocytes 37
Figure 2.5. Formyl peptide-releasing microspheres chemoattract human monocyte-derived DCs 39
Figure 2.6. Kinetics of CCL20 chemokine release from 40-75 kDa PLGA microspheres in vitro 41
Figure 2.7. Surface expression of CD11c and CCR6 on bone marrow dendritic cells on days 2 (–), 4 (–), 6 (–), 8 (–), and 9 (–) 42
Figure 2.8. CCL20-releasing microspheres elicit sustained chemoattraction of murine BMDCs 44
Figure 2.9. DCs can chemotax into direct contact with controlled release microspheres. Shown are five frames from a time-lapse imaging experiment near one isolated large PLGA microsphere (denoted in the first frame by black arrow) 46
Figure 2.10. (A) Schematic of FITC-fMLP release assay into collagen gel for estimation of diffusion characteristics of the chemokine into collagen (B) Fluorescence micrographs depicting diffusion of FITC-fMLP as a function of space and time into collagen gel. The chemokine source is located at the lower right corner of each image (C) Average fluorescence intensities for the field of view determined experimentally and obtained from Equation 10. 49
Figure 2.11. (A) Schematic of FITC-CCL20 release assay into collagen gel for estimation of diffusion profile of the chemokine into collagen (B) Fluorescence micrographs depicting diffusion of FITC- CCL20 as a function of space and time into collagen gel. The chemokine source is located along the left edge of each image (C) Diffusion profile of labeled chemokine as a function of distance from the chemokine source and time. 51
Figure 2.12. Predicted concentration profiles of fMLP using Equation 9 as a function of distance from chemoattractant source and time for (A) bolus delivery of chemokine and (B) Controlled release of chemokine for ~10 days. 53

Figure 3.1. Mean diameter of pluronic aggregates as a function of temperature in 0.04 g/mL pluronic F-68 aqueous solution containing 5.5 M NaCl with (○) or without (□) the addition of 1 mg/mL ovalbumin and 6.6 mg/mL monomers (6 mg/mL PEGMA, 0.3 mg/mL PEGDMA, and 0.3 mg/mL MAA). 71
Figure 3.2. Schematic diagram of monomer chemical structures, hydrogel particle synthesis, and functionalization with CpG oligonucleotides. 72
Figure 3.3. (A) Mean diameter of pluronic aggregates/ emulsion droplets at each stage of particle synthesis obtained by DLS. (B) Size distribution of emulsion droplets at 40 °C (□) and hydrogel particles post-polymerization (■) as measured by DLS... 74
Figure 3.4. Kinetics of CpG oligonucleotide desorption from the surface of functionalized hydrogel particles when incubated in PBS at 37 °C. 78
Figure 3.5. (A) IL-12p40 secretion at 1 μM hydrogel particle-bound CpG concentration after 48 hours of incubation of bone marrow dendritic cells with hydrogel particles adsorbed with different concentrations of poly-L-arginine as a function of CpG loading per particle; (B) IL-12p40 secretion by dendritic cells when incubated with same number of hydrogel particles but with different CpG loadings per particle.... 79
Figure 3.6. Size-exclusion chromatograms of supernatants collected after 48 h co-incubation of mixtures of 200 μg/mL cathepsin D 81
Figure 3.7. (A) Fluorescence images of ova-containing hydrogel particles stained with either anti-ova (left) or isotype control (right) primary antibody followed In both cases by Alexa fluor 488-conjugated IgG secondary antibody. (B) Histogram of fluorescence intensities from anti-ova-labeled particles (solid line) and isotype control-stained particles (dashed line)..... 83
Figure 3.8. Hydrogel particle uptake by dendritic cells. Dendritic cells were incubated with DQ-ovalbumin-containing particles (A) or control medium (B) for 1 h. Extracellular and membrane-bound fluorescence was quenched with trypan blue, and cells were then imaged by fluorescence microscopy. 84
Figure 3.9. Cell viability assessed by propidium iodide when dendritic cells were cultured with hydrogel particles for 24 h..... 85
Figure 3.10. Antigen delivery to dendritic cells by soluble protein, hydrogel particles, and CpG-coated hydrogel particles after 1, 4, and 18 hours of incubation. Grey histograms represent unmanipulated cells and solid lines represent corresponding samples..... 86
Figure 3.11. (A) Expression of SIINFEKL-K^b on the surface of dendritic cells based on staining with 25-D1.16 antibody after incubating dendritic cells with antigen for 18 hours. Solid histogram represents isotype control staining, dotted line is solution control, and solid lines are samples; (B) Shown are the mean fluorescence intensity (MFI) values obtained for SIINFEKL-K^b staining on dendritic cells and % cells with peptide-MHC I complex expression above isotype control..... 88
Figure 3.12. Surface phenotype of dendritic cells incubated with different agents for 24 hours followed by staining with specific antibodies. 90
Figure 3.13. Secretion of various cytokines – (A) IL-12p40; (B) IL-12p70; (C) IL-6; (D) TNF-α; and (E) IL-10 – by dendritic cells when incubated with soluble CpG (♦), unmodified particles (■), and CpG-coated particles (▲)..... 92

Figure 3.14. IL-2 secretion by primed T cells when incubated for 48 h with bone marrow dendritic cells and unmodified ova-loaded hydrogel particles (■) or soluble ovalbumin (♦)..... 93
Figure 3.15. Naïve T cell activation by dendritic cells incubated with hydrogel particles. 95
Figure 3.16. Anti-ovalbumin total IgG titers in the serum of C57Bl/6 mice 1, 3, 5, and 7 weeks after s.c. immunization with 100 μg ovalbumin in different forms: soluble ova, soluble ova mixed with 8.5 μg CpG, hydrogel nanoparticles, nanoparticles coated with 8.5 μg CpG, or ova emulsified in CFA. Antibody titers were calculated by endpoint dilution assay. Asterisks denote 7 week data statistically different from ova + soluble CpG ($p < 0.01$); **, statistically different from CpG-particles at 7 weeks ($p < 0.05$). Data shown from one representative of two independent experiments.... 97
Figure 3.17. C57Bl/6 mice were immunized with antigen in different forms and lymphocytes from the inguinal (draining) lymph nodes (hashed bars) and spleen (solid bars) were restimulated *in vitro* with MHC class II or class I peptides to measure (A) $CD4^+$ and (B) $CD8^+$ T cell responses, respectively. Shown are IFN-γ levels measured in supernatants of restimulated lymphocytes after 48 hrs. Asterisks denote samples statistically different form PBS control ($p < 0.05$). Data shown from one representative of two independent experiments. 99
Figure 3.18. (A) C57Bl/6 mice were immunized with ova nanoparticles without CpG, soluble CpG, and particle-bound CpG. Splenocytes were isolated after 1 week and restimulated with MHC class I or class II peptides and IFN-γ levels were measured after 48 hrs as described in Section 3.3.8.2. Asterisks denote samples statistically different from PBS control ($p < 0.05$), and ** denote statistically significant difference from ova nanoparticles delivered along with soluble CpG ($p < 0.05$). (B) Splenocytes from experiment in (A) were stained with anti-CD8α and ova-tetramer, and analyzed by flow cytometry to determine frequency of ova-specific CTLs in immunized mice. Shown are the density plots with $CD8^+$ $tetramer^+$ cells in upper-right quadrant. (C) Mean frequency ($n = 4$) of ova-specific CTLs for ova nanoparticles delivered without CpG, soluble CpG, or particle-bound CpG..... 101
Figure 3.19. Mice were immunized as described in Section 3.3.8.2 followed by intravenous injection of CFSE-labeled syngeneic splenocytes loaded with SIINFEKL peptide after 60 days. Memory response was quantified as % cytolytic activity. Shown are cell populations depicting control ($CFSE^{lo}$) and ova peptide-pulsed target splenocytes ($CFSE^{hi}$). Grey solid histograms represent results from immunized animals and black solid lines are cells recovered from a sham-immunized control. The values shown in the histogram charts are the mean values of cytolytic activity. 102
Figure 4.1. (A) Chemical structure of alginate. G = Guluronic Acid and M = Mannuronic Acid. (B) Schematic diagram for encapsulation of hydrogel nanoparticles and chemokine in alginate microparticles. 116
Figure 4.2. Fluorescence micrographs of alginate microparticles containing (A) DQ-ova-containing hydrogel nanoparticles (B) Alexa fluor 594-labeled CCL20. (C) Particle size distribution data and circularity of alginate microspheres obtained by Vi-Cell Counter. 117

Figure 4.3. Release profile of CCL20 from alginate microparticles in complete RPMI medium at 37 °C. 120
Figure 4.4. Uptake of DQ-ova-containing nanoparticles loaded in alginate microspheres by DCs visualized by timelapse videomicroscopy. Region where DC phagocytoses the nanoparticle is encircled..... 121
Figure 4.5. Antigen uptake by bone marrow dendritic cells from alginate microparticles synthesized using different amounts of calcium chloride. 122
Figure 4.6. (A) Schematic diagram of bone marrow dendritic cell migration to alginate microparticles in 3D collagen gel set up. (B) Nanoparticle uptake by dendritic cells as a function of CCL20 loading per particle. Dashed line represents nanoparticle uptake with alginate microparticles without chemokine..... 124
Figure 4.7. (A) Images from timelapse videomicroscopy of bone marrow dendritic cell migration to alginate microparticle in 3D collagen gel. Green fluorescence in the overlay derives from fluorescent ova-labeled nanoparticles in the alginate carriers. This example shows two alginate microcarriers near the center of the image. (B) Cell paths for migration in response to CCL20-loaded alginate microparticles (left) or control alginate microparticle (right) (C) Distribution of distances migrated by BMDCs in response to CCL20 gradients created by alginate microparticles in 3D collagen..... 126
Figure 4.8. Nanoparticle uptake by $CD11c^{+}$-BMDCs in collagen after 24 h culture when incubated with alginate microparticles containing DQ-ova-containing nanoparticles with or without CCL20. 128
Figure 4.9. Flow cytometry analysis of dendritic cells after 24 h culture in collagen gel with different doses of alginate microparticles with or without CCL20 for (A) antigen uptake and (B) DC maturation. 129
Figure 4.10. Images from timelapse videomicroscopy for migration of dendritic cells towards alginate microparticles (red) by CCL20 in a co-culture of macrophages (blue) and dendritic cells (green)..... 131

1. Introduction and Background

1.1 Adaptive immunity and the role of dendritic cell

The immune system functions to defend the body from extracellular infectious agents. In addition, it attempts to restrict the growth of tumor cells and virally-infected cells. The immune system is comprised of innate immunity and adaptive immunity. Innate immunity is nonspecific and acts as a first line of defense against pathogens through the recruitment of epithelial cells, macrophages, and dendritic cells. On the other hand, adaptive immunity develops and adapts according to the encountered antigen, and is divided into cell-mediated and humoral immunity (Figure 1.1). Cell-mediated immunity involves activation of T-lymphocytes within secondary lymphoid organs (SLO), which then migrate to the site of infection and destroy the pathogen or infected cells by means of cytokines or cytolytic activity. In contrast, humoral immunity is comprised of B-lymphocytes that when activated form antibody-secreting plasma cells, and these secreted antigen-specific antibodies neutralize the pathogen [1-3].

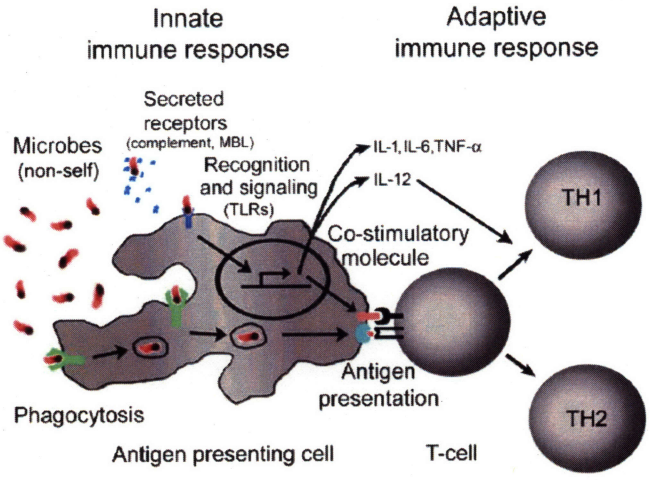

Figure 1.1. Schematic Diagram of Innate Immunity and Adaptive Immunity linked through Antigen Presenting Cells [4].

In the primary immune response, dendritic cells, a class of antigen-presenting cells, phagocytose (and macropinocytose) foreign antigen at sites of infection in peripheral tissues, process them in the endosomes and/or cytosol, and present peptides thus obtained on their surface using a multi-subunit protein complex called Major Histocompatibility Complex (MHC). MHC molecules are subdivided into class I and class II MHC; MHC class I molecules present antigen to $CD8^+$ cytotoxic T-lymphocytes (CTL) whereas MHC class II molecules are used to present antigen to $CD4^+$ helper T-lymphocytes (T_H-cells). CTLs destroy infected cells presenting the antigen against which they have been activated. T_H-cells, on the other hand, release soluble mediators called cytokines that initiate a cascade involving proliferation of macrophages to engulf and destroy the antigen (Figure 1.2) [5]. Successful elimination of a pathogen is accompanied by generation of memory T cells to control any future exposure to the same antigen. Activation of naïve T-lymphocytes by dendritic cells (DCs) requires not only the presence of peptide loaded onto MHC molecule (pMHC) but also costimulatory signals provided by DC cell surface molecules (e.g., B7-1 and B7-2) that interact with specific receptors on T-cells (e.g., CD28) [1-3]. For the vaccine to be developed in this project, dendritic cells were targeted as they are the only professional APCs known to prime naïve T-cells (both $CD4^+$ and $CD8^+$) *in vivo* [5-7] and along with macrophages

possess a unique ability to cross present antigen [8]. B cells, in contrast to T cells, can directly bind protein antigens via their B cell receptors (membrane-tethered IgM or IgG molecules).

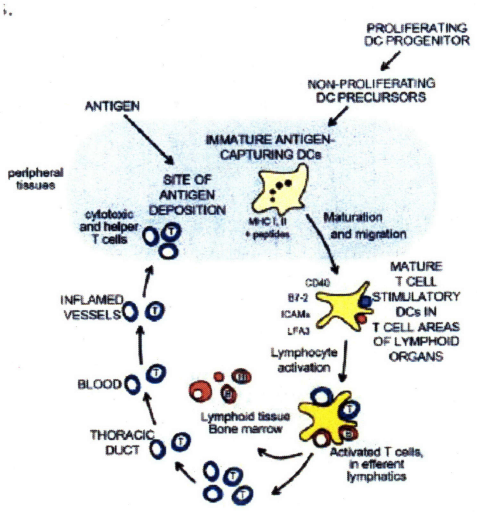

Figure 1.2. Activation of CD4+ and CD8+ T cells in cell-mediated adaptive immune response [5].

Exogenous antigens are processed in the endosomes of APCs and are presented using MHC class II molecules; in most nucleated cells, endogenous (cytosolic) antigens are typically processed in the cytosol and are presented on MHC class I molecules (Figure 1.3). Therefore, the physical location of an antigen is a determinant of whether $CD8^+$ T cells against the antigen can be generated. However, dendritic cells are known to transport antigens from endosomes to the cytosol as a result of which antigenic peptides are presented on MHC class I as well as class II molecules [9]. This phenomenon that allows DCs (and macrophages) [10] to present antigens captured from the extracellular milieu to both $CD4^+$ and $CD8^+$ T cells is called *cross priming* or *cross presentation*; the detailed mechanism of this process are still not clear but formation of ER-phagolysosome fusions has been proposed [11].

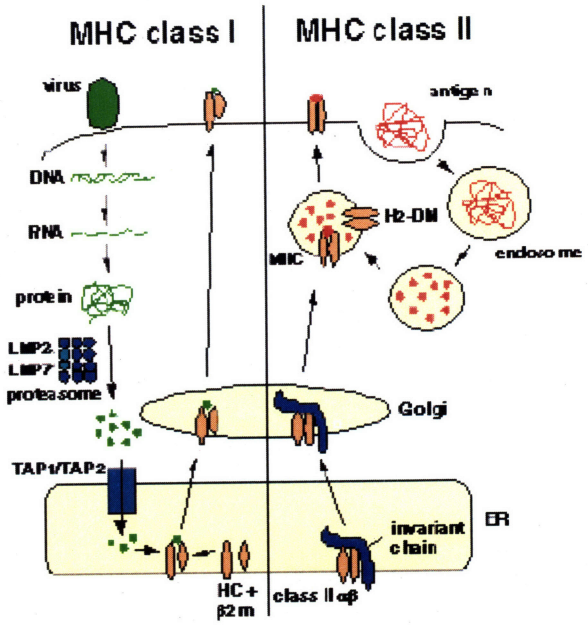

Figure 1.3. Mechanisms of antigen presentation on MHC class I and class II molecules [12].

1.2 Role of chemokines in immune response

The homing and migration of lymphocytes and dendritic cells is determined by chemoattractants called chemokines. Different cell types are associated with characteristic chemokine receptors and their cognate ligands, and similarly, expression of chemokine receptors by dendritic cells depends on the state of the DC (Table 1.1) [13]. Chemokines are involved in several processes such as angiogenesis, dendritic cell and lymphocytes homing, wound healing, and organogenesis. Chemokines are able to specifically target the cells of primary importance and cause concentration and/or organization of cells of interest at the site of action via the process of chemotaxis. Immature DCs have a high expression of CCR6, which binds the chemokines MCP-3, CCL20 and β-defensins [14-16]. Another set of receptors for immature DCs comprises the formyl peptide receptor (FPR) and the formyl peptide-like receptor (FPLR), which bind to the bacterially-derived peptide fMet-Leu-Phe (fMLF, commonly written as fMLP) and related peptides [17,18]. These receptors are thought to direct immature DCs to sites of infection for antigen loading. Maturing DCs, on the other hand, downregulate

CCR6 and FPR, and upregulate CCR7, the lymph node homing receptor that binds macrophage inflammatory protein-3β (MIP-3β) or CCL21 [5,19].

Table 1.1. Expression of various chemokine receptors in cells of immune system.

Receptor	Cellular Distribution	Ligands
CCR1	N. M. T. NK. B. Ms. As. Nn	RANTES. MIP-1α. HCC-1. MCP-2.3. MIP-5. Ckβ8
CCR2A	M	MCP-1.3.4
CCR2B	M. T. B. Bs	MCP-1.2.3.4. HIV
CCR3	Eo. Bs. T	Eotaxin. Eotaxin-2.3. RANTES. MCP-2.3.4. MIP-5
CCR4	T. P	TARC. MDC
CCR5	T. M. DC	RANTES. MIP-1α.β. MCP-2. M tropic HIV-1
CCR6	Memory T. B: immat. DC	MIP-3α
CCR7	Naïve T. B: mat. DC	MIP-3β. SLC. ELC
CCR8	M. Thymus	I-309
CCR9	T. Thymus	TECK
CCR10	Skin-homing T	CTACK
CCR11	Heart. small intestine. lung	MCP-1.2.4

1.3 Dendritic cell activation

As outlined in Figures 1.1 and 1.2, the two key early steps for dendritic cell function are antigen uptake and dendritic cell maturation. Maturation is caused by various agents most of which have been obtained from bacterial and viral sources like lipopolysaccharide (LPS), bacterial oligonucleotides with unmethylated CpG motifs, lipoteichoic acid (LTA), and Papillomavirus-like particles (VLP) [20-22] and is characterized by several phenotypic changes. These maturation agents also known as Pathogen-Associated Molecular Patterns (PAMPs) or 'danger signals' bind with surface receptors on antigen-presenting cells called Toll-like receptors (TLRs) resulting in initiation of a signaling pathway and transcription of various inflammation-associated genes causing molecular and cellular-level changes in APCs. Most of the Toll-like receptors are present on the cell surface where they bind their ligand but TLR3 and TLR9 which bind dsRNA and unmethylated CpG oligonucleotides are localized in the endosomes of dendritic cells and macrophages. First, maturation triggers an increase in the surface expression of MHC and costimulatory molecules, secretion of inflammatory

cytokines, and a switch in chemokine receptor expression as mentioned above. Second, phagocytosis/endocytosis of extracellular antigen, which is avid in immature DCs, is greatly reduced and peptide-MHC complexes are exported to the cell surface for antigen presentation to T cells. If either of these steps (antigen uptake or maturation) is missing, it can result in generation of tolerance to the antigen or autoimmunity. Failure to specifically chemoattract immature DCs may reduce the efficacy of a vaccine as mature DCs, being inefficient phagocytes, may not be able to out-compete other phagocytic cells such as macrophages and neutrophils in antigen uptake. Removal of antigen delivery from the sequence of events may lead to autoimmunity as the expression of costimulatory signals will be upregulated for self-antigens [23]. Alternatively, DCs that receive antigen but no maturation signal may promote tolerance to the antigen [24]. Thus, it is important to be able to provide DCs with both antigen and activation stimuli in a programmed manner and with high efficiency, possibly similar to infection of cells by viruses.

1.4 Vaccines in practice and study

Since the first vaccine against small pox was discovered by Edward Jenner, a tremendous effort has been made to develop prophylactic vaccines against various bacterial and viral infections. In addition, therapeutic vaccination for patients with persistent viral infections such as HIV, and cancer are envisioned. Traditional vaccines such as live or attenuated virus/ bacteria; inactivated viruses; recombinant envelope protein; and the use of neutralizing antibodies [25,26] have led to successful immunizations against self-limiting infections including smallpox, mumps, measles, hepatitis B, and polio. Several of these traditional approaches are unable to generate an effective CTL responses and immunological memory in cases of persistent viral infections (Table 1.2) [27,28], which has led to interest in vaccines like plasmid DNA encoding for cytokines; live recombinant bacteria; fusion proteins (e.g., antibody + pMHC); dendritic cell vaccine therapy; antisense RNA; and adoptive T-cell therapy. Some of these have shown promising results but still suffer from the same limitations as traditional vaccines (Table 1.2) [27,28].

Table 1.2. Categories of vaccines currently in practice or in study, their mechanisms, and limitations associated with them.

Vaccine	Mechanism	Observed limitations
Live, attenuated virus/bacteria [29]	Immune response against bacteria/viruses; *in vitro* culture reduces mutation frequency	Danger of pathogenicity
Inactivated viruses with adjuvants [30,31]	Immune response against viral envelope proteins; mutation frequency reduced	Absence of CTLs
Recombinant envelope protein [32]	Generation of immune response against pathogenic protein	No neutralizing antibodies; Absence of CTLs
Neutralizing antibodies [25,26]	Antibodies bind to epitopes and initiate immune response	Diversity of antigens; no immunological memory
Plasmid DNA [33]	Cytokines produced by infected cells to initiate immune response	Poor DNA delivery to target cells
Live recombinant bacteria [34]	Immune response against bacteria; bacteria has low pathogenicity	Limited immunogenicity, limited experience in humans
Fusion proteins [35]	Anti-CD3 and pMHC coupled to activate CTLs	Low efficacy
Dendritic cell vaccine therapy [36]	Dendritic cells cultured *ex vivo* with tumor antigen to activate immune system when transplanted back	Laborious process, diversity of human MHC
Antisense RNA [37]	Double stranded mRNA formation; removal of regulatory markers	Non-specificity, RNA delivery
Adoptive T-cell therapy [38]	T-cells withdrawn, activated against antigen and injected back into the patient	Laborious process, low and non-specific *in vivo* activity of transferred cells, autoimmunity

1.5 Significance and design of the proposed vaccine

Vaccines that fail to induce cytotoxic T cells often lead to incomplete immunity, and current evidence supports the idea that activation of $CD8^+$ T cells will be a critical component of a successful vaccine for HIV and other persistent viral infections. Tumors and virally-infected cells share several common features in their resistance to the immune system [39]. Using the proposed vaccine, we propose to generate an immune response against the infected cells by providing corresponding antigen (e.g., tumor-

associated antigen or spike proteins) as well as maturation signals to the dendritic cells to generate an effective CTL response as well as immunological memory to the antigen.

The proposed vaccine sought to meet the following cellular and molecular level objectives, while offering better safety than live vectors: 1) specifically employ DCs in their efficient antigen-loading immature state; 2) concentrate DCs at the vaccine site to obtain a strong response; and 3) provide antigen and maturation signal in a coupled manner for effective dendritic cell activation and to prevent any tolerance or autoimmunity (Figure 1.4). In order to achieve a high concentration of immature DCs at the immunization site, we used controlled release systems to create suitable concentration gradients of CCR6 and/or FPR ligands that chemoattract immature DCs. To initiate a primary effective immune response, it is necessary that recruited DCs take up both antigen and a maturation agent; this was achieved with the help of hydrogel nanoparticles that delivered both components to DCs. Particulate delivery of antigen was able to induce cross-presentation thus facilitating MHC class I presentation.

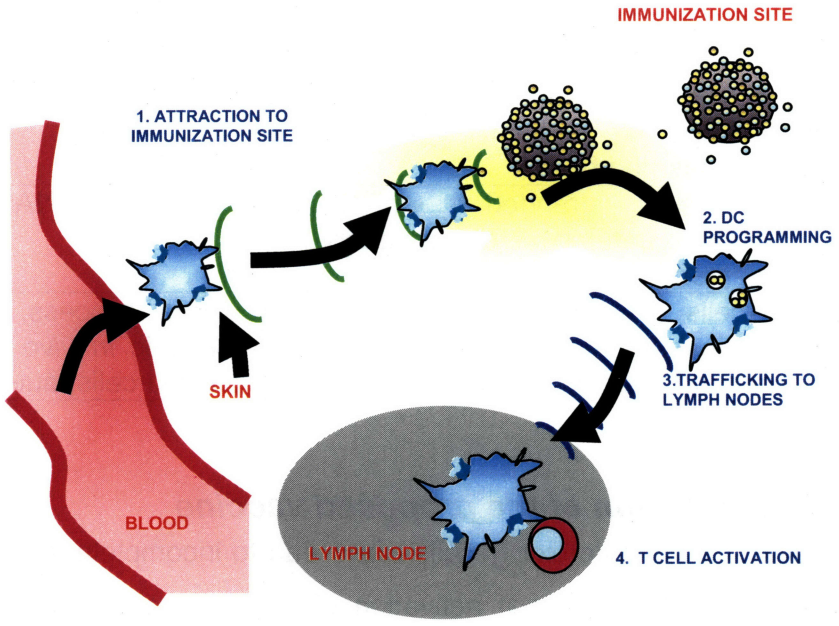

Figure 1.4. Schematic diagram depicting the mechanism of action of the proposed vaccine.

Once the DCs are matured, they migrate towards the lymph node. Through cross priming, antigen is loaded onto MHC class I as well as class II molecules to provide effective CTL and T_H responses, respectively. It was shown by Shen *et al.* that antigen immobilized on microspheres increased antigen presentation on both MHC class I and class II by as much as two orders of magnitude compared to soluble forms of the antigen [10]. Kumamoto et al. constructed a device made from poly(ethylene-co-vinyl) acetate in which MIP-3β and a tumor-associated antigen were loaded in two separate controlled release devices [40,41]. The implant chemoattracted mature DCs and loaded them with the antigen; the subsequent immune response resulted in tumor regression. However, we hypothesized that attraction of immature DCs can provide more potent immune responses, and provide a better control over as well as understanding of the working of the vaccine. Furumoto *et al.* demonstrated that expression of CCL20 chemokine at the tumor site results in a more effective anti-tumor response resulting in complete tumor regression [42]. Similarly, Sumida *et al.* showed that intramuscular injection of plasmids that recruit and expand DC population at the site of immunization resulted in strong humoral and cellular responses against vaccinia virus [43]. Collectively, these studies suggest that increasing the recruitment of dendritic cells at the site of immunization directly correlates with higher efficacy of immune response. For the design of the vaccine, the materials we used were biocompatible materials and have been approved by FDA for clinical use.

1.6 Overall objectives and specific aims

The steps required to prepare dendritic cells (DCs) for the desired initiation of an effective primary immune response are primarily antigen loading and maturation of immature DCs. We hypothesized that these two steps may be triggered in a programmed manner by mimicking structural aspects of pathogens in a synthetic particulate antigen-delivery system. In addition, we hypothesized that immune responses could be enhanced by mimicking the chemoattraction of immature DCs to an infection site in the context of a vaccine. To test these hypotheses, we developed a vaccine in the form of injectable biodegradable microparticles that could elicit a tailored response from the immune system. Our approach was based on a general theory of

vaccination, which in principle may be used to develop vaccines for a variety of cancers or persistent viral infections such as HIV and hepatitis C, and possibly diseases in genetically immunodeficient persons.

To trigger potent immune responses, the vaccine was designed to first chemoattract immature DCs to the site of immunization. Chemoattractants specific for immature dendritic cells were encapsulated in biodegradable microspheres and released the chemoattractant in a controlled fashion, thereby creating and maintaining a chemoattractant gradient in the environment around the microspheres. Chemoattracted immature DCs were then delivered hydrogel particles containing antigen and maturation factors (Figure 1.5). Uptake of hydrogel particles delivered antigen and maturation signals intracellularly to dendritic cells and antigen was presented on MHC class I and class II molecules. The maturation signals induced significant upregulation of expression of costimulatory molecules- MHC II, CD40, CD86 and CD80, and secretion of inflammatory cytokines such as IL-12, IL-6, and TNF-α; DC maturation is also associated with downregulation of CCR6 receptor and upregulation of CCR7 receptors on dendritic cells surface. After maturation *in vivo*, these matured DCs will migrate towards the nearest lymph nodes for interaction with T-lymphocytes.

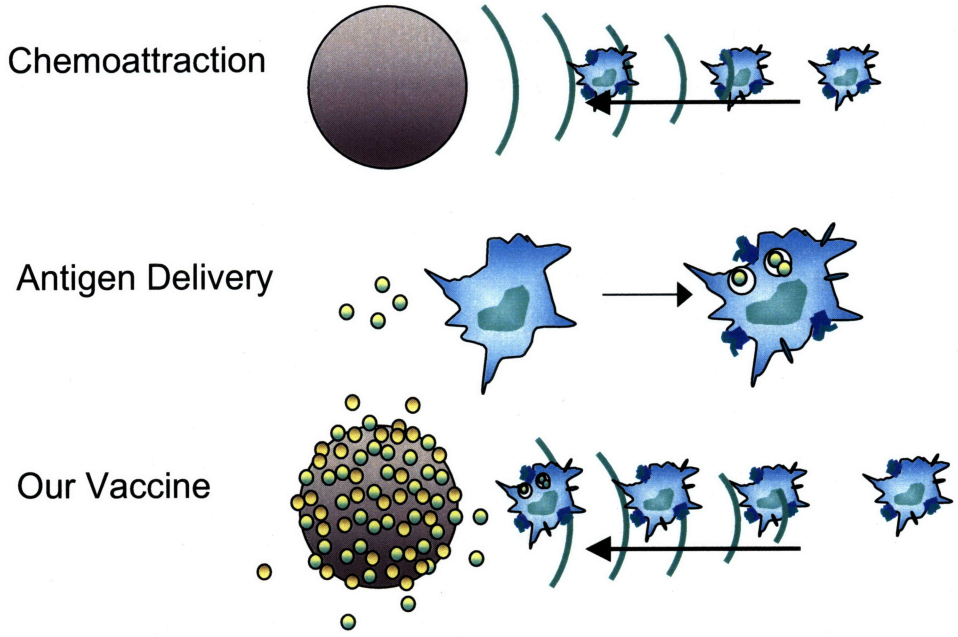

Figure 1.5. Schematic diagram of the proposed vaccine depicting function of individual components.

Based on this design concept, the specific aims of this research were as follows:

1. Chemoattraction:
    a. Identification and encapsulation of suitable chemoattractant(s)
    b. Study of controlled release of the chemoattractant(s)
    c. Response of DCs and DC precursors to the chemoattractant gradient(s) thus created.
2. Antigen delivery:
    a. Encapsulation of antigen in hydrogel nanoparticles
    b. Study of cross-priming for stimulation of $CD8^+$ T cells by class I peptide-MHC
    c. Study of class II peptide- MHC loading for activation of $CD4^+$ T cells
3. Maturation agent delivery:
    a. Identification of a suitable maturation agent
    b. Immobilization of the maturation agent
    c. Study of the maturation of (chemoattracted) immature dendritic cells.
4. *In vivo* T cell and B cell activation with hydrogel nanoparticles
5. Assembly and functional testing of the device:
    a. Co-encapsulation of chemokine and hydrogel nanoparticles for coincident delivery to dendritic cells
    b. Analysis of antigen uptake by dendritic cells and DC responses *in vitro*.

2. Reverse Targeting of Dendritic Cells by Chemotaxis

2.1 Introduction

Cells of immune system exhibit complex patterns of trafficking among the primary and secondary lymphoid organs and the peripheral tissues as part of homeostasis and immune surveillance [44-46]. Spatial and temporal orchestration of lymphocyte migration is achieved by a diverse family of chemokines, typically ~ 10 kDa polypeptides, which bind related families of G protein-coupled receptors [47-49]. Chemokines and other chemoattractant molecules are produced at local sites and diffuse to form soluble or solid-phase concentration gradients; cells expressing the appropriate chemokine receptors typically migrate up chemoattractant gradients towards their source. Chemokines and cognate receptors are now known, which guide naïve T and B cells to their local niches within secondary lymphoid organs [50,51]; attract antigen-presenting cells (APCs), effector and memory T and B cells, and innate immune cells to sites of infection [52]; and guide antigen-loaded APCs to lymph nodes [53].

The sensitivity of immune cells to specific chemokines might be exploited in the design of novel immunotherapies and vaccines, by inducing specific cell types to concentrate local depot of antigen. For example, primary immune responses are

initiated when professional APCs known as dendritic cells (DCs) engulf foreign antigens and become activated, migrate to draining lymph nodes, and present these captured antigens to T cells to initiate T cell activation [5,54,55]. In the presence of a pathogen, stromal and inflammatory cells in the periphery initiate this cascade by secreting chemokines that selectively attract immature (unactivated) DCs and their precursors (e.g., monocytes) to the sites of infection or inflammation [55,56]. A number of chemoattractants are known to elicit directed migration of DCs and monocytes in this context, including monocyte chemotactic protein-1 (MCP-1), MCP-2, MCP-3, macrophage inflammatory protein-1α (MIP-1α), MIP-1β, Regulated upon Activation Normal T cell Expressed and Secreted (RANTES), C5a, β-defensins, and bacterially-derived formyl peptides [15,16,18,57-60]. Because the frequency of DCs in blood and peripheral tissues is low (typically ~1% of cells or fewer [61,62]), vaccines that mimic DC recruitment to inflamed tissues by creating a local chemoattractant source may significantly enhance immune responses. Attraction of resting 'immature' DCs to an immunization site could increase the number of DCs loaded with antigen, and subsequently, the number of naïve T cells activated in draining lymph nodes. Recently, Martin-Fontecha *et al.* showed that naïve T cell activation increases in proportion to the number of antigen-loaded DCs injected subcutaneously in a mouse [63].

Several prior studies have sought to develop vaccines that apply this principle, by immunizing with DNA plasmids that encode an antigen of interest as well as a chemoattractant molecule [42,64-69]. This approach has been shown to trigger enhanced DC infiltrates at injection sites and improved protection against tumors and model pathogens. However, DNA immunization provides little control over the amount of chemokine produced or the time course of its expression, which limits the ability of this approach to control magnitude and duration of DC attraction. These characteristics also make DNA immunization an intractable method for dissecting the biology of chemokine functions in immune cell trafficking.

As an alternative, Kumamoto *et al.* [40,41] demonstrated that implanted poly(ethylene-*co*-vinyl acetate) (EVAc) rods releasing a model protein antigen and MIP-3β (a chemoattractant for activated 'mature' DCs) drew DCs to the implant site and resulted in enhanced protection against E.G7 and 3LL tumors in mice. This approach

allowed a known amount of chemokine to be implanted with defined release kinetics. However, the use of non-degradable polymer rods that require implantation and eventual retrieval is not attractive for a practical vaccine. In addition, EVAc releases protein rapidly, over a course of ~24 hours due to rapid swelling of the matrix with water; such a system cannot deliver chemokine over longer time periods which may be optimal for maximization of the immune response [42].

Given these promising prior results, we developed a system which could serve both as a potential platform for manipulating lymphocyte trafficking in immunotherapies and as a basic tool for quantitatively studying the role of chemokines in controlling immune cell migration *in vitro* and *in vivo*. We prepared degradable poly(lactide-*co*-glycolide) controlled release microspheres as an injectable formulation that could mimic the generation of chemoattractant gradients generated in situ in natural acute infections and enrich professional APCs at an immunization site. Two chemoattractants with different physical properties were chosen for these studies: a hydrophobic formyl peptide variant formyl-Nle-Leu-Phe-Nle-Tyr-Lys (fN'LFN'YK), representative of pathogen-derived chemoattractants present during bacterial infections [70] and the 7.9 kDa C-C chemokine MIP-3α (CCL20) [71-73]. These chemokines attract immature dendritic cells and their monocyte precursors, via binding to the formyl peptide receptor and CCR6, respectively. To assay the ability of controlled release microspheres to guide migration of DCs and monocytes to a local site, we developed an assay for chemotaxis based on time-lapse videomicroscopy observation of live cell migration through three dimensional (3D) collagen gels *in vitro*, which is related to direct observation assays used in prior cell migration studies of immune cells [74-76] and other cell types [77]. Chemoattractants released from PLGA microspheres were found to elicit strong, sustained attraction of human DCs and monocytes as well as murine DCs for at least 8 hours. Slow release of chemokine from microspheres was found to provide significantly stronger attraction compared to bolus delivery of freely diffusing attractant. These microspheres allow defined total amounts of chemokine to be delivered to known sites with known release kinetics, making them of interest both for the design of improved vaccines and as tools for dissecting the role of chemoattractants in immunobiology. In addition, control of cellular chemotaxis via chemoattractant-

releasing biomaterials could be a powerful strategy for tissue engineering (e.g., for guided angiogenesis), where guided physical organization of multiple cell types according to wound healing or developmental principles is of interest.

2.2 Materials and Methods

2.2.1 Dendritic cell migration through a membrane filter in Boyden Chamber

Various dilutions of fN'LFN'YK or CCL20 ranging from 10 μg/mL to 0.1 μg/mL were prepared in phosphate-buffered saline with 1% BSA; 31 μl of chemokine solution was added to each well of a 96-well Boyden chamber (NeuroProbe, USA). A membrane (5 μm pore size) was placed on top of the wells and 50 μl bone marrow-derived dendritic cells (day 6) (1 x 10^6 cells/mL) labeled with 10 μM Carboxyfluorescein succinimidyl ester (CFSE) dye (as described in the Appendix) were pipetted onto each well of the Boyden chamber. The plate was incubated at 37 °C/ 5% CO_2 for 90 min followed by incubation at 4 °C for 20 min. Membranes were then removed and the total fluorescence from cells that migrated into the lower chamber was measured for each well using a spectrafluorometer (SpectraMax Gemini, Molecular Devices) at $\lambda_{ex}/\lambda_{em}$ of 490/510 nm. Migration of cells as a function of chemokine concentration was reported as a Chemotactic Index defined as the ratio of number of cells with directed migration to number of cells with random migration and was calculated as:

$$Chemotactic\ Index = \frac{Fluorescence\ Intensity\ with\ Chemokine}{Fluorescence\ Intensity\ without\ Chemokine} \qquad [1]$$

2.2.2 Encapsulation of fN'LFN'YK in PLGA Microspheres

PLGA microspheres encapsulating the hydrophobic peptide fN'LFN'YK or fN'LFN'YK-FITC (Sigma-Aldrich, USA) were synthesized by a solid-in-oil-in-water emulsion process [78,79]. Ten milligrams of formyl peptide was added to 200 mg PLGA

(Sigma, 40-75 kDa; Alkermes, 4.4 kDa) in 1 mL of dichloromethane (DCM) and the mixture was vortexed for 1 min to form a uniform suspension. The organic mixture was then emulsified in 20 mL of 2% w/v (aq) polyvinyl alcohol (PVA, 25 kDa, 88 mol% hydrolyzed, Polysciences) solution by homogenizing (Ika, Ultra-Turrex T-25) at 10,000 rpm for 1 min at 20 °C. The suspension was stirred at 1000 rpm for 4 h at 20 °C to evaporate DCM followed by centrifugation and washing (4x). The resulting microspheres were lyophilized and stored at 4 °C until used.

2.2.3 Encapsulation of CCL20 in PLGA microspheres

CCL20 was encapsulated in PLGA microspheres by a water-in-oil-in-water double emulsion process. First, 20 μg CCL20 and 20 mg Bovine Serum Albumin (BSA) were co-dissolved in a 2% (w/v) aqueous PVA solution and then emulsified in an organic phase comprising 100 mg PLGA in 1 mL dichloromethane by homogenization at 10,000 rpm for 1 min at 20 °C. Microspheres were formed by homogenizing the first emulsion in 50 mL of 2% (w/v) aqueous PVA at 10,000 rpm for 1 min at 20 °C. The resulting double emulsion was diluted in 100 mL of 1% (w/v) aqueous PVA solution and stirred at 400 rpm for 3-4 h at 20 °C to evaporate dichloromethane. The particles were collected by centrifugation, washed in milliQ water 4x, and lyophilized. The freeze-dried particles were stored at 4 °C until used.

2.2.4 Microsphere Characterization

2.2.4.1 Chemokine Loading, Encapsulation Efficiency, and Particle Size

The microspheres were analyzed for encapsulation efficiency by degrading the PLGA matrix in alkaline medium and analyzing the released protein concentration by bicinchoninic acid (BCA) colorimetric assay (Pierce Chemical Co., USA). Ten milligrams of particles were suspended in 3 mL of 0.5 M NaOH/2% sodium dodecyl sulfate (SDS) solution, and incubated at 37 °C overnight. The protein/peptide concentration in solution was then estimated by the BCA assay following the manufacturer's instructions. Chemokine loading and encapsulation efficiency were calculated as follows:

$$Chemokine\ Loading = \frac{Protein\ concentration\ as\ determined\ by\ BCA\ assay \times 3}{10\ mg\ microspheres} \quad [2]$$

$$Encapsulation\ Efficiency = \frac{Measured\ Chemokine\ Loading}{Theoretical\ Chemokine\ Loading} \times 100\,\% \quad [3]$$

Endotoxin contamination in microspheres was measured by the LAL assay (Cambrex, USA); endotoxin levels were ≤ 0.15 EU/mL.

Microsphere sizes were determined using a Coulter Counter (Beckman Coulter Multisizer II). Mean diameters were calculated from the measured particle size distribution curves as:

$$Mean\ Particle\ Diameter = \frac{\sum Particle\ Size \times Number\ of\ Particles\ in\ the\ interval}{\sum Number\ of\ Particles\ in\ the\ interval} \quad [4]$$

2.2.4.2 Measurement of bulk chemokine release kinetics

Release of formyl peptides from microspheres was quantified *in vitro* using BCA assay. Microspheres (20 mg) were suspended in 5 mL phosphate-buffered saline (PBS), 0.1% Tween 20 and shaken at 37 °C for 30 days. Every 24 h, microspheres were pelleted by centrifugation and supernatant was removed for analysis; fresh buffer was added to replace the removed supernatant.

The kinetics of CCL20 release from double emulsion microspheres were analyzed following a similar procedure. Chemokine present in the release medium was quantified using a sandwich ELISA kit (R&D Systems, USA) according to manufacturer's instructions and as described in Appendix.

2.2.5 Monocyte and monocyte-derived dendritic cell culture

Freshly elutriated human monocytes were obtained from Advanced Biotechnologies Inc. (Columbia, MD). Cells were resuspended in 10% DMSO/ 90% fetal calf serum (FCS), and stored at -80 °C until used. For migration assays using

monocytes, cells were thawed rapidly at 37 °C and cultured in complete RPMI medium, and used in gel microscopy assay after 48 h.

Human monocyte-derived dendritic cells were generated as previously reported [80] by plating 1 x 10^6 monocytes in 1000 U/mL GM-CSF and 1000 U/mL IL-4 (R&D Systems) in 1 mL complete RPMI medium. Cytokines were replenished in the culture on days 2, 4, and 6 by addition of 100 mL complete RPMI containing 1000 U/mL GM-CSF and 1000 U/mL IL-4. Cells were used for migration on days 7-9.

2.2.6 Collagen gel direct visualization migration assay

In vitro chemotaxis of cells in response to chemokine-loaded microspheres or control samples was measured by direct visualization in 3-D collagen gels. Purified low-endotoxin bovine type I collagen (BD Biosciences, USA) was diluted in an equal volume of complete RPMI 1640 medium to 1.2 mg/mL and cast (2 mL) in 35 mm tissue culture polystyrene dishes around plastic inserts suspended from the dish lids, which molded wells ~7 mm in diameter and ~1 mm depth in the resulting gels. Two different geometries were used for the videomicroscopy experiments as illustrated in Figures 2.1A and 2.1B. In the first geometry (2.1A), two wells were molded in the collagen separated by a 5 mm gap. In this configuration, microspheres and cells were each added separately to the wells after gelling of the collagen matrix. In the second geometry (2.1B), a single well was molded in the collagen gel surrounded by cells suspended at a density of 1.5 x 10^6 cells/mL in collagen. In this case, collagen was diluted to the desired concentration (1.2 mg/mL) with complete RPMI 1640 medium containing cells. For all samples, the collagen matrix was gelled at 37 °C/ 5% CO_2 for 30 min. After gelling, samples prepared with the two-well geometry were completed by adding microspheres suspended in 25 μl collagen to one well, and 5 x 10^4 cells suspended in 25 μl collagen to the second well; cell migration at the 'cell source' well was then immediately tracked by time-lapse videomicroscopy. For samples prepared in a single-well geometry, microspheres suspended in collagen were added to the source well and time-lapse imaging was immediately begun adjacent to the source well.

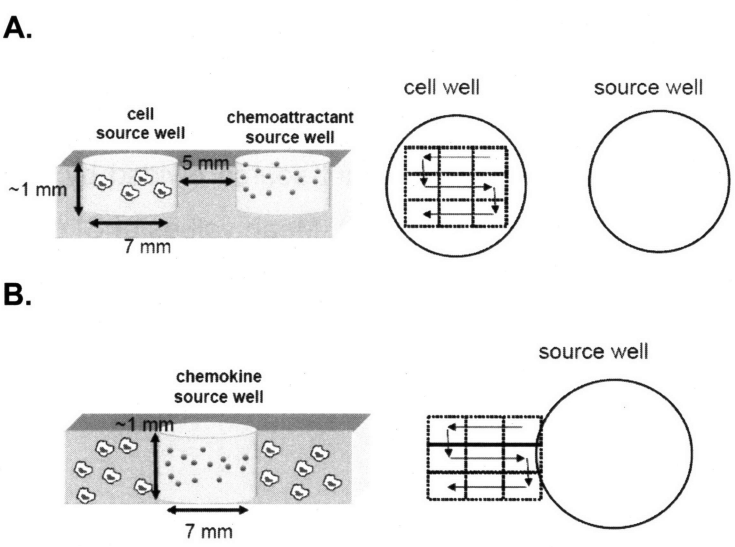

Figure 2.1. Schematic of two-well (A) and single-well (B) time-lapse videomicroscopy migration assays.

Time-lapse videomicroscopy was carried out using a Zeiss Axiovert 200 microscope equipped with a motorized stage (Ludl), Roper Scientific CoolSnap HQ CCD camera, and an environmental chamber (Zeiss), which maintained samples at 37 ^{o}C with a 5% CO_2 atmosphere. A total field of view of 2600 x 1910 μm^2 was recorded every 1 min by rapid collection of 9 adjacent brightfield images using a 10x objective, where each single field of view was 900 x 670 μm^2 and the 9 fields collected formed a 3 x 3 array in the *x-y* plane of the overall observation area (Figure 2.1). Image acquisition and the motorized stage were controlled using MetaMorph software (Universal Imaging Corp.).

2.2.7 Analysis of cell migration data

Individual cells from the nine visualized fields in each experiment were tracked via a software-assisted centroid determination algorithm using MetaMorph imaging software. Cells areas in each frame were identified by auto-thresholding the intensity of brightfield images, and centroid tracking (*x-y* position as a function of time) was performed using the thresholded area. Cells leaving the field of view of migrating out of

focus in the z-direction were discarded from analysis. Endpoint position and cell path data were pooled from 2-5 independent experiments.

The chemotactic index (CI) was defined after method of Moghe *et al.* [76] as the distance traveled by each cell in the direction of attractant source divided by the total path length (a ratio also known as McCutcheon Index [81]). Mean values of CI over time (‹CI›) were calculated by averaging the CI of 20 individual cells selected randomly from the nine fields of observation at each time point.

2.3 Results

2.3.1 Dendritic cell migration in response to formyl peptide and CCL20 in a modified Boyden chamber

We first measured the response of murine bone marrow-derived dendritic cells (BMDCs) to formyl peptides or CCL20 using a Boyden chamber equipped with a 5 μm filter that separated the chemokine source from the dendritic cells by a distance of 100 μm. Both formyl peptide and CCL20 induced significant migration of BMDCs through the membrane filter and a chemotactic index > 1 was observed over a range of chemokine concentrations. The chemotactic index peaked at 2.0 for CCL20 and 1.5 for formyl peptide at 1 μg/mL and 10 μg/mL respectively, and was observed to be reduced at higher and lower chemoattractant concentrations (Figure 2.2). This reduction in cell migration at high concentration of chemokine is possibly due to the saturation of chemokine receptors and consequent inability of cells to sense the chemokine concentration gradient effectively. In addition to absolute concentration, the specific gradient (1/c dc/dx)is a second important factor in chemotaxis, and must be in a limited range appropriate for support of chemotaxis [76,82,83]. Theoretical [83] and experimental analyses [76,83] suggest that soluble chemokines must form a specific gradient on the order of ~5-10 cm^{-1} to elicit a directed migration, corresponding to a minimum 0.5% change in attractant concentration over the length of a typical cell (10 μm in diameter). Moreover, in addition to chemokine receptor saturation, cells may endocytose chemokine receptors upon binding of chemokine molecules, resulting in

desensitization of the cell and reduced migration. The concentration for maximum chemotactic index is representative of the binding affinity of the chemokines to their cognate receptors. Formyl peptide binding to formyl peptide receptors occurs with a binding affinity (K_D) of 30 nM [84] whereas signaling through murine CCR6 is triggered by ~0.01 – 0.1 nM CCL20 and has a K_D of ~ 1 nM for CCL20 binding [73].

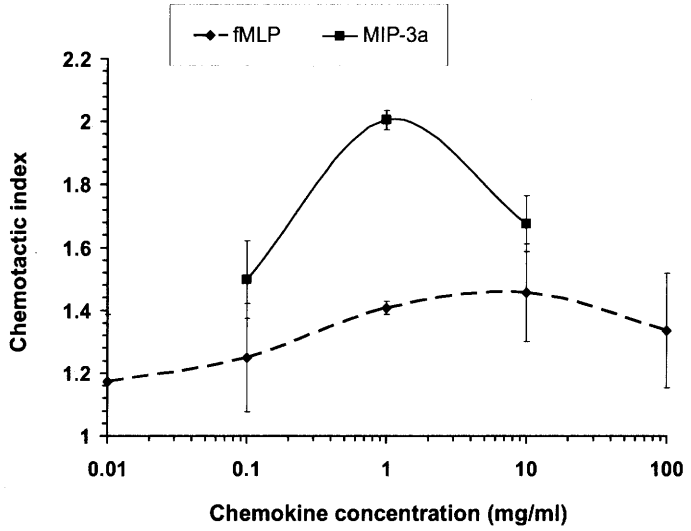

Figure 2.2. Chemotactic index for murine BMDC migration to different doses of formyl peptide and CCL20 as measured in a modified Boyden chamber assay.

2.3.2 Encapsulation and release of formyl peptides from PLGA microspheres

To experimentally examine controlled release of chemoattractants for DCs and monocytes, we fabricated degradable microspheres encapsulating either the chemoattractant peptide fN'LFN'YK or the C-C family chemokine MIP-3α (CCL20). In choosing these two molecules, we sought to test delivery of two attractants with significantly different properties: fN'LFN'YK is a hydrophobic, low molecular weight (824 Da) peptide with low water solubility, while CCL20 is a more hydrophilic polypeptide with ~10-fold greater molecular weight (7.9 kDa). To provide sustained slow release, the chemoattractants were encapsulated in degradable poly(lactide-*co*-glycolide) (PLGA) microspheres. We also studied the effect of the molecular weight of PLGA on release

kinetics by encapsulating formyl peptide in microspheres formed from low (4.4 kDa) and high (40-75 kDa) molecular weight PLGA.

Table 2.1. Characteristics of formyl peptide and CCL20-loaded microspheres.

Chemokine encapsulated	Matrix PLGA MW (KDa)	Encapsulation efficiency (wt %)	Total chemokine encapsulated (μg chemokine/mg microspheres)	Mean microsphere diameter (μm)
fN'LFN'YK	75	90	45	4.8
fN'LFN'YK	4.4	80	40	5.0
fN'LFN'YK-FITC	75	80	40	6.6
CCL20	75	50	0.1	4.3

First, the hydrophobic formyl peptide and its fluorescein-labeled derivative were encapsulated by a s/o/w emulsion process using dichloromethane as the oil phase. Characteristics of the resulting microspheres are given in Table 2.1. Peptides were efficiently encapsulated (Encapsulation Efficiency = 80-90%, Chemoattractant loading = 40-45 μg/mg microspheres) in microspheres prepared from high or low molecular weight PLGA. The kinetics of fN'LFN'YK and fN'LFN'YK-FITC release from microspheres into well-mixed PBS at 37 °C are shown in Figure 2.3. As shown in Figure 2.3A, fN'LFN'YK was steadily released for at least 3 weeks when encapsulated in a high molecular weight matrix. As observed for other PLGA drug release systems [85], the initial release rate increased when the molecular weight of the matrix was decreased to 4.4 kDa and the chemokine was released in less than a week from the matrix. The burst release of the unlabeled chemoattractant from 75 kDa PLGA microspheres over the first several hours was low (typically 10-15%) and the release rate remained greater than 50 ng (mg microspheres)$^{-1}$ h^{-1} for more than 1 week (Figure 2.3B). Encapsulated fN'LFN'YK-FITC showed a significantly greater burst release at short times relative to the unlabeled peptide, followed by a slowly decaying release rate on days 2-10.

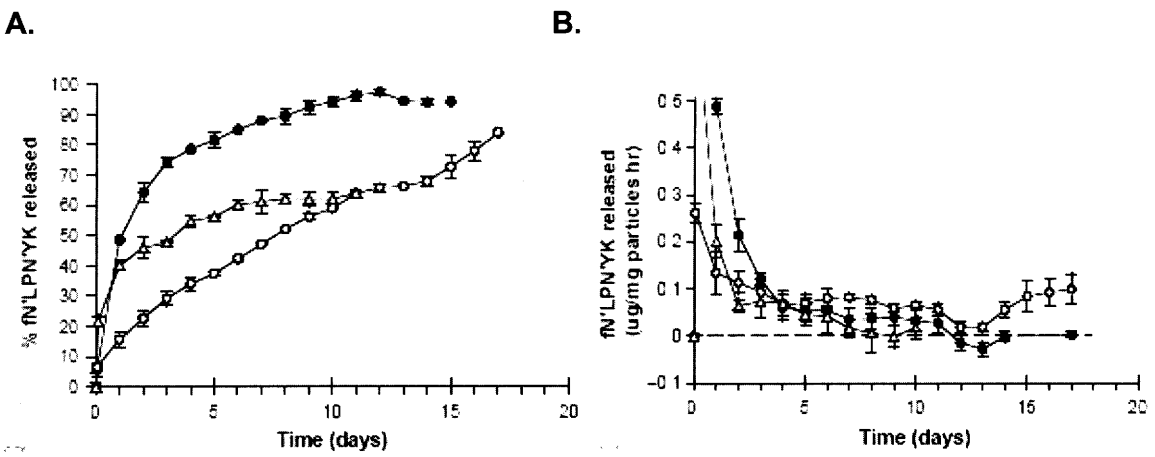

Figure 2.3. Kinetics of fN'LFN'YK chemoattractant release from PLGA microspheres in vitro. (A) Percentage of encapsulated peptide-released versus time in well-stirred PBS solution at 37 °C. (B) Release rates calculated from release profiles shown in (A). Measurements were made for fN'LFN'YK encapsulated in (•) 4.4 kDa PLGA or (○) 40-75 kDa PLGA microspheres and fN'LFN'YK-FITC encapsulated in 40-75 kDa PLGA (Δ).

2.3.3 Chemoattraction of human monocytes and DCs toward formyl peptide-releasing microspheres *in vitro*

Human monocytes and DCs express a formyl peptide receptor that binds to formyl-Met-Leu-Phe and structurally related peptides with an affinity of ~30 nM [84], and these cells chemotax in response to concentration gradients of formyl peptides. To determine the effect of microsphere-mediated formyl peptide release on human monocyte and dendritic cells chemotaxis, cell migration through 3-D collagen gels was assayed in the presence of fN'LFN'YK-FITC-releasing microspheres by time-lapse videomicroscopy. Though the release characteristics of fluorophore-labeled peptide were inferior to those of unlabeled formyl peptide (higher burst release, lower and more rapidly decaying release rate), we performed migration experiments with the labeled chemoattractant in order to have a qualitative marker of fN'LFN'YK gradients present (by collecting fluorescence images to detect FITC gradients) during the assays. Because the high burst release of the labeled peptide could lead to saturation and downregulation of the responding cells' formyl peptide receptors, fN'LFN'YK-FITC

microspheres were 'pre-released' in PBS for 48 h prior to use in the chemotaxis assays, to remove burst and provide release kinetics starting at ~75 ng/h (mg microspheres).

For these experiments, collagen gels were molded in a two-well geometry (Figure 2.1A). Monocytes or monocyte-derived dendritic cells were suspended in collagen in one well, while 0.25 mg microspheres in collagen (or collagen alone) were added to opposite well. Upon addition of cells and microspheres, the samples were placed at 37 ^{o}C, 5% CO_2 on the microscope stage, and time-lapse imaging of central region of the cell well was initiated. Brightfield images were recorded at 1-min interval over 1-3 h to track cell migration. From the resulting time-lapse images, individual cell paths were determined using software-assisted single cell tracking. Migration of cells in the absence of microspheres was compared to that observed when the chemokine source well was loaded with empty microspheres (no peptide encapsulated) or microspheres releasing fN'LFN'YK-FITC.

Representative paths for motile monocytes in the *x-y* plane over 3 h are shown in Figures 2.4 for cells responding to source wells containing no microspheres, empty microspheres, and microspheres releasing fN'LFN'YK-FITC, respectively. Each trace on the 4-quadrant plots identifies the *x-y* path of a single cell relative to its starting point (placed at the origin); tracks for 10 individual cells are shown overlaid on each plot. The bold arrows indicate the direction toward chemoattractant source well in each case. In the absence of microspheres, migrating cells showed persistent random walk motion, but no preferential migration toward or away from the opposite (empty) collagen well (Figure 2.4A). The migration behavior of monocytes was similar to when empty PLGA microspheres were loaded in the opposite well of the gel (Figure 2.4B). In contrast, when fN'LFN'YK-FITC- loaded microspheres were added to the attractant source well, monocytes migrated with a strong bias toward the microsphere well (Figure 2.4C). This directed migration response was seen in the entire monocyte population. Endpoint positions of 50 individual cells at the end of 3 h are shown in Figures 2.4D and 2.4E for cells responding to empty microspheres or formyl peptide-releasing microspheres, respectively. In response to microsphere-released fN'LFN'YK, 90% of the cells at the end of 3 h observation period occupied an x position closer to the microspheres, while empty microspheres elicited a random distribution of cell endpoints in the *x-y* plane

(48% and 52% of cells ended with an x position closer or farther from the chemoattractant well, respectively). Thus peptide release from the microspheres elicited strong directed migration from human monocytes.

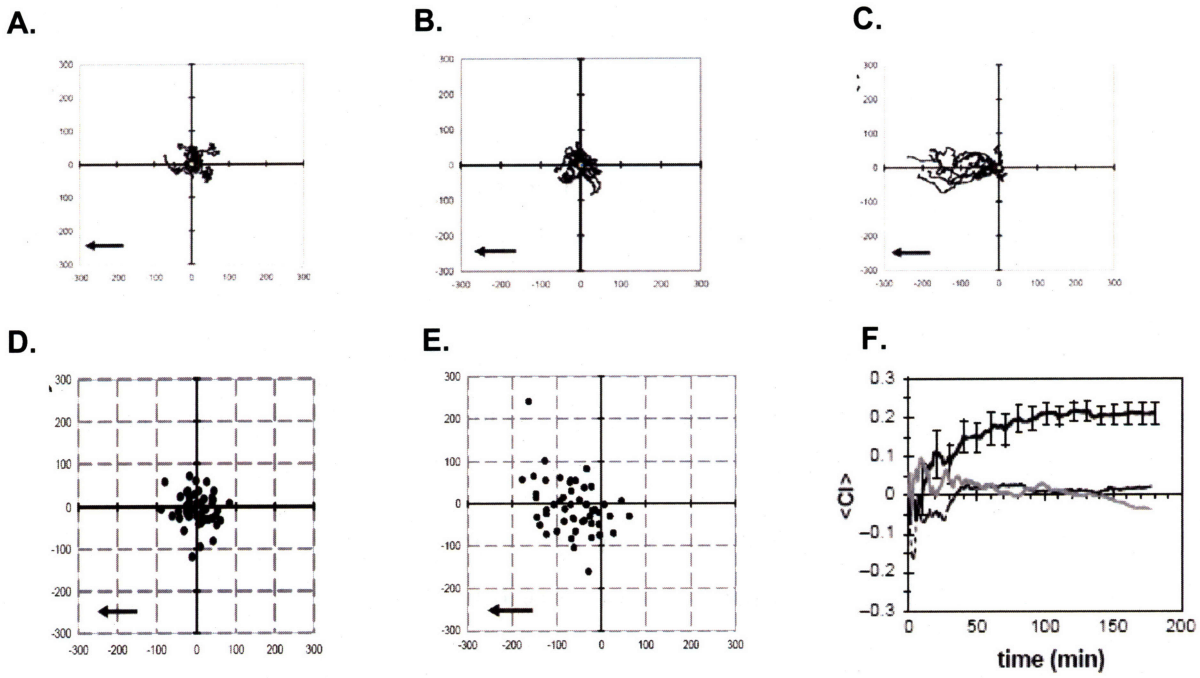

Figure 2.4. Formyl peptide chemoattractants released from PLGA microspheres induce directed migration of human monocytes. (A-C) Paths of 10 single cells in the *x-y* plane from time 0 to 3 h are shown overlaid, with each cell's starting positions placed at the origin. Shown are the paths of the cells in the two-well migration assay responding to source wells loaded with (A) no chemoattractant, (B) 0.25 mg blank PLGA microspheres, or (C) 0.25 mg fN'LFN'YK-FITC-releasing microspheres. (D, E) Endpoint relative positions of 50 cells after 3 h in the two-well migration assay. The starting point of each cell is placed at the origin. Shown are cell responses to source wells containing (D) empty microspheres or (E) fN'LFN'YK-FITC-releasing microspheres. Axes in (A-E) are distances in μm and arrows denote direction toward the chemoattractant source well. (F) Time evolution of the mean chemotactic index <CI> for monocytes migrating in response to source wells containing no chemoattractant (dashed line), blank PLGA microspheres (solid gray line), or fN'LFN'YK-FITC-releasing microspheres (solid black line).

To provide a quantitative measure of the response for the cell population examined, we determined the CI, defined as the mean total distance migrated by each cell toward the attractant source well divided by the cell's total path length. A mean CI (‹CI›) was determined by averaging the chemotaxis index obtained from 20 cells at each time point. As shown in Figure 2.4F, the chemotaxis index of responding monocytes evolved over the first ~60 min of the experiment, plateauing to a value of ~0 for cells responding to empty microspheres and cells incubated without microspheres-indicative of random migration (each cell equally likely to migrate toward or away from the attractant source well). In response to chemokine released from microspheres, the ‹CI› steadily rose to a maximum value of 0.21 ±0.06 over 3 h, comparable to the maximum chemotactic response observed for human neutrophils responding to chemoattractants in fibrin gels [76]. The lack of any downturn in ‹CI› over time course indicates that monocytes were continuously attracted throughout the observation period.

We next assayed the migration response of human monocyte-derived dendritic cells (MDDCs) to fN'LFN'YK-FITC-releasing microspheres (Figure 2.5). Shown in Figures 2.5A and 2.5B are 10 overlaid single-cell paths for MDDCs recorded over 1 h for the case of an empty attractant source well or a source well containing 0.25 mg fN'LFN'YK-FITC-loaded microspheres. Similar to the results obtained with monocytes, the population of MDDCs migrated in all four *x-y* quadrants approximately equally when no chemoattractant was present, while MDDCs responding to the fN'LFN'YK-release microspheres exhibited strongly biased migration toward the microsphere source well. Similar behavior was exhibited by majority of cells as shown by the 1 h path endpoint plots shown for MDDCs incubated with no chemokine (Figure 2.5C) or fN'LFN'YK-FITC-release microspheres (Figure 2.5D). The ‹CI› achieved by MDDCs responding to microspheres-released fN'LFN'YK plateaued after ~2 h, reaching a mean value of 0.32±0.07 indicating significantly biased migration toward the microspheres, while MDDCs migrating in the absence of chemokine had a ‹CI› ~0.

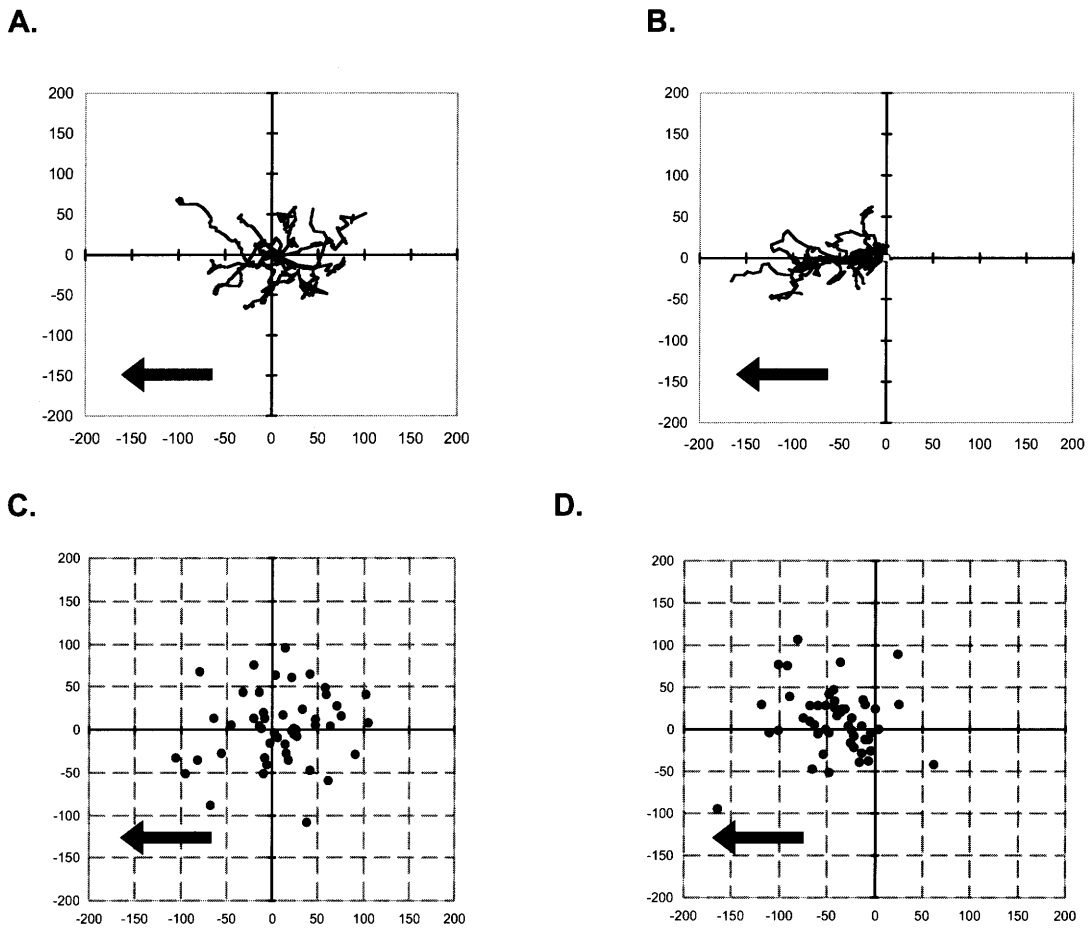

Figure 2.5. Formyl peptide-releasing microspheres chemoattract human monocyte-derived DCs. Shown are plots of DC migration over 1 h in the absence of chemoattractant (empty chemoattractant well) (A,C) or in response to 0.25 mg fN'LFN'YK-FITC-releasing PLGA microspheres (B,D). (A,B) Representative paths of 10 single cells in the *x* – *y* plane over 1 h are shown overlaid, with each cell's starting position placed at the origin. (C,D) Endpoint relative positions of 50 cells after 1 h, with the starting position of each cell placed at the origin. Axes are distances in μm, and arrows denote direction toward chemoattractant source well.

2.3.4 Encapsulation and release of CCL20 chemokine from PLGA microspheres

The results obtained with slow release of formyl peptide from PLGA provide a proof of concept that microspheres can induce sustained attraction of responsive

monocytes and MDDCs. However, formyl peptides are not highly selective chemoattractants for monocytes and unactivated, immature DCs; these peptides also attract neutrophils, eosinophils, and macrophages [86,87]. To avoid competition among cells for the chemoattractant and maximize the specific cellular infiltrate desired for priming of immune responses, we examined a second chemokine, MIP-3α (CCL20), whose receptor CCR6 is expressed by immature (unactivated) DCs, but not mature DCs, macrophages, eosinophils, or neutrophils [72,73,88,89]. In addition, to preface *in vivo* testing in mice, we encapsulated murine CCL20, and tested the response of mouse bone marrow-derived DCs (BMDCs) to these microspheres.

CCL20 was co-encapsulated in PLGA (40-75 kDa) with an excess of the carrier protein, bovine serum albumin (BSA) to protect the chemokine during encapsulation by a double emulsion process. Because CCL20 has been shown to trigger calcium signaling in CCR6-expressing cells at concentrations as low as < 0.1 nM, we encapsulated lower total amounts of protein in the CCL20 microspheres compared the formyl peptide experiments, to avoid paralyzing cells with saturating levels of chemokine, as indicated in Table 2.1.

Release of CCL20 from the PLGA microspheres was assayed *in vitro* at 37 °C using sandwich ELISA, to detect conformationally intact chemokine in solution. As shown in Figure 2.6A, the microspheres exhibited sustained release over 2 weeks. The release rate decayed gradually from ~1.5 ng/mg-h after 1 day to ~0.25 ng/mg-h at 7 days (Figure 2.6B). By day 15, ~90% of the encapsulated chemokine was detected by the ELISA in the microsphere supernatant, indicating that the carrier protein was effective in protecting the chemokine from degradation.

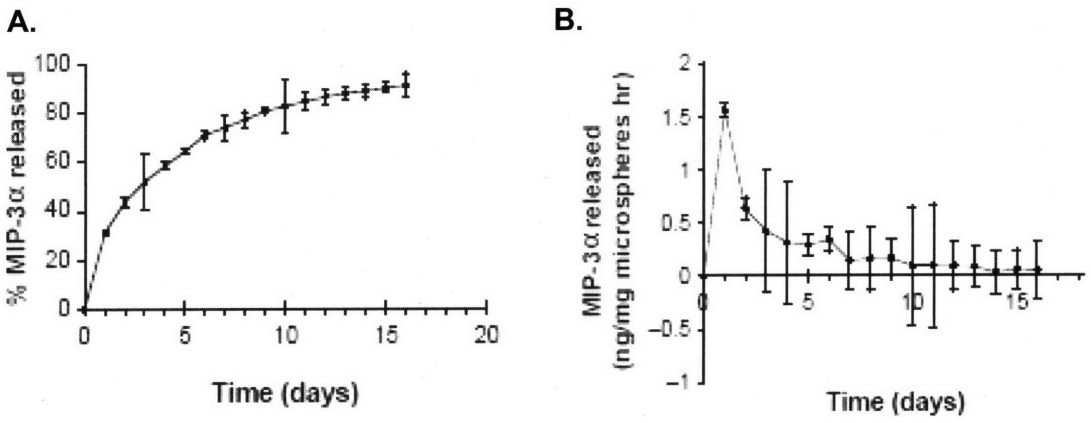

Figure 2.6. Kinetics of CCL20 chemokine release from 40-75 kDa PLGA microspheres in vitro. (A) Percentage of chemokine released versus time into well-stirred PBS at 37 °C. (B) Release rate calculated using data from (A).

2.3.5 Phenotyping of murine BMDCs for kinetics of CCR6 expression on cell surface

Bone marrow cells from femur and tibia of a 6-8 weeks old C57Bl/6 mouse were plated in a 24-well tissue culture polystyrene plate in complete RPMI 1640 medium with 5 ng/mL rmGM-CSF. Cells were pipetted on days 2, 4, 6, 8, and 9, stained with CD11c-FITC and CCR6-phycoerythrin and analyzed by flow cytometry for the expression of these surface markers. As shown in Figure 2.7 depicting the overlays of CD11c and CCR6 expressions on different days, CCR6 expression increases as bone marrow cells differentiate into dendritic cells (characterized by the increase in $CD11c^+$ cells); CCR6 is expressed on ~ 50% cells on day 6 and reaches a maximum of ~70% on day 8. BMDCs were therefore used between days 7-8 for all migration experiments.

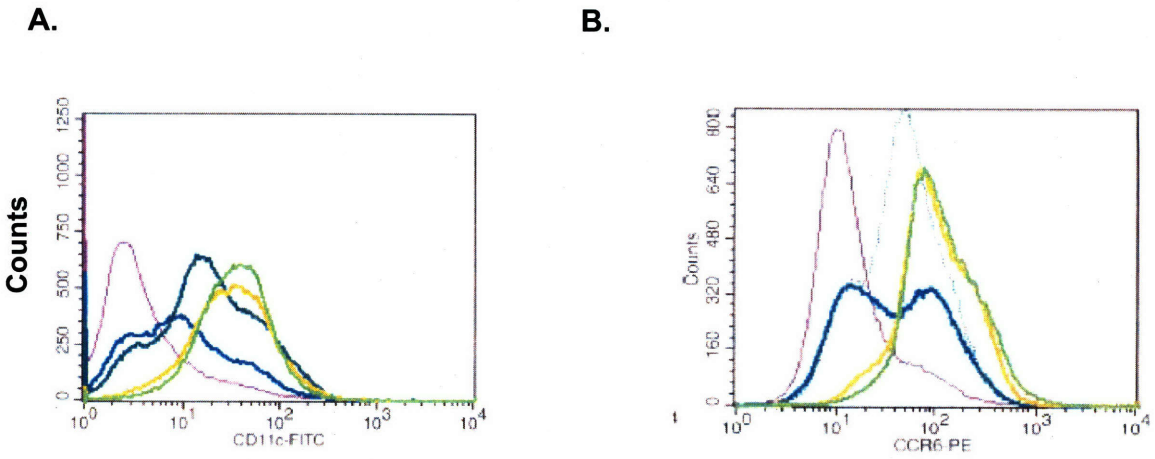

Figure 2.7. Surface expression of CD11c and CCR6 on bone marrow dendritic cells on days 2 (–), 4 (–), 6 (–), 8 (–), and 9 (–)

2.3.6 Chemoattraction of murine BMDCs toward CCL20 -releasing microspheres

Attraction of murine BMDCs to CCL20 microspheres was tested *in vitro* using the collagen gel videomicroscopy assay. For these experiments, we sought to better approximate the situation for immunotherapy/ vaccination, where microspheres might be co-injected with antigens and other adjuvant factors; ideally, immature DCs and DC precursors would be attracted from an immediately surrounding tissue to within very close proximity of the microsphere depot where antigen and DC activation factors have been co-localized. To model this situation, collagen gels with single wells were formed, with BMDCs suspended throughout the gel surrounding the 'immunization site' (Figure 2.1B). Microspheres and collagen were then added to the source well, and the migration of BMDCs near the source well was tracked by time-lapse videomicroscopy.

Time-lapse imaging experiments were carried out, recording nine fields adjacent to attractant source well for 8 h in 1-min intervals. Similar to experiments with fN'LFN'YK, control microspheres containing no protein or containing carrier protein BSA only elicited no chemoattraction of BMDCs. In contrast, Figure 2.8A shows path endpoints for *x-y* migration of cells in response to microspheres releasing CCL20, where pronounced chemoattraction toward the microsphere source was observed. BMDCs

were continuously attracted toward the microspheres during the course of 8 h migration assays. Figure 2.8B shows representative instantaneous velocities for two single cells, demonstrating that DCs were continually motile during the time-course of the experiment, as opposed to exhibiting transient motility followed by paralysis. The mean velocity for chemotaxing DCs in our collagen gel system was 3.2 μm/min, comparable to the rates of DC migration measured in intact lymph nodes *ex vivo* [90] and *in vivo* by intravital imaging [91]; the constant stop-and-go motion of these cells observed is also qualitatively similar to data reported in these prior studies.

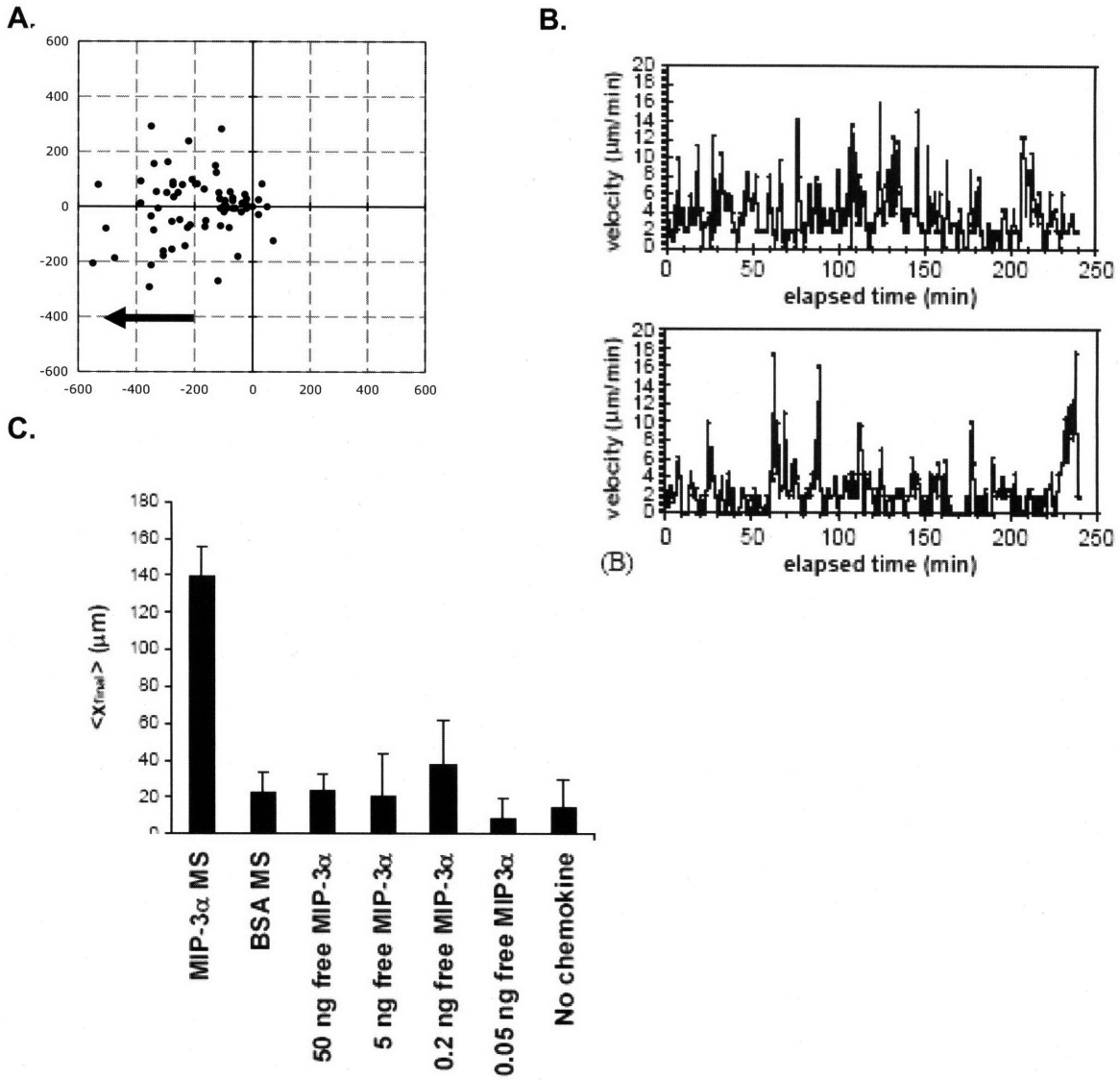

Figure 2.8. CCL20-releasing microspheres elicit sustained chemoattraction of murine BMDCs. (A) Path *x* – *y* endpoints for the migration of 50 single cells after 8 h in the single-well migration assay, with their relative initial positions placed at the origin. Axes are distances in μm, and the arrow denotes the direction toward the attractant source well. (B) Example of single-cell instantaneous velocities over 3 h at 1-min intervals for DCs responding to CCL20 -releasing microspheres. (C) Mean final *x* positions for DCs responding to attractant source wells loaded with CCL20-releasing microspheres, BSA-containing microspheres, or different amounts of freely diffusing CCL20. Positive $\langle x_{final} \rangle$ values denote migration toward the attractant source.

We next compared the migration of BMDCs toward a source well containing bolus CCL20 to DC migration toward a source well containing microspheres releasing CCL20. Initial screens of BMDC chemotaxis in response to freely diffusing CCL20 revealed maximal attraction to ~0.2 ng of free chemokine in our collagen gel assay. We thus tested the chemotaxis of BMDCs to 25 μg of CCL20 -releasing microspheres (which release 0.2-0.3 ng CCL20 over 8 h). Shown in Figure 2.8C is the mean final x position of cells relative to their starting points in the gel after 8 h in response to CCL20 microspheres or different doses of free CCL20; positive values of $\langle x_{final} \rangle$ indicate net motion toward the chemokine source well. Microsphere-released CCL20 was significantly more potent in attracting BMDCs relative to comparable total doses of chemokine delivered as a bolus at time zero. In addition, higher doses of free chemokine could not compensate for this weaker attraction, as seen in the $\langle x_{final} \rangle$ data. This result agrees with the expectation that higher concentrations of chemokine lead to chemokine receptor saturation/ desensitization and blockade of directed cell migration.

BMDCs up to ~2.5 mm from the source (the maximum distance from the source monitored in the assay) exhibited directed migration in response to the CCL20-releasing microspheres during the assay. Strikingly, BMDCs migrating in response to microsphere-released chemokine did not appear to exhibit receptor saturation-driven paralysis or loss of directed motion over the course of 8 h of observation, and the cells could be attracted to the point of contact with CCL20-releasing microspheres. Large discrete microspheres occasionally observed at the edge of the gel source well potently attracted large number of DCs in a 'swarming' motion to their surface, and retained these cells over several hours, as illustrated by the time-lapse images of Figure 2.9. Thus, chemokine-releasing microspheres can potently attract cells over prolonged time periods (here, evaluated for 8 h) and draw DCs over distances of several hundred microns to the point of contact with attracting microspheres.

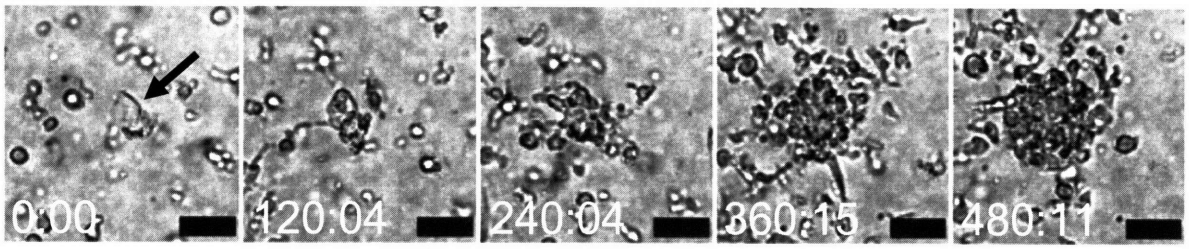

Figure 2.9. DCs can chemotax into direct contact with controlled release microspheres. Shown are five frames from a time-lapse imaging experiment near one isolated large PLGA microsphere (denoted in the first frame by black arrow). DCs continuously accumulated around this particle over 8 h of observation. Elapsed times (min: s) are shown in the lower left of each frame and the scale bars are 50 mm. A quicktime movie of this time-lapse data can be viewed at: http://web.mit.edu/biomaterials/swarm.html; password: swarm.

2.3.7 Modeling spatio-temporal chemokine concentration profiles in collagen

As shown in Figure 2.1, chemoattractants diffuse from 'vaccination site' source well into a relatively large volume of collagen gel. To understand the diffusion of chemoattractants into collagen and attraction of dendritic cells and DC precursors, we modeled the chemoattractant diffusion into collagen by approximating the system as diffusion of chemoattractant from a point source into a semi-infinite sink. We first determined the diffusion coefficient for formyl peptide and CCL20 in collagen gel using this model, and then used the model to predict spatio-temporal concentration profiles of formyl peptide in collagen gel for bolus delivery and controlled-delivery of the chemoattractant. The simplified model of our system has the limitation that it assumes the 'vaccination site' is maintained at a constant concentration and ignores the end effects of the system. Moreover, chemokines are known to bind to the ECM, which means that diffusion may not be the only process determining the concentration profile of chemoattractants. For diffusion from a point source into a semi-infinite sink, Fick's law for diffusion of chemokine in direction x defines flux as:

$$J_x = -D\frac{\partial c_x}{\partial x}; \frac{\partial c_x}{\partial t} = -\frac{\partial J_x}{\partial x} = D\frac{\partial^2 c_x}{\partial x^2} \quad [5]$$

where,

J_x = Flux of chemokine in *x*-direction

D = Diffusion coefficient of chemokine through matrix

The initial and boundary conditions for chemokine diffusion into collagen from a source well into an infinite sink are:

c = 0 at t = 0 for all x > 0	I.C.
$c = c_o$ at x = 0 for all t	B.C. 1
c = 0 at x → ∞ for all t	B.C. 2

The solution to Equation 5 with the above initial boundary conditions to estimate concentration profile as a function of space and time is:

$$c = c_o\, erfc\left[\frac{x}{2\sqrt{Dt}}\right] \quad [6]$$

Since, MetaMorph can provide us average fluorescence intensity in a given field, we decided to reduce Equation 9 into a form containing one variable only. Equation 6 was further averaged over distance *x* (0^+ to L) to estimate average concentration, <c> as a function of time:

$$\frac{<c>}{c_o} = erfc\left(\frac{L}{2\sqrt{Dt}}\right) + \frac{2\sqrt{Dt}}{L\sqrt{\pi}}\left(1 - e^{\frac{L^2}{4Dt}}\right) \quad [7]$$

2.3.7.1 Determination of diffusion coefficient of formyl peptide in collagen gel

The diffusion coefficient of formyl peptide in collagen gels was calculated from direct observation of fluorophore-labeled peptide. The peptide, fN'LFN'YK-FITC (1 μg/mL) was mixed with collagen (1.2 mg/mL, 40 μl) and gelled in a corner of an eight-well labtek chamber slide followed by addition of collagen gel (1.2 mg/mL, 400 μl) to create an infinite sink (Figure 2.10A); time-lapse videomicroscopy was initiated immediately by taking green-fluorescence images for 2 hours at 5-min intervals using a 40x objective lens (Figure 2.10B). The average fluorescence intensity for plane of

observation next to the source well was fit with Equation 7 and the diffusion coefficient was estimated to be 6 x 10^{-10} m^2/sec, which indicates that formyl peptide diffuses freely into collagen.

When this experiment was repeated with fN'LFN'YK-FITC-loaded microspheres, average fluorescence intensity was observed to fit very closely with Equation 10 using the diffusion coefficient in collagen determined above (Figure 2.10B). It must be noted that fluorescein has poor photostability resulting in photobleaching when exposed to light. Therefore, the intensities observed do not necessarily reflect the chemoattractant concentrations in the collagen gel accurately.

A.

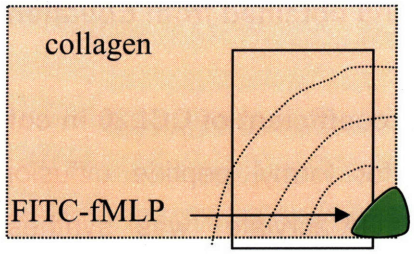

B.

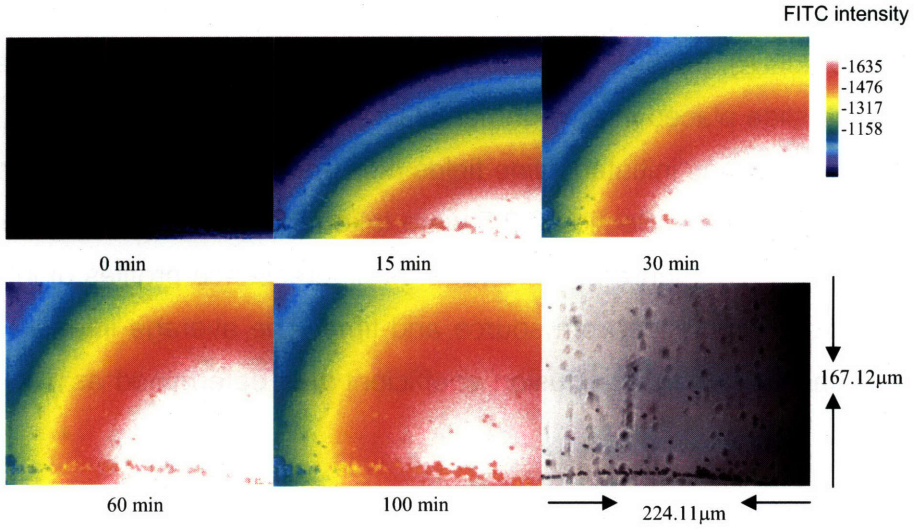

C.

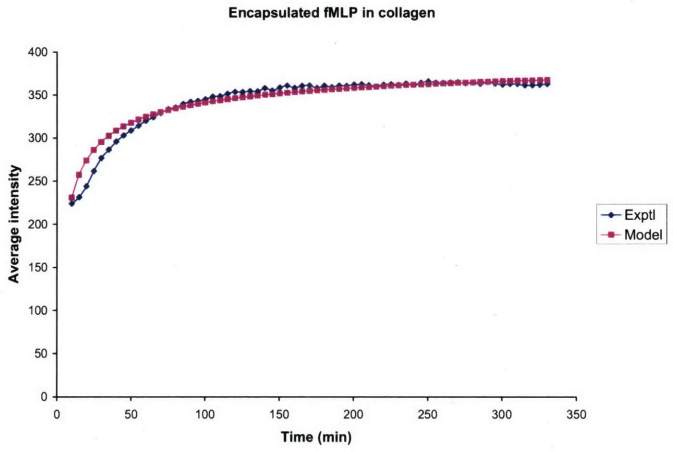

Figure 2.10. (A) Schematic of FITC-fMLP release assay into collagen gel for estimation of diffusion characteristics of the chemokine into collagen (B) Fluorescence micrographs depicting diffusion of FITC-fMLP as a function of space and time into collagen gel. The chemokine source is located at the lower

right corner of each image (C) Average fluorescence intensities for the field of view determined experimentally and obtained from Equation 10.

2.3.7.2 Determination of diffusion coefficient of CCL20 in collagen gel

Similar to the experiment for formyl peptide diffusion in collagen, triblock copolymer (acrylate-PLGA-PEG-PLGA-acrylate) was synthesized as described in Appendix 11 and polymerized along with CCL20 conjugated to FITC (Appendix 7) by photopolymerization initiated by Irgacure^{TM} for 2 min in the center of a 2-well labtek chamber slide (Figure 2.11A). Following polymerization, 1 mL of 2.4 mg/mL of collagen gel was added and the slide placed in environmental chamber maintained at 37 °C, and time-lapse videomicroscopy was initiated. Nine fields adjacent to triblock copolymer in a 3 x 3 array as described above in Section 2.2.5 were taken for green-fluorescence and phase contrast (Figure 2.11B). Figure 2.11C shows the fluorescence profiles of labeled chemokine as a function of distance from source and time. The average intensity was again fit with the Equation 7 and the diffusion coefficient was determined as 1×10^{-11} m^2/sec.

A.

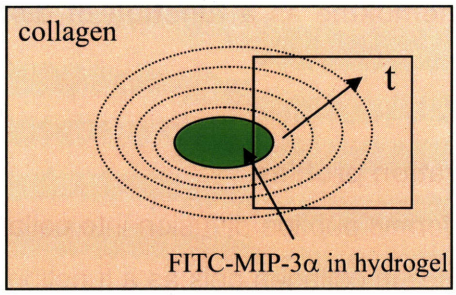

B.

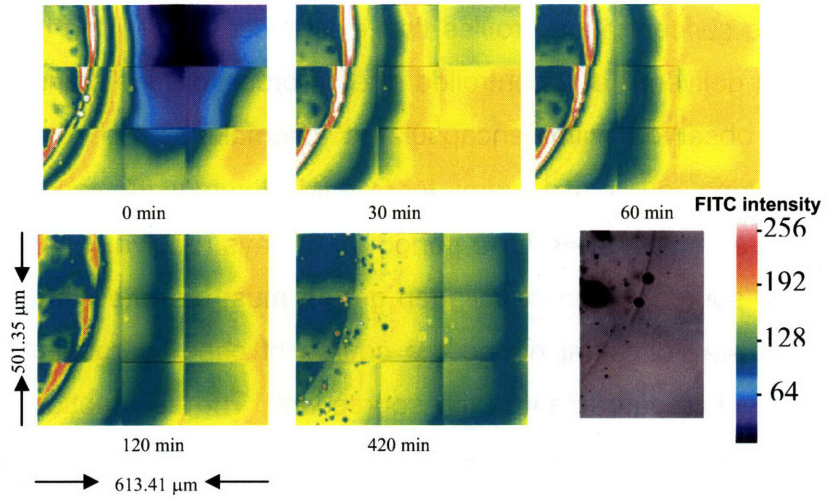

C.

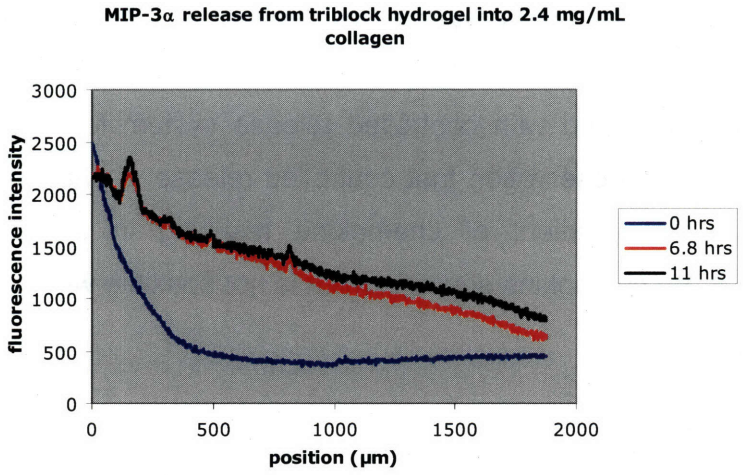

Figure 2.11. (A) Schematic of FITC-CCL20 release assay into collagen gel for estimation of diffusion profile of the chemokine into collagen (B) Fluorescence micrographs depicting diffusion of FITC- CCL20 as a function of space and time

into collagen gel. The chemokine source is located along the left edge of each image (C) Diffusion profile of labeled chemokine as a function of distance from the chemokine source and time.

2.3.7.3 Prediction of chemokine concentration profiles

Based on the diffusion coefficient of formyl peptide diffusion into collagen gel, we predicted the chemokine concentration profiles in collagen gels as a function of distance from the chemokine source and time by fitting the parameters into Equation 6. These predictions were used to compare concentration profiles that exist when chemokine is delivered as a bolus versus when delivered at a controlled rate, in order to understand the sustained chemoattraction observed with encapsulated chemokine. For the predictions, we assumed a chemokine source at 1 μg/mL for free fMLP versus the same amount of chemokine released at a constant rate for a period of 10 days (equivalent to a release rate of ~1 pg/mL/sec in source region of collagen gel). It must be noted that the source concentration will not stay constant during the course of chemoattractant diffusion due to limited amount of chemoattractant in the source well. The assumption that source concentration is constant may however be valid during the initial time points. Figures 2.12A and 2.12B depict the predicted concentration profiles for bolus chemokine and controlled release of chemokine, respectively. As can be seen in the plots, the concentration of chemokine rises quickly in bolus delivery situation reaching near-saturating concentration of chemokine in about 1 h. On the other hand, sub-saturating conditions could be maintained with controlled release system for several hours to days, which agrees with our observation that controlled release of chemokine creates and maintains an optimal gradient of chemokine resulting in sustained chemoattraction of cells towards the chemokine source, which is not possible with bolus delivery of chemokine.

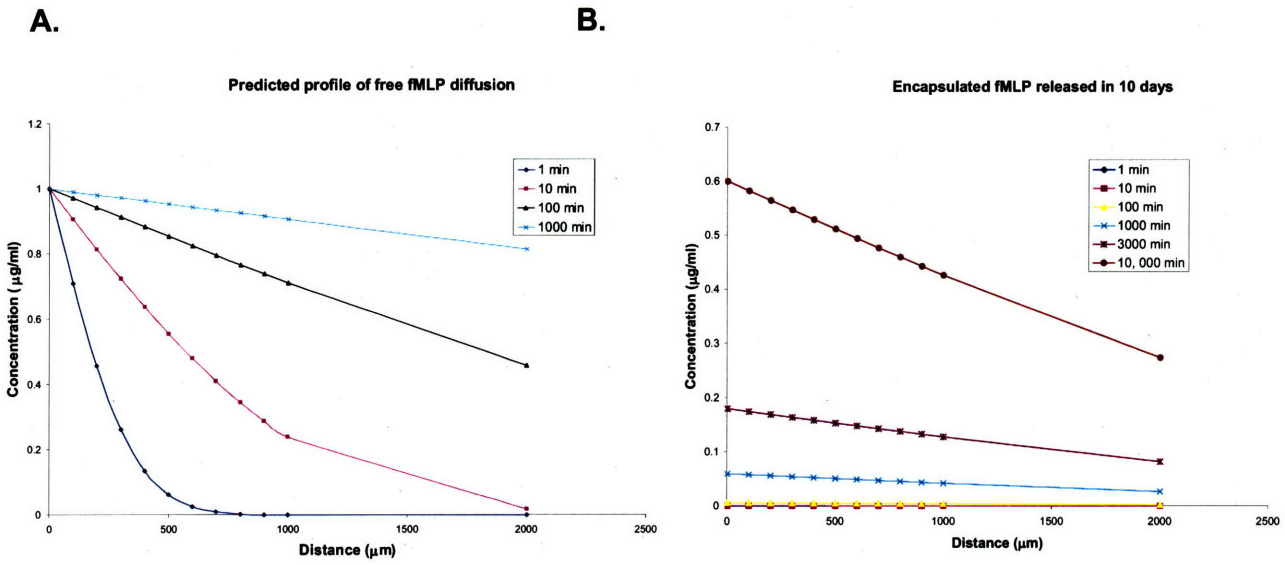

Figure 2.12. Predicted concentration profiles of fMLP using Equation 9 as a function of distance from chemoattractant source and time for (A) bolus delivery of chemokine and (B) Controlled release of chemokine for ~10 days.

2.4 Discussion

Chemotaxis is a ubiquitous mode of directed cell migration in development [92], wound healing [93,94], disease states [48,95,96], and proper function of the immune system [49,97]. In immunity, chemotaxis controls many aspects of cellular trafficking. For example, during induction of a primary immune response, resting (immature) DCs and other inflammatory cells chemotax to sites of infection, DCs activated (matured) by interactions with pathogens or inflammatory cytokines chemotax to the draining lymph nodes to activate T cells, and naïve T cells chemotax to lymph nodes from the blood to rendezvous with DCs [47,49,53,55,97].

Of particular interest for the design of vaccines is the role of chemotaxis in controlling DC (and DC precursor) recruitment to sites of infection. Studies examining DC attraction to an immunization site *in vivo* by a single bolus injection of freely diffusing chemokines have shown that DC attraction in this situation is transient (peaking at ~24 h) [98], as expected given the relatively fast diffusion rates of these small molar mass attractants. By simply sustaining the concentration of a chemoattractant at the injection

site, controlled release of chemokines could thus be expected to offer enhanced DC accumulation.

Based on promising prior studies seeking to trigger chemotaxis in the setting of immunization and the results of this theoretical analysis of controlled release versus bolus chemokine delivery, we sought to develop an injectable, biodegradable, controlled release formulation that would allow the total dosage of chemokine delivered, its location, and its release rate to be tailored. Biodegradable controlled release microspheres could meet these requirements, and poly(lactide-*co*-glycolide) is an attractive first choice as a matrix material due to its long record of safe application *in vivo* and use in clinically licensed products. Polylactide and PLGA microspheres have previously been studied as carriers for the delivery of vaccine antigens in the form of peptides [99], recombinant proteins [100-102], inactivated virus preparations [103,104], or DNA [105-107] and have been shown to enhance both antibody production [100,102-104,106] and T cell immune responses [99,102,105-107] *in vivo*. Microspheres releasing chemokines could be readily combined with these or other antigen delivery strategies, or even co-encapsulate antigen with chemokine – drawing DCs directly to the spatial center of delivered antigens.

We encapsulated two different types of chemoattractants in PLGA microspheres. Formyl peptides are inexpensive, low molecular weight chemoattractants that can be prepared by solid-phase synthesis methods. They attract immature DCs, but also numerous other inflammatory cell types. In contrast, CCL20 is currently produced as a recombinant protein, making it significantly more expensive (an important issue in design of vaccines [108]). However, CCL20 offers enhanced selectivity for attraction of immature DCs to the immunization site: it is the only chemokine known to bind CCR6 and binds only to CCR6, while in contrast most chemokine receptors bind multiple chemokines, and many chemokines are promiscuous in their receptor binding [14]. CCR6 expression is restricted to DCs and memory lymphocytes [73], and CCL20 is the most potent attractant known for several subtypes of human DCs and their precursors [52,56].

We found that both formyl peptides and CCL20, when released from PLGA microspheres, could trigger chemotaxis in DCs millimeters away from the attractant

source, elicit directed migration of up to 500 mm toward the source, and maintain attraction for at least 8 h *in vitro* through a 3D collagen gel model of the extracellular matrix. A limiting factor in chemotaxis is the potential for receptor saturation and/or downregulation, blocking directed migration at high chemoattractant concentrations [76]. As shown in Figure 2.9, DCs could chemotax to the point of contact with controlled release microspheres without exhibiting paralysis or loss of directionality. Based on the experimental release data and modeling results, we hypothesize that this is due to the low, sustained rate of chemokine delivery from the microspheres. It is also likely that the concentration profile of free chemokine very near individual microspheres is modulated at late times by binding to the high density of DCs in the immediate vicinity.

What temporal characteristics are appropriate for chemokine delivery in the setting of an optimal vaccine? Ideally, chemoattractant-releasing microspheres would increase the number of recruited DCs significantly and this amplifies the number of subsequently trafficking DCs to lymph nodes for T cell activation. Daily bolus injections of free CCL20 into tumors have been found to be insufficient to promote significant anti-tumor immunity, under conditions where continuous production of CCL20 (via transduced tumor cells expressing the chemokine) led to tumor regression [42]. Similarly, other studies of chemoattractant-encoding DNA vaccines reporting improved immune responses have observed enhanced DC infiltration at immunization sites from 5 to 15 days post-immunization [65,66,69]. These results suggest that continuous maintenance of a chemokine gradient up to several weeks may be important for sustaining DC influx to an injection site and obtaining enhanced immune responses.

In addition to their potential application directly to vaccine design, chemokine-releasing microspheres should be a powerful tool for the study of chemotaxis *in vitro* and *in vivo*. The ability to create local gradients of one or more factors, which at the extreme can be delivered from single large microspheres as 'point' sources is of interest for studies of cell trafficking in immunity, development, and angiogenesis. These characteristics are complementary to other recent tools developed for the study of chemotaxis such as the use of laminar flows in microfluidics to control chemokine concentrations [109] and enhanced diffusion chambers for the study of cells migrating at different rates [77].

Several issues are relevant in regard to application of chemokine-releasing microspheres *in vivo*. Concentration profiles of chemokines *in vivo* may be modulated by uptake by cells, proteolysis, binding to ECM components, as well as efflux into blood and lymph [110]. Chemokines are known to bind heparin sulfate and other proteoglycan *in vivo* and may be functional from the solid phase [111-113], which will also alter the dynamics of chemotaxis. Thus, optimal release rates and doses *in vivo* may differ from those observed *in vitro*. In addition, microsphere size must be carefully considered in an application to real vaccines. DCs and macrophages have been shown to phagocytose particles smaller than ~ 5 μm (including PLGA microspheres and other synthetic particles) both *in vitro* and *in vivo* [114-119]. Small microspheres may only transiently attract cells prior to internalization and removal by phagocytic cells; to obtain a sustained depot of chemoattractant, large microspheres may be required to avoid phagocytic removal from the injection site. Though the microspheres in the present study had mean diameters of ~ 5 μm, the size of PLGA microspheres prepared by emulsion techniques is readily varied vial alteration of several of fabrication conditions, including continuous phase viscosity, relative oil/water phase volumes, surfactant concentrations, stirring speeds, and choice of solvents [120,121]. Finally, in order to selectively attract target immune cells, the controlled release matrix itself must not trigger unintended chemotaxis e.g., due to chemoattractive breakdown products or the induction of inflammatory chemokines triggered in surrounding tissue. In the present *in vitro* studies carried up to 8 h in culture, we did not observe chemotaxis triggered by empty PLGA microspheres or microspheres loaded only with the carrier protein. However, *in vivo* and over longer times *in vitro*, acid breakdown products from PLGA could influence the cellular response.

2.5 Conclusions

Injectable, biodegradable PLGA microspheres releasing chemoattractants that induce directed cell migration have been developed. Microspheres releasing either formyl peptide attractants or the chemokine CCL20 elicited sustained chemotaxis of human and mouse DCs over distances up to 500 μm and sustained the attraction of

these cells up to 8 h in an *in vitro* collagen gel model. DCs could be attracted directly into contact with controlled release microspheres, suggesting that they could be effective for enriching DCs at the immunization site *in vivo* under conditions where the dosage, release rate, and location of the chemoattractant could be fully predetermined by the composition of the microspheres. The use of such controlled release microspheres to create defined gradients of chemoattractants *in vitro* and *in vivo* offers the possibility to both quantitatively probe the role of specific attractants in chemoattraction and to manipulate cell migration for therapeutic purposes.

3. Delivery of antigen and maturation factor by hydrogel nanoparticles

3.1 Introduction

Synthetic vaccines designed to prime the adaptive immune system are sought for a broad range of infectious diseases and for the treatment of cancer, in both prophylactic and therapeutic settings [122-124]. From a conceptual point of view, vaccines are comprised of an antigen- the biomacromolecule component that the immune system must be primed to recognize- and an adjuvant, a second component that may play multiple roles in augmenting the immune response generated against the antigen, such as 'depoting' of antigen for sustained immune stimulation or providing inflammatory signals designed to activate cells of the immune system [125]. An ideal vaccine would lead to the stimulation of two key cellular effectors, T cells and B cells, which are triggered by two very different pathways. T cell activation occurs when a cellular intermediate, the dendritic cell (DC), internalizes a protein, proteolyses this antigen into short peptides, and presents these peptides to T cells in the cleft of their major histocompatibility complex (MHC) molecules (Figure 1.1). In contrast, B cells can

directly bind protein antigens via their B cell receptors (membrane-tethered IgM or IgG molecules). DCs and B cells must also receive stimulation through 'danger signal receptors', such as the Toll-like receptors, which alert the cell to mount an immune response against the encountered protein [22,126]. Ideally, one function of adjuvants is to provide these danger signals to DCs and B cells when they encounter antigen.

It is now generally believed that protection against many of the diseases for which vaccines are currently sought (e.g., HIV, Hepatitis C, and tuberculosis) will require both T cell and B cell responses, but the design of synthetic vaccines that potently stimulate both arms of adaptive immunity remains a significant challenge [127-130]. In contrast, natural pathogens such as viruses and bacteria potently elicit both T cell and B cell activation. Naïve $CD8^+$ and $CD4^+$ T cell responses to pathogens are triggered when DCs present pathogen-derived peptides to the T cells on class I or class II MHC molecules, respectively. Exogenous foreign proteins are normally internalized by dendritic cells, processed in endosomes, and presented on MHC class II molecules [5,10,131], while MHC class I molecules are typically loaded with peptides derived from intracellular molecules (Figure 1.3). Dendritic cells and macrophages have the unique capability to present exogenous (extracellular) proteins on MHC class I molecules by a process called cross-presentation [11,132]. Cross-presentation is not efficient for soluble protein antigens and is typically observed only when high concentrations of exogenous protein are used. However, it has been shown that whole intact microbes (or purified protein antigens adsorbed to latex particles) taken up by phagocytosis can elicit cross-presentation of the delivered antigen very efficiently; these antigens are then processed and presented on MHC class I molecules to naïve $CD8^+$ T cells [10,132,133]. Cross presentation of particulate antigens allows dendritic cells to potently activate both $CD4^+$ and $CD8^+$ naïve T cells in response to microbes such as bacteria. For B cells, the natural repeating molecular motifs present on the surface of pathogens allows multiple B cell receptors to bind to a single pathogen particle, causing receptor aggregation and strong B cell activation [129,130]. The required immunostimulatory signals are thus 'built in' to the physical structure of pathogens, such that multiple danger signal receptors on DCs and B cells are triggered when pathogens are bound/internalized [134].

Given these favorable characteristics, it has been recognized that synthetic vaccines mimicking pathogens structurally and/or functionally might take advantage of the evolutionarily engineered response of the immune system to these particulate antigens [135,136]. Examples of antigen carriers previously studied in this context include degradable poly(lactide-*co*-glycolide) microspheres[137-140], latex particles with surface-adsorbed protein [10,141], and gel particles [142-145]. Shen et al. showed that when a dendritic cell clone internalized latex particles coated with the model protein antigen ovalbumin, cross-presentation was induced, and DCs were capable of stimulating IL-2 secretion by a $CD8^+$ T cell clone at >100-fold lower doses of antigen given to DCs compared to antigen delivered to DCs as soluble protein [10]. Mimicking pathogen danger signals, Kempf *et al.* immobilized antibodies against Fc-γ receptors, CD40, or integrin receptors on the surface of PLGA microspheres [146]. These microparticles triggered enhanced maturation of human dendritic cells as well as upregulation of surface markers and IL-12 cytokine secretion.

Based on the wealth of information on activation of naïve T cells and B cells *in vivo*, synthetic vaccines have been designed to co-deliver antigen and activation signals (often Toll-like receptor ligands) in concert. Different strategies have been employed to co-deliver antigen and maturation signals such as co-injection of the two agents into the host [24,147-149], use of DNA plasmids encoding for antigen of interest that contain unmethylated CpG motifs or co-express inflammatory cytokines [150,151], conjugation of antigen with maturation factors such as ova-CpG conjugates [152,153], or co-encapsulation of antigen and maturation factors into polymeric microparticles [102,135,154]. *In vivo*, immunization of mice with antigen and CpG oligonucleotides co-encapsulated in cationic liposomes elicited enhanced cytokine secretion by lymphocytes and antibody titers were observed to increase an order of magnitude compared to that elicited by immunization with soluble antigen [155]. Similarly, a hepatitis B vaccine based on the hepatitis B core antigen and the immunostimulatory molecule monophospholipid A (MPLA) encapsulated in poly(lactide-co-glycolide) nanoparticles elicited a stronger cellular immune response than immunization with soluble protein antigen mixed with MPLA [156]. Virus-like particles formulated directly from viral membrane components have also been successfully developed to provide coincident

antigen and activation signal delivery in nonliving vaccines [157-159]. Co-delivery of antigen and maturation factor to dendritic cells using the above strategies resulted in strong immune responses compared to delivery of antigen alone.

Ongoing practical challenges facing many of these approaches are (1) maximizing antigen loading in carriers (to elicit robust immunity with reasonable vaccine doses), (2) avoiding denaturation/destruction of protein antigens during synthesis and storage within the carrier prior to release, and (3) minimizing toxicity associated with vaccine carriers and adjuvants to acceptable levels for clinical applications. Typically, the amount of antigen delivered per total mass of carriers is low (observed weight fractions of antigen in particulate carriers are typically < 15 wt% for protein encapsulation in PLGA microspheres [137-140], ≤ 5 wt% for adsorption on latex particles [10,132,141,148], and ~1 wt% for hydrogel particles [142-144]). Low protein loading limits the levels of antigen that can be delivered in an immunization. Encapsulation of proteins in synthetic polymers like PLGA microspheres is also known to lead to antigen degradation both during the encapsulation process itself and during 'storage' within the particles, limiting the effective dose delivered in such vaccines [125,160-163]. In addition, various adjuvants used in conjunction with particulate antigen delivery carriers such as lipopolysaccharide, cholera toxin, Quil-A, Freund's adjuvant, and lipid-based adjuvants (e.g., murapalmitine and murametide [148,164]) have unacceptable levels of toxicity and therefore have limited clinical application [127,165].

A direct examination of the value of presenting immunostimulatory and antigenic epitopes together at the surface of synthetic particulate vaccines is lacking, but data from prior studies is consistent with a potential positive impact of such structural mimicry on immunological outcomes [136]. Prior studies have demonstrated that intact protein antigens immobilized to the surface of biodegradable microparticles significantly enhance B cell and T cell responses [148,166,167]; although the objective of this strategy was to prevent degradation of the antigen during encapsulation, it is possible that microspheres transported to draining lymph nodes were directly accessed by B cells, enabling improved B cell stimulation via multivalent, microsphere-bound antigen. Likewise, peptide antigens tethered to the surface of synthetic nanoparticles have been

shown to elicit highly elevated antibody responses relative to soluble peptide antigen [148,168]. Other strategies utilized for particulate delivery of surface-displayed antigen epitopes include conjugation of antigen to immune complexes [9], liposomes [169-172], and the use of virus-like particles [21]. To our knowledge, surface co-display of TLR ligands and antigen by synthetic particle vaccines has not been tested. However, conjugation of CpG oligonucleotides (short single-stranded DNA sequences mimicking bacterial DNA, which bind TLR9) directly to model protein antigens [152,153], mixing of CpG-bearing particles with antigen-bearing particles [106], and co-encapsulation of antigens and TLR ligands within biodegradable particles [102,173,174] have all been found to enhance both T cell and antibody responses. In addition, the potency of TLR ligands is enhanced by particulate delivery, allowing significantly lower total doses of the TLR ligands to be used, which may alleviate potential side effects from these strong immunostimulatory signals [175].

Based on these earlier findings, we sought to develop a particulate protein carrier synthesis strategy that would allow high levels of protein to be encapsulated under aqueous conditions that preserve the integrity of the antigen, provide antigen accessible at the surface of the carrier for binding to B cell receptors, and permit subsequent functionalization of the particle surfaces with immunostimulatory 'danger' signals to drive naïve T and B cell responses. To this end, we investigated a two-phase aqueous miniemulsion polymerization to encapsulate protein within submicron hydrogel particles in the absence of organic solvents. Near-saturated salt solutions of a poly(ethylene oxide-*b*-propylene oxide-*b*-ethylene oxide) (PEO-PPO-PEO) triblock copolymer, pluronic^{TM} F-68, mixed with the model protein antigen ovalbumin (ova) and the methacrylate monomers poly(ethylene glycol) methacrylate, methacrylic acid, and poly(ethylene glycol) dimethacrylate, phase separated on heating to 40°C to form a stable emulsion. Free radical polymerization of the emulsion provided submicron-sized (~500 nm diameter) hydrogel particles encapsulating up to ~750 μg ova per mg of dried particles. The particles were surface-functionalized post-synthesis by electrostatic adsorption of CpG oligonucleotides, to provide immunostimulatory signals to dendritic cells or B cells encountering the particles. These mesoscale particles, which mimic pathogens in size and in their functional co-delivery of antigen and activation signals,

were avidly phagocytosed by dendritic cells, and DCs that internalized ovalbumin-loaded particles primed naïve $CD4^+$ and $CD8^+$ T cell responses at ~10-fold lower doses of protein than DCs pulsed with soluble ovalbumin (ova). Dendritic cells were effectively matured by hydrogel particles, secreting inflammatory cytokines and upregulating expression of costimulatory molecules. *In* vivo, CpG-coated hydrogel particles caused activation of naïve T cells and resulted in high anti-ovalbumin IgG antibody titers. This hydrogel particle encapsulation strategy may be of utility for higher potency vaccines and drug delivery applications requiring the delivery of high levels of fragile proteins.

3.2 Materials and Methods

3.2.1 Hydrogel particle synthesis

A salting out-based miniemulsion polymerization technique was used to synthesize protein-loaded hydrogel particles. Sodium chloride (16 g) was added to 50 mL of 4% (w/vol) aqueous pluronic^{TM} F-68 (Sigma) solution in a 100 mL round bottom flask and stirred until dissolved. The solution was degassed for 15 min with nitrogen followed by the addition of 50 mg ova and (for experiments with labeled particles) 250 μg Texas Red-conjugated ova (or 1 mg DQ-conjugated ova, Molecular Probes) to the solution with stirring. Poly(ethylene glycol) methacrylate (PEGMA, 300 mg, $5.7x10^{-4}$ mol, Sigma), poly(ethylene glycol) dimethacrylate (PEGDMA, 15 mg, $1.71x10^{-5}$ mol, Sigma), and methacrylic acid (MAA, 15 mg, $1.74x10^{-4}$ mol, Sigma) were mixed and degassed with nitrogen; the monomers were then added to the pluronic/protein/salt solution with stirring to form a clear solution. The solution was heated in a water bath to 40°C, causing phase separation/emulsion formation driven by salting-out of the pluronic copolymer. Polymerization was initiated by the addition of 10 mg ammonium persulfate (Pierce Chemicals Co.) and 10 mg sodium metabisulfite (Sigma) in 1 mL of water. Owing to the rapid polymerization in miniemulsions [176,177], particles were formed and the reaction was stopped after 7 min. The resulting particle suspension was diluted with 50 mL of deionized water and the particles were collected by centrifugation. The recovered gel particles were washed with 50 mL water three times (until no free protein

was detected in the supernatant), resuspended in 5 mL of 0.4% w/vol pluronic^{TM} F-68 solution in PBS (~10 mg/mL particle concentration), and stored at 4°C until further use.

3.2.2 Electrostatic assembly of CpG oligonucleotide on hydrogel particles

To provide a high density of dendritic cell- and B cell-activating ligands at the surface of each particle, the initially anionic hydrogel particles obtained from the miniemulsion synthesis were modified by sequential adsorption of poly(L-arginine) (10 kDa, Sigma) followed by anionic CpG oligonucleotides (TCC ATG ACG TTC CTG ACG TT, Integrated DNA Technologies, USA). Hydrogel particles (10 mg in 1mL PBS) were incubated with 5 mg/mL poly-L-arginine at 37°C with shaking overnight. The poly-L-arginine coated particles were centrifuged and washed four times to remove unbound polycation. For CpG functionalization, the poly(L-arginine)-coated particles were then resuspended in 1 mL PBS, mixed with CpG oligos (final CpG concentration 100 μM), and incubated for 3 hrs at 37°C. The CpG-modified particles were pelleted by centrifugation and the supernatant was collected to measure the amount of unbound CpG remaining in solution using a spectrophotometer (ThermoElectron Spectronic^{TM} Helios^{TM} Gamma UV-Vis Spectrophotometer) via the absorption at 260 nm. Based on a standard curve determined for CpG 1826, the efficiency of CpG coupling was determined as:

$$CpG\ Conjugation\ Efficiency = [1 - \frac{CpG\,concentration\ in\ supernatant}{initial\ CpG\ concentration}] \times 100\,\% \quad [8]$$

3.2.3 Hydrogel particle characterization

3.2.3.1 Hydrogel particle size

The size distributions of hydrogel particles were characterized by dynamic light scattering using a 657 nm laser source at a fixed angle of 90° (Brookhaven 90Plus particle sizer). Typical count rates were 350,000 per second and collection times were 15 min. Surface charge on poly-L-arginine-coated hydrogel particles was characterized

by measuring the zeta potential of particle suspensions in PBS (300 μg/mL dry weight of particles) using a Zeta Pals (Brookhaven Instruments Corporation).

3.2.3.2 Protein encapsulation efficiency

To determine the amount of protein encapsulated and the protein encapsulation efficiency, supernatants from the particle synthesis were collected, pooled, and fluorescence from the tracer protein texas red ovalbumin (λ_{exc} = 584 nm, λ_{em} = 612 nm) was measured in a spectrofluorometer (Molecular Devices SpectraMax Gemini Spectrofluorometer) to detect unencapsulated protein. The protein encapsulation efficiency was calculated as:

$$Encapsulation\ Efficiency = \left[1 - \frac{Amount\ of\ protein\ in\ supernatant}{Amount\ of\ protein\ added}\right] \times 100\,\% \quad [9]$$

3.2.3.3 Determination of presence of surface protein epitopes

In order to detect the presence of encapsulated protein accessible at the surface of particles, 2 mg (10 mg/mL) particles were incubated with 50 μg/mL mouse anti-ovalbumin monoclonal antibody or with isotype control antibody for 30 min at room temperature. Particles were then washed and incubated with 50 μg/mL Alexa fluor 488-conjugated anti-mouse IgG secondary antibody for 30 min at room temperature. The labeled particles were washed again and finally imaged at 40X using a Zeiss Axiovert 200 epifluorescence microscope equipped with a CoolSnapHQ CCD camera (Roper Scientific).

3.2.3.4 *In vitro* digestion of encapsulated antigen by endosomal protease cathepsin D

To assess *in vitro* digestion and release of encapsulated ova from particles incubated with phagolysosomal proteases, hydrogel particles were resuspended (7 mg/mL particles, equivalent to 5 mg/mL ovalbumin) in 0.1 M Gly-HCl buffer pH 5.5 and incubated for 48 hours with 200 μg/mL bovine spleen cathepsin D. The sample was then centrifuged and the supernatant analyzed by size exclusion chromatography

(Hitachi LaChrom D-7000 HPLC system) in phosphate buffered saline using a Superdex200 column (Amersham Biosciences). Eluting proteins or peptide fragments were analyzed by a UV-vis detector (Hitachi L-7420) measuring absorbance at 280 nm.

3.2.3.5 Determination of hydrogel particle density in suspension

Particle concentrations obtained from each synthesis were determined by analyzing serial dilutions of fluorescent gel particle suspensions on a flow cytometer (FACS Scan, BD Biosciences), and counting the total number of events in a known volume.

3.2.3.6 Determination of water content in hydrogel particles

To estimate the water content of protein-loaded particles, 1 mL of 10 mg/mL particles were blotted on filter paper and the initial mass of the particles was measured. The sample was then dried to constant weight in a vacuum oven at 70°C for 12 hours and the dry mass was determined to calculate the weight fraction of water in the gels.

3.2.4 Hydrogel particle uptake by bone marrow-derived dendritic cells

3.2.4.1 Fluorescence imaging of hydrogel uptake and cell viability

DCs (1 million/mL) were incubated with DQ-ovalbumin-containing hydrogel particles (50 μg/mL ovalbumin) for 1 hour at 37°C in complete RPMI medium. The medium was replaced to remove free particles, and particles/DCs were imaged at 40X using the fluorescence system described above. Fluorescence from non-internalized particles bound to cells was quenched by the addition of 0.4% w/vol trypan blue [10]. Dendtitic cells incubated with hydrogel particles for 24 hours were stained with 5 μg/mL propidium iodide and analyzed by flow cytometry for cell viability.

3.2.4.2 Kinetics of antigen uptake by bone marrow-derived dendritic cells

BMDCs (1 x 10^6 cells in 1 mL) were incubated with Alexa fluor 488-conjugated ovalbumin-containing hydrogel particles (1:50 labeled: unlabeled protein) equivalent to 50 μg encapsulated ovalbumin or a corresponding amount of soluble protein with or

without soluble CpG oligonucleotide for 1, 4, or 18 hours at 37°C. Cells were washed, stained with phycoerythrin (PE)-conjugated anti-CD11c (clone HL3, Pharmingen), and uptake of antigen by DCs was determined by analyzing Alexa fluorescence of $CD11c^+$ cells on a Becton Dickinson FACS Scan flow cytometer.

To obtain a measure of the amount of class I ova peptide-MHC complexes generated following antigen pulsing in different conditions, BMDCs were incubated for 18 hrs with 50 mg soluble ova or ova-loaded particles, stained with monoclonal antibody 25.D1.16 that recognizes SIINFEKL-K^b class I ova peptide-MHC complexes [178] , followed by PE-conjugated rat anti-mouse IgG_1 antibody (clone A85-1, Pharmingen, USA). Stained BMDCs were analyzed for levels of surface antigen presentation using flow cytometry (FACS Scan, BD Biosciences).

3.2.5 Assesment of dendritic cell maturation/activation by hydrogel nanoparticles

3.2.5.1 Upregulation of costimulatory molecules on dendritic cells surface

BMDCs (1×10^6 cells/ml) were incubated 24 hrs with 1 μM soluble CpG, 100 μg nanoparticles-lacking CpG, CpG-coated hydrogel particles (100 μg particles, 1 μM equivalent CpG concentration), 1 μg/mL lipopolysaccharide (LPS), or were left untreated. Dendritic cell Fcγ-II/III receptors were blocked using anti-CD16/CD32 antibody (Pharmingen, USA), and cells were then stained with monoclonal antibodies against CD11c, I-A^b (clone AF6-120.1), CD40 (clone 3/23), CD80 (clone 16-10A1), and CD86 (clone GL1) (Pharmingen, USA) and analyzed on a BD FACS Scan flow cytometer.

3.2.5.2 Secretion of inflammatory cytokines by dendritic cells

Cytokine secretion by DCs exposed to soluble CpG or CpG-conjugated nanoparticles was measured by ELISA. BMDCs (5×10^5 cells/ml) were cultured with various dilutions of soluble CpG, hydrogel particles coated with poly(L-arginine) but not with CpG, or CpG-coated hydrogel particles in a 96-well plate for 48 hrs. Supernatants

from the cultures were analyzed for the presence of IL-12p40, IL-12p70, IL-6, TNF-α, and IL-10 by ELISA (R&D Systems, USA).

3.2.6 *In vitro* antigen presentation to T cells by dendritic cells

To determine whether protein antigen in gel particles internalized by dendritic cells was processed to allow antigen presentation to T cells, activation of naïve T cells by particle-pulsed or control DCs was assessed by measuring production of IL-2 by T cells in response to stimulation by DCs. DCs (1×10^5) were plated in 96-well round-bottom tissue culture plates and incubated with either soluble ova mixed with 1 μM CpG or CpG-modified ova gel particles (~14 nmol CpG/mg encapsulated ovalbumin) for 4 hours, after which the DCs were washed with RPMI medium to remove free antigen. $CD4^+$ or $CD8^+$ naïve ovalbumin-specific T cells were isolated from spleens of OT-II or OT-I transgenic mice (Jackson Laboratories) respectively, using $CD4^+$ or $CD8^+$ Magnetic-Assisted Cell Sorting (MACS) beads ($CD4^+$ T cell and $CD8^+$ T cell negative selection kits, Miltenyi Biotech) according to the manufacturer's instructions. Purified T-cells (1×10^5) were added to each well and co-cultured with DCs for 72 hours; IL-2 concentrations in the culture supernatants were then determined by ELISA. $CD8^+$ OT-I splenocytes were blasted for 5-7 days and co-cultured with dendritic cells as described above for naïve T cells. IL-2 secretion was measured by ELISA after 48 h to study antigen presentation to T cells by dendritic cells.

To assess the proliferation of naïve T cells upon activation by activated dendritic cells, BMDCs (1×10^5 cells/well) were incubated for four hours with 10 μg/mL ovalbumin delivered as soluble protein or hydrogel particles in a 96-well round bottom tissue culture plate. Free antigen was removed and CFSE-labeled $CD4^+$ (OT-II) or $CD8^+$ (OT-I) naïve T cells (1 x 105 cells/well) were co-cultured with equal number of dendritic cells at 37°C, 5% CO_2 for 60 h. Cells were extracted from the tissue culture plate, and stained with anti-CD4/CD8-APC (for OT-I or OT-II T cell identification) and propidium iodide (for live cells), and T cell proliferation was assessed by CFSE dilution upon cell division

3.2.7 *In vivo* activation of lymphocytes by hydrogel particles in C57Bl/6 mice

3.2.7.1 *In vivo* activation of ovalbumin-specific naïve T cells measured by *in vitro* restimulation and SIINFEKL-K^b tetramer staining

C57Bl/6 mice (8-10 weeks old) were immunized s.c. in the lower flanks with 100 μL PBS (control) or 100 μg of ova in different forms: soluble ova in 100 μL PBS, soluble ova mixed with soluble CpG (1.4 nmoles), soluble ova in 50 μL PBS emulsified in 50 μL CFA, uncoated ova nanoparticles in 100 μL PBS, or CpG-coated ova nanoparticles (1.4 nmole total CpG) in 100 μL PBS. Mice were sacrificed after 7 d, and cells were isolated from spleen or inguinal (draining) lymph nodes using 400 U/mL collagenase D (Roche Applied Science, USA) for 45 min at 37 °C. RBCs were lysed in splenocyte samples, and cells were plated at 500,000 cells/ well in 96-well round bottom plates. Dominant ovalbumin-derived peptides known to be presented by C57Bl/6 MHC class I (SIINFEKL) or class II (ISQAVHAAHAEINEAGR) (AnaSpec, USA) [133] were added at a final concentration of 5 μg/ml in each well in a total volume of 200 μl. IFN-γ secretion from the *ex vivo*-restimulated cells was determined by sandwich ELISA (R&D Systems, USA) after 48 hrs to quantify T cell activation. Statistical analysis of data was carried out by Student's *t*-test; differences were considered significant when P-values were <0.05.

To determine the role of CpG display from particle surfaces, C57Bl/6 mice (8-10 weeks old, 4 mice per condition) were immunized in lower flanks with 100 μL PBS or 100 μg ova nanoparticles in 100 μL PBS, ova nanoparticles mixed with soluble CpG (1.4 nmol), or CpG-bound nanoparticles. One week later, splenocytes were isolated by treatment with collagenase D. Splenocytes (1×10^6 cells) from each mouse were stained directly *ex vivo* with anti-CD8α and SIINFEKL-MHC class I phycoerythrin-conjugated streptavidin tetramers (a gift of Dr. Norman Letvin, Harvard Medical School), and analyzed by flow cytometry to determine the frequency of ova-specific $CD8^+$ T cells from mice immunized by each condition. In parallel, splenocytes were restimulated with class I and class II peptides as described above and IFN-γ secretion was measured in the supernatants after 48 hrs by sandwich ELISA.

3.2.7.2 Anti-ovalbumin IgG titers in sera of mice immunized with hydrogel particles

Groups of two C57Bl/6 mice (8-10 weeks old, groups of 2) per condition were immunized s.c. in their lower flanks with 100 μg total ovalbumin in different forms: soluble ova in 100 μL PBS, soluble ova mixed with 1.4 nmoles (8.5 μg) soluble CpG 1826, soluble ovalbumin (in 50 μL PBS) mixed with 50 μL complete Freund's adjuvant (CFA), ovalbumin-containing hydrogel particles in 100 μL PBS, or CpG-coated hydrogel particles (1.4 nmole (8.5 μg) total CpG) in 100 μL PBS. Control mice received injections of PBS only. Serum IgG titers were determined from blood samples collected after 1, 3, 5, and 7 weeks by sandwich ELISA using ova-coated microtiter plates. Antibody titers are reported as the serum dilution at which the sample $O.D._{450}$ was 2-fold greater than the $O.D._{450}$ measured for naive mice (Equation 10). The data was analyzed for statistical significance using Student's *t*-test; differences were considered significant when P-values were < 0.05.

:

$$Antibody\ Titer\ in\ Serum = (Serum\ dilution\ at\ which\ A_{450}^{sample} = 2 \times A_{450}^{nonimmune\ \ serum}) \quad [10]$$

3.2.7.3 *In vivo* cytolytic activity of memory T cells

To measure the induction of $CD8^+$ T cell memory, an *in vivo* CTL assay was employed [149]. C57Bl/6 mice were immunized s.c. in lower flanks with PBS, 100 μg ova in nanoparticles mixed with 8.5 μg soluble CpG, or CpG-coated nanoparticles (100 μg ova, 8.5 μg CpG). 60 days later, syngeneic splenocytes labeled with 0.5 μM (unplulsed) or 5 μM (pulsed with 1 μg/mL SIINFEKL for 1 h) were injected at 6 x 10^6 cells of each type per mouse. 24 h later, mice were sacrificed and splenocytes were analyzed for *in vivo* cytolytic activity calculated as:

$$Cytolytic\ Activity = \left[1 - \frac{ratio\ primed}{ratio\ unprimed}\right] \times 100\ \%,\ where\ ratio = \frac{CFSE^{lo}}{CFSE^{hi}} \quad [11]$$

3.3 Results

3.3.1 Hydrogel particle synthesis and characterization

To develop a strategy for all-aqueous encapsulation of antigen, we first investigated the effect of monovalent salts on the phase separation behavior of pluronic F-68 by means of dynamic light scattering. Pluronic F-68 solution (0.04 g/mL) in a near-saturated (5.5 M) NaCl solution was heated to various temperatures followed by determination of the size of block copolymer aggregates in the solution using Dynamic Light Scattering (DLS); as shown in Figure 3.1. We found that the cloud point of F-68 could be lowered from ~108°C in pure water (a theoretical value) to ~ 37°C in a near-saturated sodium chloride solution. The measured hydrodynamic diameter of pluronic aggregates in 5.5 M NaCl solution with 0.04 g/mL increased from ~35 nm at 32 °C to ~ 400 nm at 37 °C, coincident with obvious clouding of the initially clear solution. The phase separation behavior and the cloud point of pluronic F-68 in saturated salt solution was unaffected by presence of PEG monomers and protein (Figure 3.1). This is possibly a result of small relative concentrations of protein (0.1% w/v) and PEG monomers (0.66% w/v) compared to the weight fraction of pluronic F-68 (4% w/v) in the salt solution. The mesoscale polymer-rich droplets formed on heating to 37 °C (visible by light microscopy) were stable in a stirred solution and showed no change in mean diameter for up to 4 h at constant temperature.

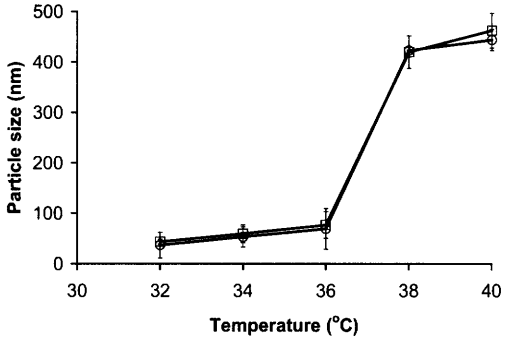

Figure 3.1. Mean diameter of pluronic aggregates as a function of temperature in 0.04 g/mL pluronic F-68 aqueous solution containing 5.5 M NaCl with (○) or without (□) the addition of 1 mg/mL ovalbumin and 6.6 mg/mL monomers (6 mg/mL PEGMA, 0.3 mg/mL PEGDMA, and 0.3 mg/mL MAA).

For synthesis of hydrogel particles, a model protein antigen, ovalbumin, and the gel precursor monomers PEGMA, PEGDMA, and MAA were added to a 5.5 M NaCl solution containing 0.04 g/mL pluronic F-68. Heating of the solution to 40 °C followed by addition of the free-radical initiator ammonium persulfate (APS) led to rapid polymerization of monomer within protein/ polymer-rich phase of the emulsion, and hydrogel particles formed by this process were recovered by centrifugation of the resulting suspension (Figure 3.2).

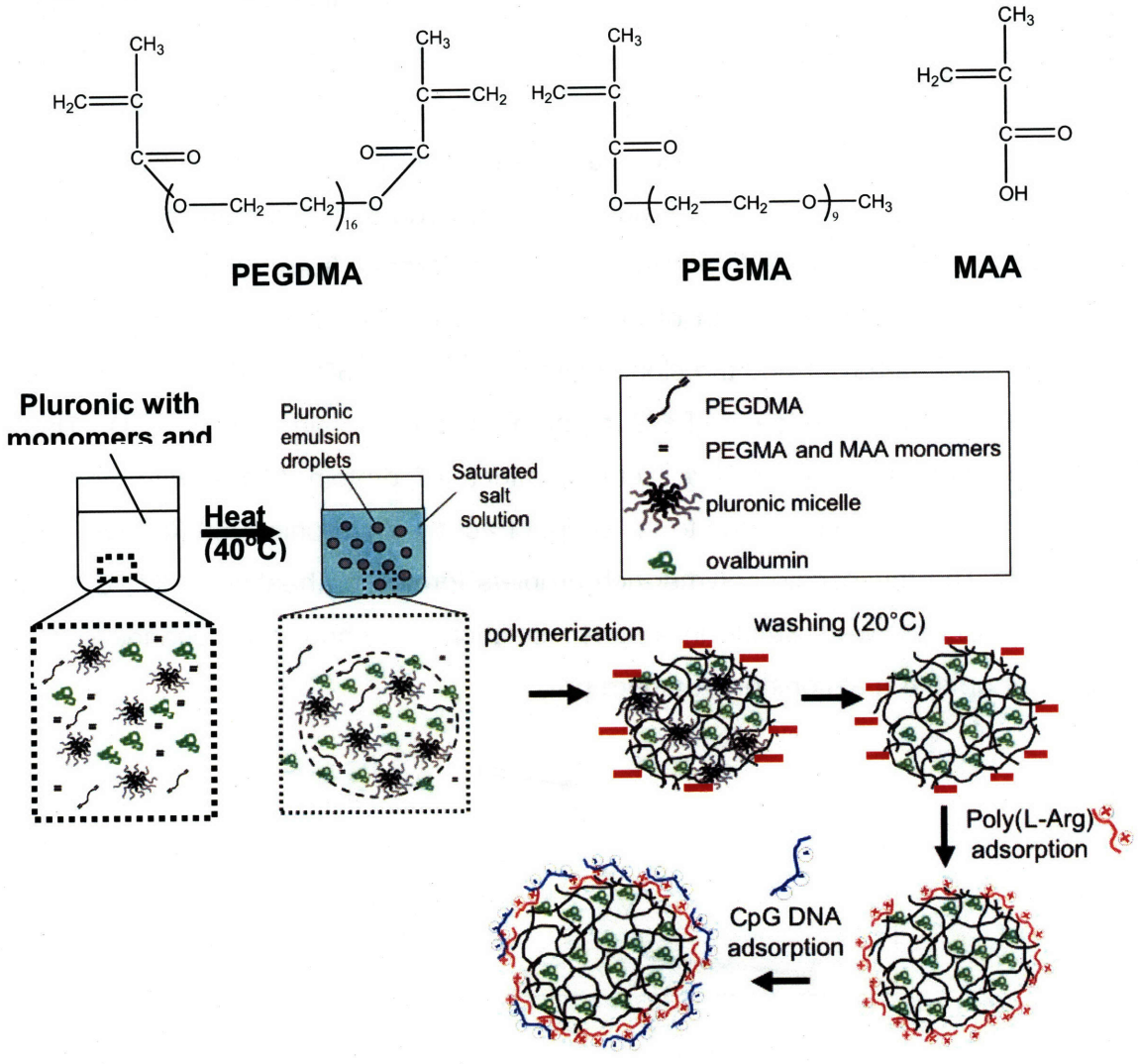

Figure 3.2. Schematic diagram of monomer chemical structures, hydrogel particle synthesis, and functionalization with CpG oligonucleotides.

To characterize the steps in this synthesis, dynamic light scattering was used to monitor the state of the emulsion at each step before and after polymerization (Figure 3.3). The pluronic (0.04 g/mL) in pure water at 25°C is well below its Critical Micelle Temperature (CMT) (~37°C); F-68 unimers had a measured hydrodynamic diameter of 4.5 nm, in agreement with previously reported values. Addition of 5.5M sodium chloride induced the formation of micelles at 25°C (measured diameters ~23nm). The size of these aggregates is somewhat larger than that reported for F-68 micelles formed in pure water at temperatures above the CMT (13-15.6 nm); this discrepancy in the size of aggregates formed by temperature- vs. salt-driven assembly has also been observed for F-68 in potassium fluoride aqueous solutions [179]. Addition of protein to the pluronic/salt solution at 25°C did not cause a statistically significant change in the aggregate size detected by DLS. Addition of the hydrogel precursor monomers to the pluronic/salt/protein solution caused a further increase in the size of the (still unimodal) aggregate population to ~33 nm. Upon heating of the solution containing pluronic, protein, and monomer to 40°C, the pluronic phase separated as in the absence of protein and monomer, forming an emulsion with relatively monodisperse droplets 440 nm in diameter (Figures 3.1 and 3.3A), the same size as droplets formed by pluronic alone in salt solution. The pluronic-dominated phase behavior of the system is consistent with the lower relative concentrations of protein and monomers present (4% w/v pluronic versus 0.1% w/v ovalbumin and 0.66% w/v monomers). The particles formed after polymerization had diameters by DLS slightly larger than the size of the emulsion droplets detected prior to initiation (490 ± 30 nm after polymerization, Figure). The uniform submicron size of the particles formed was also confirmed by direct observation of rhodamine-labeled particles by fluorescence microscopy (data not shown and Figure 3.7 discussed below).

A.

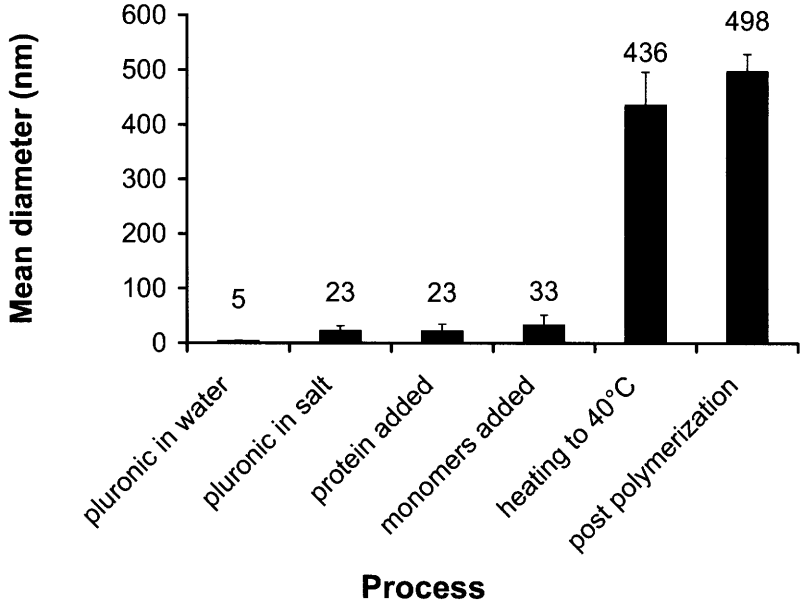

B.

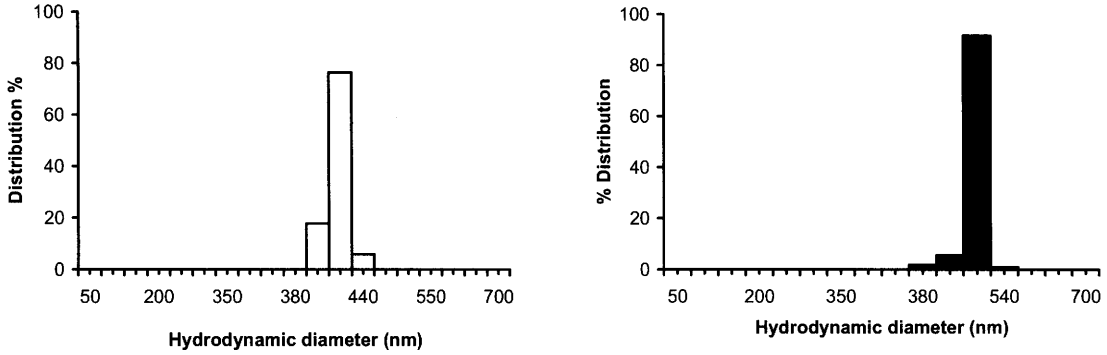

Figure 3.3. (A) Mean diameter of pluronic aggregates/ emulsion droplets at each stage of particle synthesis obtained by DLS. (B) Size distribution of emulsion droplets at 40 °C (□) and hydrogel particles post-polymerization (■) as measured by DLS.

Notably, no particles were recovered if salt, initiator, or gel precursor monomers were excluded from the synthesis. Exclusion of protein from the synthesis resulted in a significantly reduced yield of particles that were difficult to pellet. Typically ~50 mg of

particles (dry mass) were obtained from the synthesis, comprised of ~37.5 mg ova (discussed below) and 12.5 mg polymer, a yield of 75% protein encapsulated and 4% of the monomers incorporated into the particles. Measurement of the 'wet' mass of the as-synthesized particles by blotting on a filtration membrane followed by drying to constant mass revealed a water content of 74±14 wt% in the hydrogels. The density of polymerized particles formed during the synthesis, based on the measured particle size and mass of the hydrated particles, was 6.24×10^{10}/mL, in good agreement with the average density of particles directly measured by flow cytometry (5.35×10^{10}/mL). The stability of the mesoscale pluronic emulsion droplets and relatively close correspondence between the pre-polymerization emulsion droplet size and the diameter of the resulting gel particles is consistent with a miniemulsion mechanism of polymerization in this system, where individual emulsion droplets template the final gel particles formed.

Based on the measurements above, the total polymer concentration within the gel particles is approximately 65 mg/mL. Because the pluronic exists in the unimer state below 36°C in pure water at concentrations below 0.05 g/mL, we believe that any pluronic in the particles should be largely removed during washing of the gels into water at 25°C post-synthesis, due to its small molecular size (Scheme). Assuming the polymer measured in the dried particles is comprised solely of crosslinked poly(PEGMA-co-MAA) chains formed during polymerization, the mesh size of the network making up the gel particles, ξ, can be calculated using the theory of Canal and Peppas [180]:

$$\xi = C_n^{1/2} Q^{1/3} N^{1/2} l \qquad [12]$$

where, ξ is the mesh size of the polymer network, C_n is the characteristic ratio of the polymer, Q is the degree of swelling = $V_{swollen}/V_{dry}$, N is the degree of polymerization between crosslinks, and *l* is the bond length in the polymer backbone. Using these values, ξ is determined to be 6.04 nm, which should facilitate retention of the encapsulated ova protein, which has a hydrodynamic diameter of 6.1 nm.

Table 3.1. Ovalbumin-loaded hydrogel particle characteristics as a function of Pluronic F-68 concentration in synthesis.

Pluronic™ F-68 content (w/v)	1%	2%	4%	6%	8%
Particle size	Flocs >10 μm	Flocs >10 μm	488 ± 30 nm	520 ± 20 nm	504 ± 20 nm
Encapsulation Efficiency	83%	85%	73%	52%	34%
Protein content (mg protein/mg dry particles)	0.735	0.739	0.735	0.634	0.523

High protein encapsulation efficiency and protein loading in particle-based vaccines are desirable to maximize immune responses. In the present system, we found that the concentration of pluronic was a key parameter controlling the formation of particles, the protein encapsulation efficiency, and net protein loading per particle, as shown in Table 3.1. Macroscopic aggregates formed if the pluronic content was reduced from 4% (wt/vol) to 2% or lower. For pluronic concentrations ranging from 4% to 8%, mesoscale particles were obtained with a mean particle diameter of ~500 nm. However, as the pluronic content increased, both the net amount of protein encapsulated per particle and the protein encapsulation efficiency decreased significantly. Maximal protein encapsulation (0.74 mg protein/mg dry particles) and encapsulation efficiency (73%) were achieved at an intermediate pluronic concentration of 4%. These high values are a notable strength of this aqueous encapsulation strategy. This technique also appears to have at least moderate generality as the same procedure also allowed the successful encapsulation of bovine albumin and human serum albumin, in addition to ovalbumin (data not shown).

3.3.2 Functionalization of hydrogel particles with CpG oligonucleotide

To provide activation signals to dendritic cells and B cells for a productive immune response, short single-stranded CpG oligonucleotides, ligands for Toll-like receptor 9 (TLR9) known to promote robust DC and B cell activation, were bound to the surface of particles by a two-step electrostatic self-assembly process (Figure 3.2). First, poly(L-arginine) was adsorbed to the anionic (methacrylic acid)-containing hydrogel

particles to obtain a positively charged particle surface, followed by electrostatic adsorption of the negatively-charged CpG oligonucleotides. The amount of CpG adsorbed depended strongly on the zeta potential of the particles and thus on the poly(L-arginine) concentration used in the first adsorption step (Table 3.2). As the concentration of poly(L-arginine) was increased from 0.5 mg/mL to 5 mg/mL, the CpG adsorption efficiency in the second step increased from 30% to ~100% (Table 3.2) in parallel with the steadily increasing zeta potential of the poly(L-arginine)-coated particles.

We initially sought to synthesize cationic hydrogel particles directly by encapsulating protein in gel networks containing the monomer 2-aminoethyl methacrylate instead of methacrylic acid, but these particles, which presumably contained their positive charges distributed throughout the particle volume instead of concentrated at the surface, had a lower zeta potential (+1.05 mV) and bound CpG inefficiently (~20% of CpG adsorbed). Adsorbed oligonucleotides were well retained on the surface of polyarginine-coated particles; functionalized particles were observed to release only ~10% of the adsorbed CpG oligos after incubation in PBS at 37°C for one week (Figure 3.4), and less than 10% of the initially bound CpG desorbed from particles stored three weeks at 4°C in PBS. This simple electrostatic functionalization approach should also be applicable to a variety of other DC-stimulating ligands, including anionic single- and double-stranded RNAs (ligands for Toll-like receptors 3, 7, and 8).

Table 3.2. Zeta potential and CpG conjugation efficiency for hydrogel particles coated with poly(L-arginine).

Poly-L-arginine concentration in first adsorption step (mg mL^{-1})	Zeta Potential of poly(L-arginine)-coated particles (mV)*	CpG conjugation efficiency in second adsorption step (%)†
0.5	-14.77	30
1.0	-14.47	50
2.0	-1.45	88
5.0	+5.13	98

*Uncoated particles = -16.40mV.
† 100 % CpG conjugation efficiency = 10 nmol CpG ODN/mg dried hydrogel particles

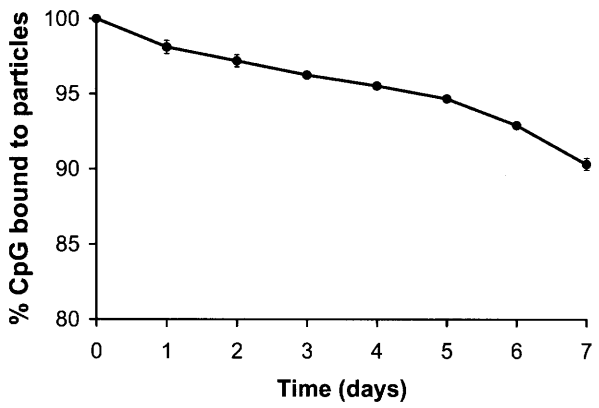

Figure 3.4. Kinetics of CpG oligonucleotide desorption from the surface of functionalized hydrogel particles when incubated in PBS at 37 °C.

To determine whether there was an optimal density of CpG per particle for DC stimulation, dendritic cells were first incubated with particles functionalized with different quantities of CpG; the total amount of particles added to the cells was varied so that in each case a fixed total amount of CpG (1 nmole/ 10^6 cells/ mL) was added to each culture. As shown in Figure 3.5A, significant IL-12p40 secretion was observed even at the lowest density of CpG/particle tested ($3.4x10^5$ oligos per particle). IL-12 production was increased when fewer nanoparticles bearing more CpG/particle were added to DCs. (Note that even at the highest CpG-per-particle density the particles were in significant excess over the number of DCs (particle:DC ratio ~540:1)). When DCs were instead incubated with a fixed number of particles (particle:DC ratio 540:1) coated with different quantities of CpG (Figure 3.5B), a dose-dependent response was observed with an onset of IL-12 production triggered by ~$5.5x10^5$ oligos/particle. Based on these results, for subsequent studies we fixed the CpG density at ~10^6 oligos per particle, the highest density tested, which gave maximal IL-12 secretion from DCs among the conditions tested.

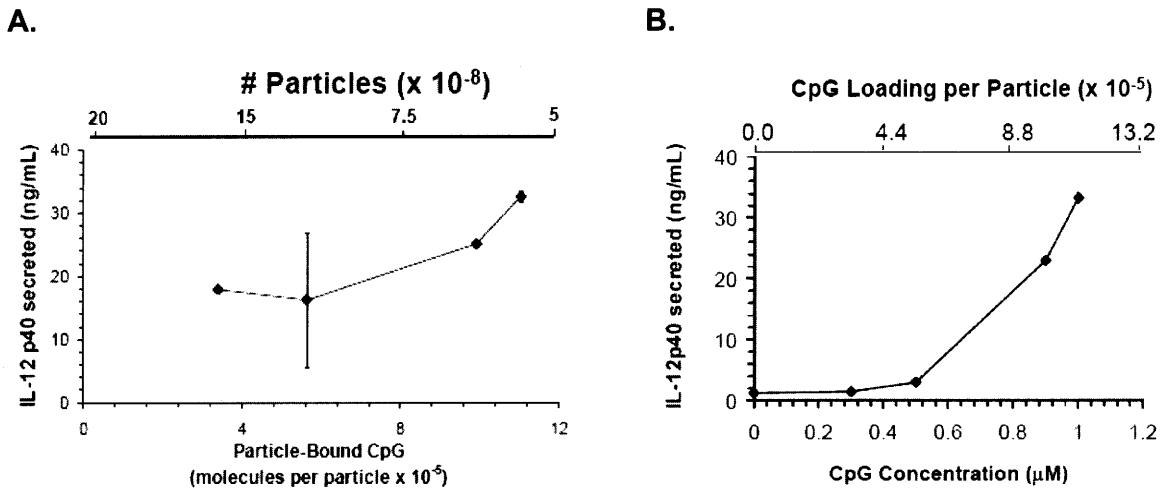

Figure 3.5. (A) IL-12p40 secretion at 1 μM hydrogel particle-bound CpG concentration after 48 hours of incubation of bone marrow dendritic cells with hydrogel particles adsorbed with different concentrations of poly-L-arginine as a function of CpG loading per particle; (B) IL-12p40 secretion by dendritic cells when incubated with same number of hydrogel particles but with different CpG loadings per particle.

3.3.3 Encapsulated antigen release by protease digestion of hydrogel particles

We hypothesized that by encapsulating protein in a hydrogel network, DC proteolytic enzymes with sizes smaller than the mesh size of the gel particle network might directly diffuse into the network and cleave entrapped protein antigen; the resulting low molar mass peptides would readily diffuse back out of the gel particle, to be processed by the native antigen presentation machinery of the dendritic cell. To test of this hypothesis, we determined the effect of incubating ova-loaded gel particles with a phagolysosomal protease *in vitro*. The enzyme tested, cathepsin D (catD), is a ubiquitous protease involved in antigen processing in the endosomes/phagosomes of antigen presenting cells, which is known to digest ova. Though catD is one of the larger known phagosomal proteases, it has a reported end-to-end distance (~4.5nm) smaller than the estimated size of the particle network mesh size, and also eluted later than ovalbumin in size exclusion chromatography experiments (discussed below). CpG-

modified, ovalbumin-loaded hydrogel particles were incubated at a phagosomal pH of 5.5 with catD for 48 hrs, and the supernatant from this co-incubation was then analyzed for the presence of protein/peptide fragments by size exclusion chromatography. The resulting chromatogram (Figure 3.6A) showed the production of fragments ranging in approximate molecular size from 2-30 KDa, and was comparable to that observed for soluble ovalbumin digestion by catD (Figure 3.6B) as well as previously reported gel electrophoresis data on catD proteolysis of ova. The supernatant from particle digestion was clearly demarcated from controls containing catD alone (Figure 3.6C) or undigested ova (not shown), and no peptide fragments were detected in the supernatant of ovalbumin particles incubated in the absence of the catD enzyme. In the absence of specific protease treatment, ova was stably encapsulated; < 5% of the encapsulated protein was released after incubation of gel particles in serum-containing medium at 37°C for one week. Thus, protein antigens encapsulated in the gel particles are stable in the presence of serum, but can be degraded by acid proteases normally present in the phagolysosomal compartments of dendritic cells.

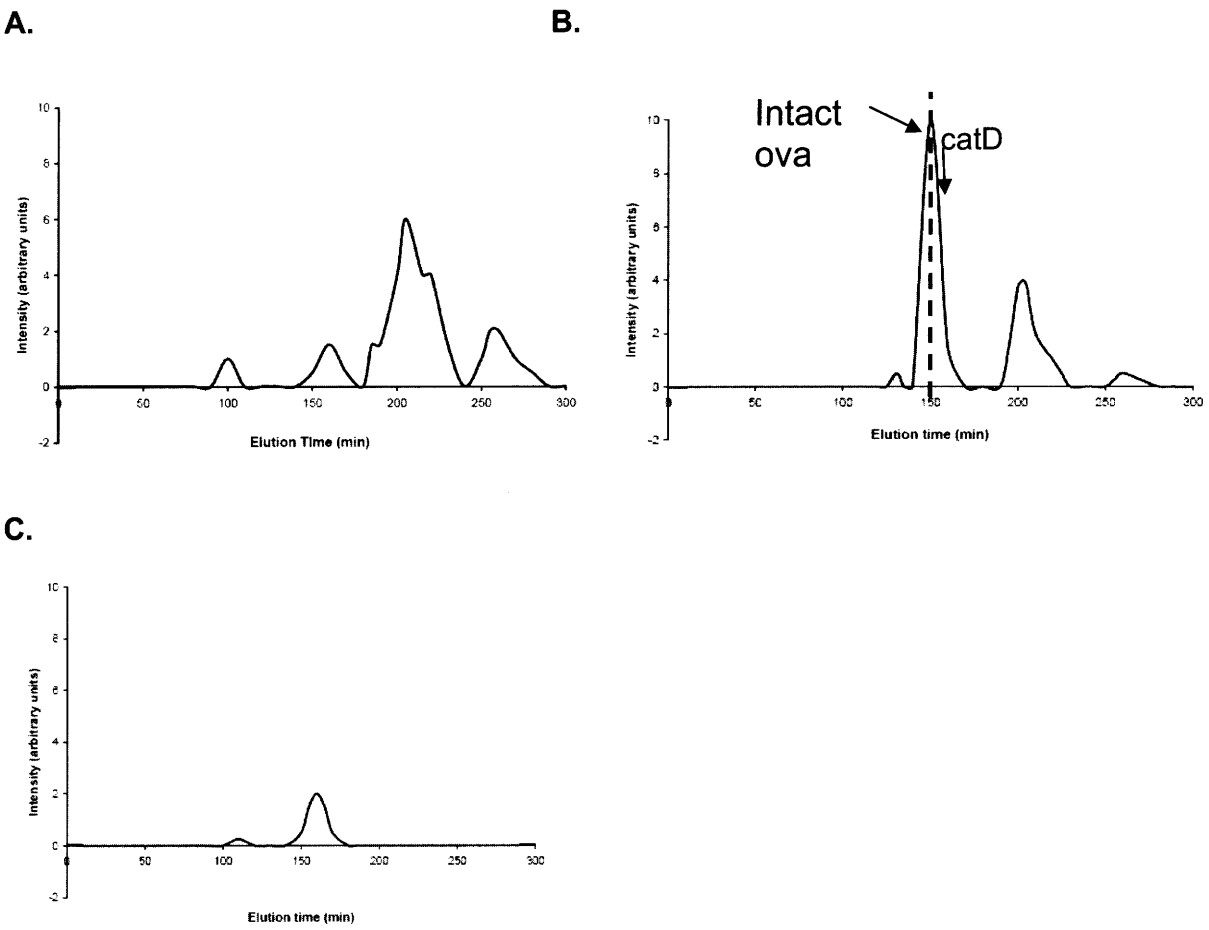

Figure 3.6. Size-exclusion chromatograms of supernatants collected after 48 h co-incubation of mixtures of 200 μg/mL cathepsin Dwith (A) 5 mg/mL CpG-modified ova hydrogel particles, (B) 5 mg/mL soluble ova, or (C) catD alone. Arrows mark the elution times for intact soluble ova and catD.

3.3.4 Accessibility of native protein epitopes at the surface of hydrogel particles

We hypothesized that the entrapment of protein antigens at or near the surface of gel particles during synthesis might permit direct binding of antibodies to exposed antigen epitopes. To examine this possibility, CpG-modified, ova-loaded gel particles were stained with mouse anti-ovalbumin monoclonal antibodies and imaged by fluorescence microscopy (Figure 3.7). The hydrodynamic diameter for these IgG molecules measured by DLS was 11.9 nm, significantly larger than the calculated mesh size of the gel particle network; we thus expected that antibody binding would reflect

ova epitopes available primarily at or near the surface of the gel particles. The clear specific staining of the gel particles by anti-ova antibody implies that the encapsulated protein is in a native state and is accessible from the particle surface. Surprisingly, similar intensities of specific antibody staining were observed for gel particles that had not been coated with polyarginine and CpG oligos (not shown), suggesting that the thin polyelectrolyte bilayer formed during the gel particle surface modification does not significantly obscure access to protein near the particle surface. In line with this *in vitro* result demonstrating accessibility of encapsulated antigen to antibody binding, we found that immunization of mice subcutaneously with hydrogel particles primed >100-fold greater anti-ova IgG antibody titers *in vivo* compared to soluble ova immunization as discussed in Section 3.3.8.2.

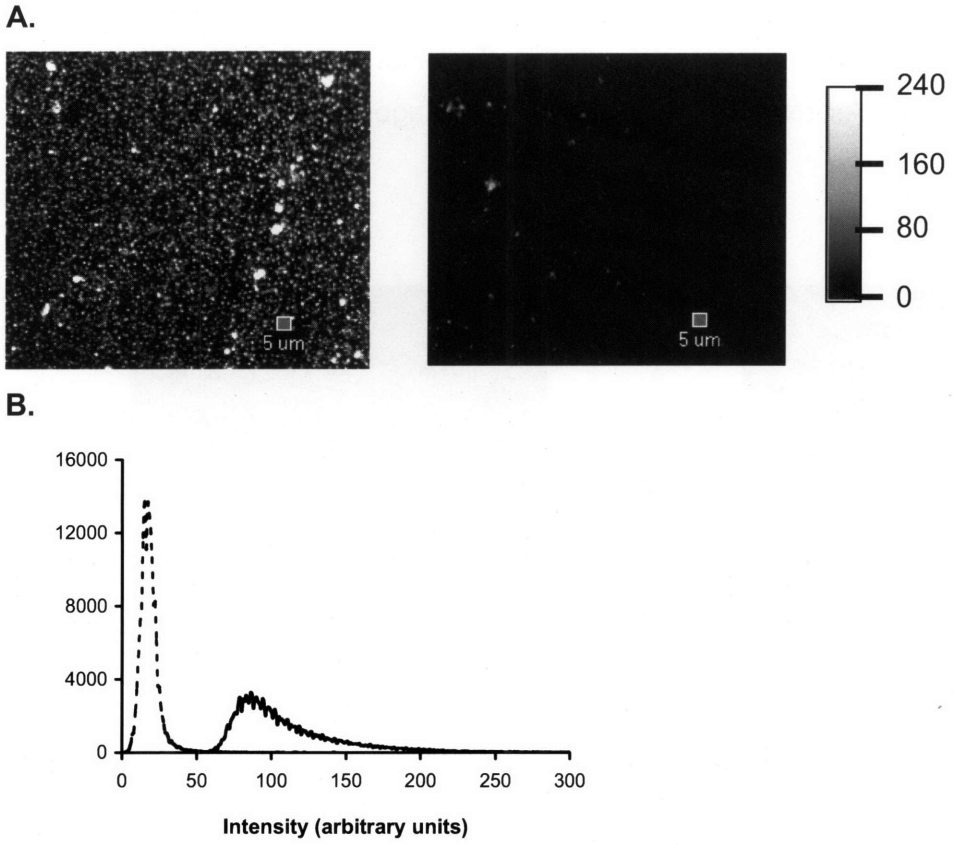

Figure 3.7. (A) Fluorescence images of ova-containing hydrogel particles stained with either anti-ova (left) or isotype control (right) primary antibody followed In both cases by Alexa fluor 488-conjugated IgG secondary antibody. (B) Histogram of fluorescence intensities from anti-ova-labeled particles (solid line) and isotype control-stained particles (dashed line).

3.3.5 Hydrogel particle uptake and cross-presentation of antigen by dendritic cells

3.3.5.1 Fluorescence imaging of hydrogel particle uptake by BMDCs

Professional antigen presenting cells such as dendritic cells are highly efficient phagocytes, and rapidly internalize submicron-sized biological or synthetic particles. To assess the uptake of ova-loaded gel particles by dendritic cells, murine bone marrow-derived DCs were incubated with fluorescent DQ-ovalbumin-loaded hydrogel particles (50 μg/mL ovalbumin) for 1 hour, washed to remove unbound particles, and then

imaged by fluorescence microscopy. Trypan blue (0.4% w/v) [10] was added to the medium to quench extracellular fluorescence and confirm that visualized particles were internalized by the cells. As expected, DCs efficiently phagocytosed the gel particles (Figure 3.8).

A. **B.**

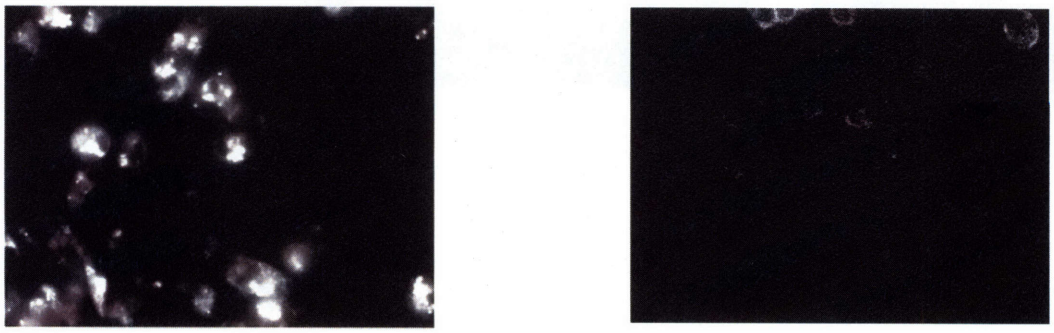

Figure 3.8. Hydrogel particle uptake by dendritic cells. Dendritic cells were incubated with DQ-ovalbumin-containing particles (A) or control medium (B) for 1 h. Extracellular and membrane-bound fluorescence was quenched with trypan blue, and cells were then imaged by fluorescence microscopy.

3.3.5.2 Toxicity of hydrogel particles in dendritic cell culture

Nontoxicity of vaccine carriers and adjuvants is required for clinical application, and cytotoxicity is a limitation of several studied vaccine adjuvants despite their ability to effectively activate cells of immune system. To test for potential toxicity associated with internalization of the nanoparticles, DCs were incubated for 24 hours with hydrogel particles followed by staining with propidium iodide to assay cell viability by flow cytometry. As shown in Figure 3.9, the hydrogel particles were non-cytotoxic and cell viability was indistinguishable from control samples. These hydrogel particles were also well-tolerated *in vivo* in mice with no apparent inflammation at sites of injection.

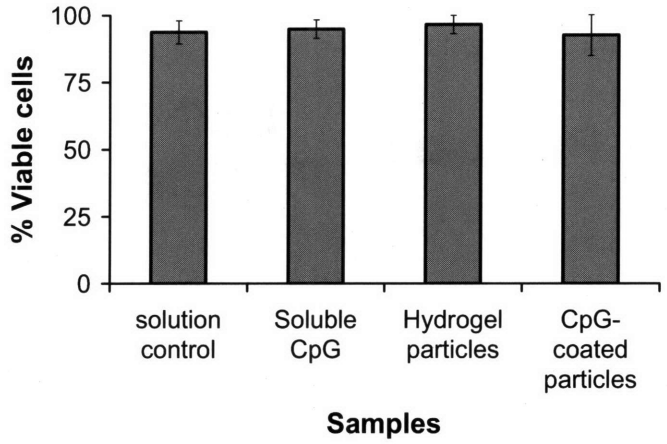

Figure 3.9. Cell viability assessed by propidium iodide when dendritic cells were cultured with hydrogel particles for 24 h.

3.3.5.3 Enhanced antigen uptake by dendritic cells

Dendritic cells are highly phagocytic and have been observed to avidly phagocytose particulate antigen in their environment [115,181-183]. In order to quantify the efficiency of ova-loaded particle uptake by dendritic cells relative to internalization of soluble ova, DCs were incubated with alexa fluor 488-conjugated ova-containing gel particles (50 μg total ovalbumin, 1:50 labeled: unlabeled protein) or 50 μg soluble ova for 1-18 hrs and the amount of internalized protein was analyzed by flow cytometry. Alexa fluor 488, unlike fluorescein, is a relatively pH-insensitive dye and does not undergo quenching in the phagosomal/ lysosomal environment, enabling tracking of antigen into these acidic intracellular compartments [184]. DC internalization of ova-loaded nanoparticles was significant within 1 hr (31% and 38% ova^+ cells after incubation of DCs with nanoparticles or CpG-modified nanoparticles, respectively), whereas almost no soluble antigen was detected in DCs at this time-point (Figure 3.10). After 18 hrs of incubation, ~1.5-fold more DCs were ova^+ when incubated with ova nanoparticles relative to soluble antigen, and the median amount of ova per cell was 2.2-fold higher for DCs incubated with CpG-modified ova particles. CpG-modified particles were internalized slightly more efficiently than unmodified ova particles, suggesting that DNA receptors on the DC surface enhanced their binding/internalization.

This result is in agreement with prior studies that have shown enhanced uptake of soluble ova when the protein is conjugated to CpG oligos [152].

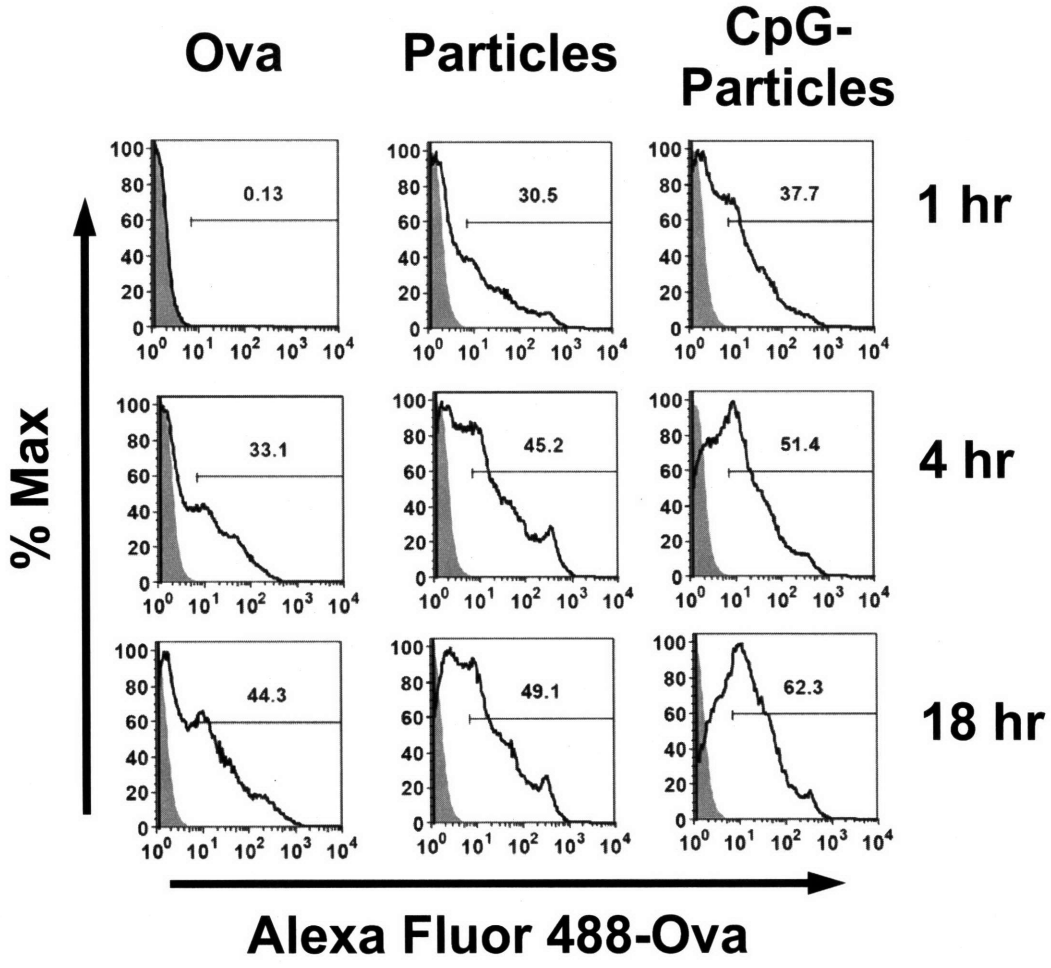

Figure 3.10. Antigen delivery to dendritic cells by soluble protein, hydrogel particles, and CpG-coated hydrogel particles after 1, 4, and 18 hours of incubation. Grey histograms represent unmanipulated cells and solid lines represent corresponding samples.

3.3.5.4 Cross-presentation of antigen by dendritic cells

Once internalized, protein antigen must be processed into peptides and loaded onto class I and class II MHC molecules for presentation to T cells. Exogenous antigens taken up by antigen presenting cells are normally processed and presented only by

class II MHC molecules. However, dendritic cells and macrophages are capable of loading peptides derived from exogenous antigens onto class I MHC molecules for presentation to $CD8^+$ T cells via a set of processes collectively termed cross-presentation [11,132], and particulate systems for delivery of protein antigen have been found to strongly promote cross-presentation [10,132,185]. To determine whether hydrogel nanoparticle delivery of ova promoted cross-presentation of ova peptides, we analyzed the expression of ova peptide-MHC class I complexes generated by DCs incubated with ova protein or ova nanoparticles for 18 hrs. The monoclonal antibody 25-D1.16, which recognizes the ova-derived peptide SIINFEKL bound to H-$2K^b$ class I MHC molecules, was used to detect ova peptide-MHC I complexes on the surface of DCs by flow cytometry [178,186,187]. The frequency of ova peptide-MHC I^+ cells was 5.3-fold greater for DCs incubated with nanoparticles compared to soluble ova, and the mean expression level of K^b-SIINFEKL complexes was 4.4-fold higher for DCs incubated with ova particles (whether CpG-modified or not) relative to DCs incubated with soluble ovalbumin (Figure 3.11A and B). The presence of CpG on the surface of hydrogel particles did not enhance the expression of peptide-MHC complexes, indicating that particulate delivery of the antigen alone induced significant cross-presentation of antigen, without the additional cross-presentation signals provided by CpG [178,186-191]. Thus, the hydrogel particles not only deliver antigen efficiently to dendritic cells but trigger cross-presentation, enabling enhanced presentation of peptide to naïve $CD8^+$ T cells compared to soluble antigen.

A.

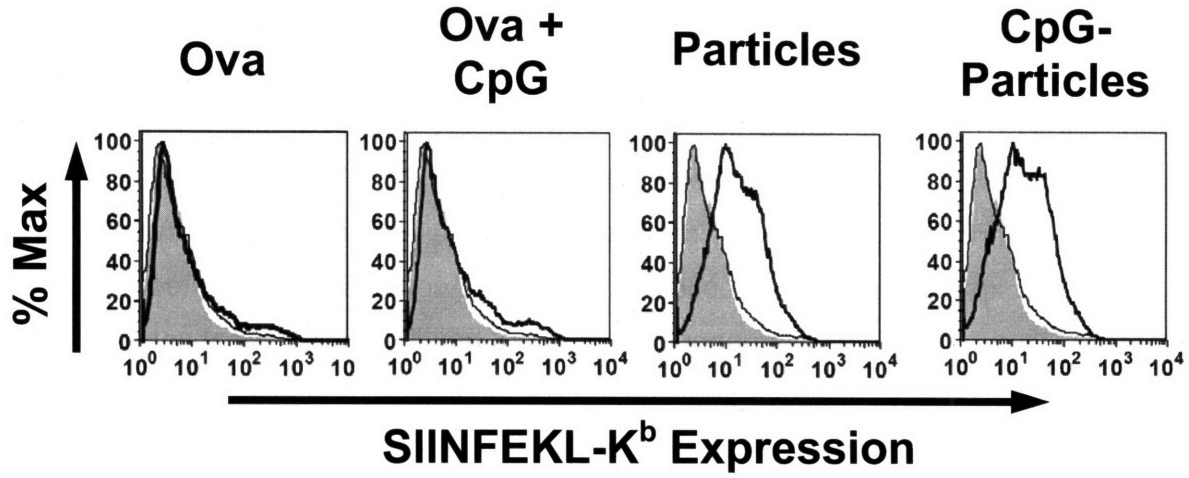

B.

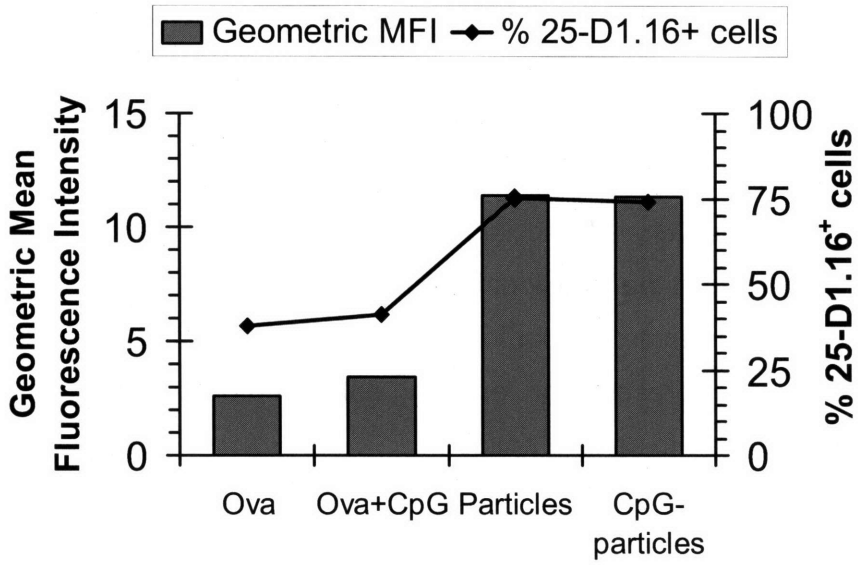

Figure 3.11. (A) Expression of SIINFEKL-K^b on the surface of dendritic cells based on staining with 25-D1.16 antibody after incubating dendritic cells with antigen for 18 hours. Solid histogram represents isotype control staining, dotted line is solution control, and solid lines are samples; (B) Shown are the mean fluorescence intensity (MFI) values obtained for SIINFEKL-K^b staining on dendritic cells and % cells with peptide-MHC I complex expression above isotype control.

3.3.6 Dendritic cell maturation by CpG-coated hydrogel particles

3.3.6.1 Upregulation of costimulatory molecules on dendritic cell surface

CpG oligonucleotides bound to the surface of protein-loaded nanoparticles are expected to drive maturation and activation of dendritic cells that internalize the particles via signaling through Toll-like receptor-9 [192,193]. Maturation of dendritic cells incubated with soluble CpG oligonucleotides or CpG-coated particles was quantified by analyzing the surface expression of MHC II and costimulatory receptors on DCs incubated for 24 hrs with 1 μM soluble CpG or an equivalent concentration of CpG coated on hydrogel nanoparticles. After incubation, DCs were stained for MHC class II, CD40, CD80, and CD86 and analyzed by flow cytometry; DCs left untreated or treated with 1 μg/mL LPS were also analyzed for comparison. Interestingly, although CpG coating was required for the nanoparticles to trigger cytokine secretion by DCs, both CpG-coated and uncoated particles induced upregulation of all 4 cell surface markers on DCs relative to untreated cells (Figure 3.12). However, upregulation of MHC II and CD40 on DCs with uncoated particles was less pronounced than with CpG-coated particles (Figure 3.12A). CpG-functionalized nanoparticles triggered stronger upregulation of the costimulatory ligand CD86 than soluble CpG (Figure 3.12B), while soluble CpG triggered slightly greater CD40 upregulation than CpG-particles (Figure 3.12A).

A.

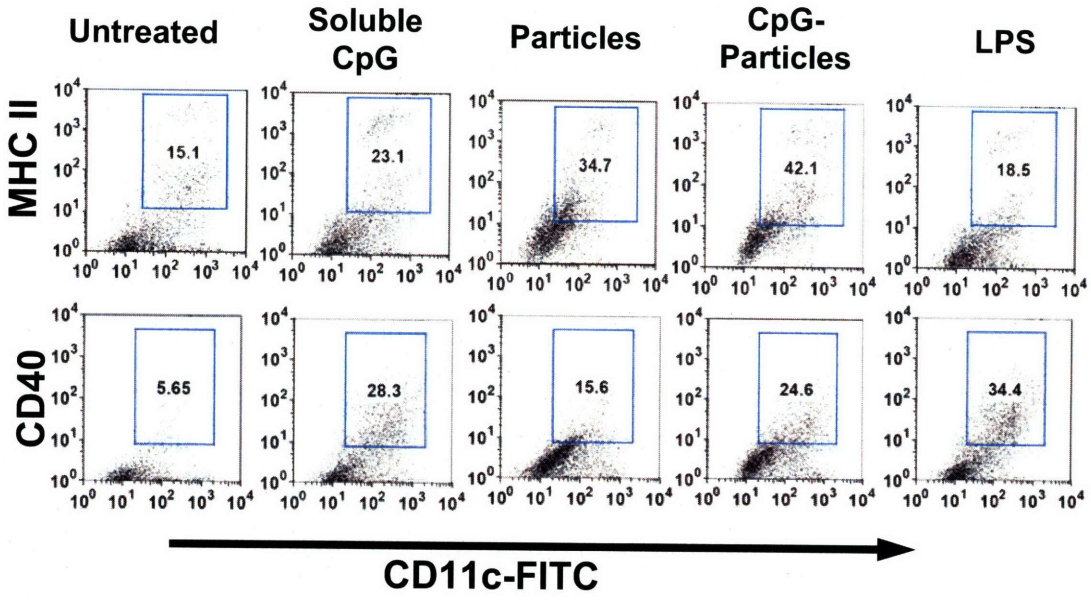

B.

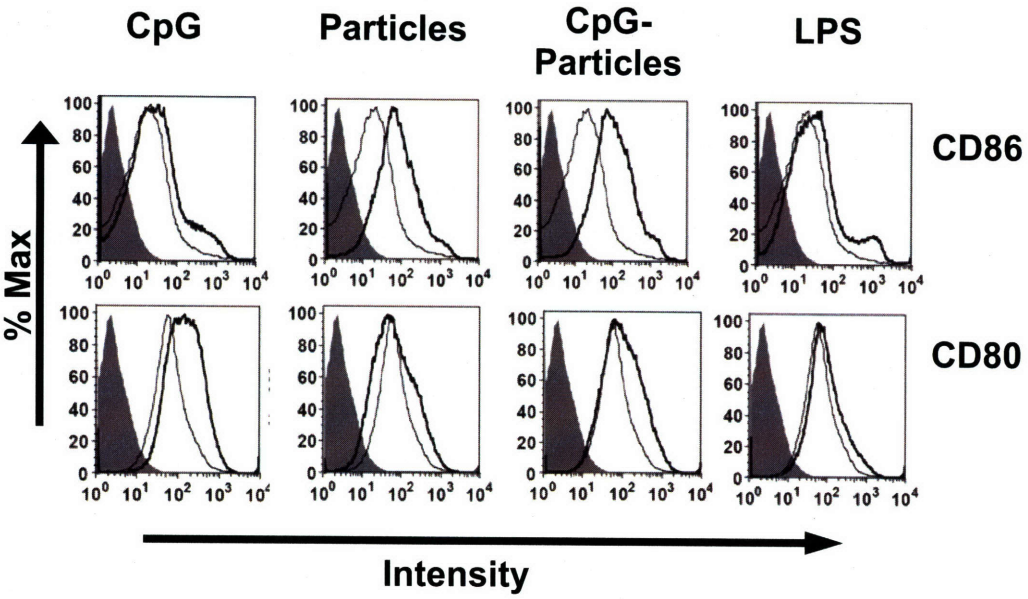

Figure 3.12. Surface phenotype of dendritic cells incubated with different agents for 24 hours followed by staining with specific antibodies. (A) Expression of IA^b and CD40 versus CD11c on bone marrow dendritic cells. The numbers in marked regions represent fraction of maximally matured dendritic cells; (B) Grey histograms represent corresponding isotype controls, dotted lines represent solution control, and solid lines represent samples.

3.3.6.2 Secretion of inflammatory cytokines by dendritic cells

Activated dendritic cells secrete a battery of pro-inflammatory cytokines such as IL-12, IL-6, and TNF-α. We thus examined the secretion of inflammatory cytokines by DCs incubated with CpG-modified nanoparticles, compared to the cytokine production elicited by culturing DCs in the presence of equivalent amounts of soluble CpG or with particles lacking CpG. Uncoated ova particles triggered low/neglible levels of IL-12p40, IL-12p70, IL-6, and TNF-α [194,195] (Figure 3.13A-D). In contrast, DCs incubated with CpG-coated hydrogel particles secreted high levels of these inflammatory cytokines, and in comparison to soluble oligonucleotides, the onset of cytokine secretion was triggered by ~10-fold lower total CpG doses using CpG-coated nanoparticles. By contrast, IL-10 secretion (Figure 3.13E) was low in response to both soluble CpG and CpG-coated hydrogel particles treatment.

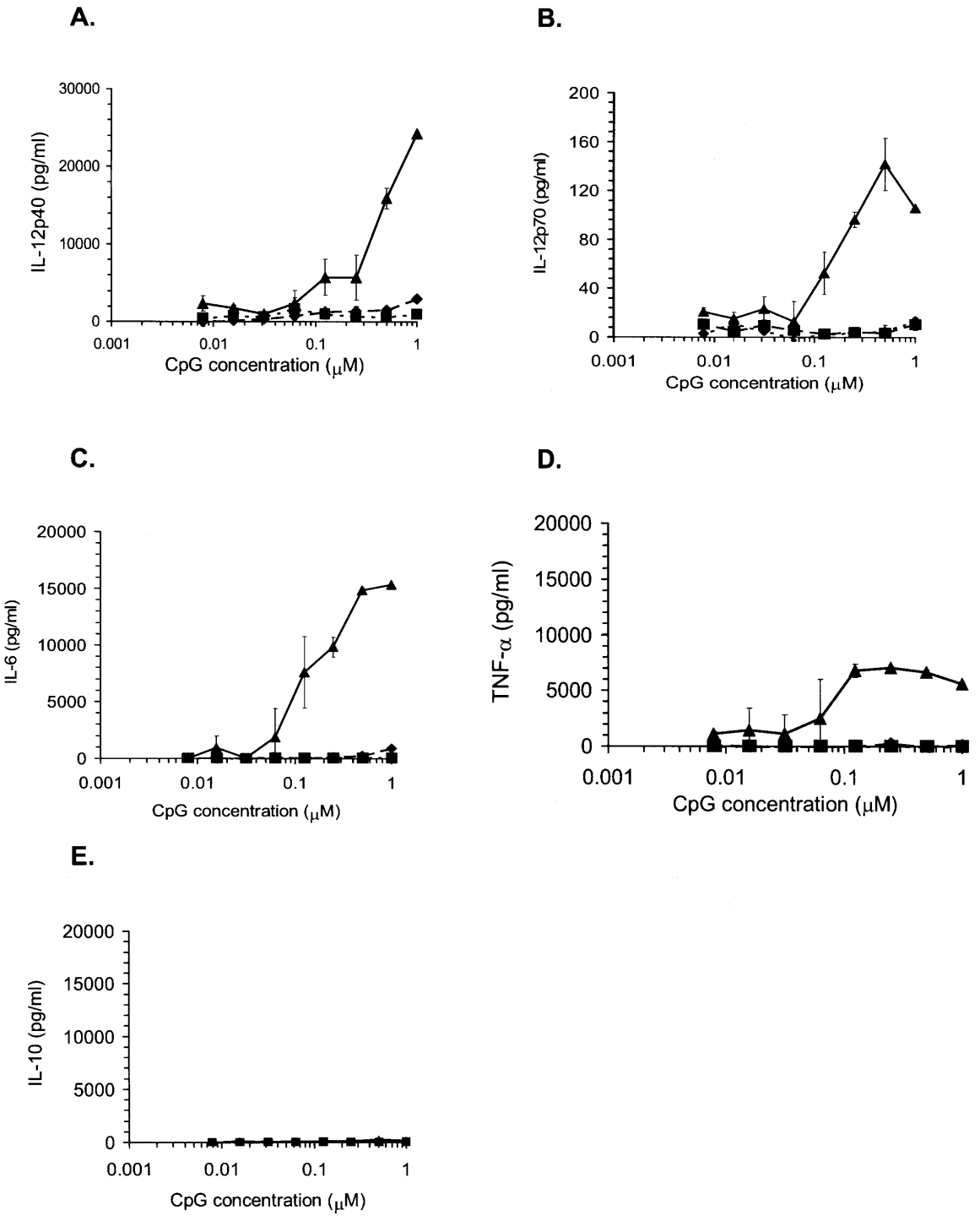

Figure 3.13. Secretion of various cytokines – (A) IL-12p40; (B) IL-12p70; (C) IL-6; (D) TNF-α; and (E) IL-10 – by dendritic cells when incubated with soluble CpG (♦), unmodified particles (■), and CpG-coated particles (▲).

3.3.7 *In vitro* T cell activation by activated dendritic cells

3.3.7.1 *In vitro* activation of primed T cells

In order to study the effect of efficient antigen delivery to dendritic cells on T cell activation, antigen-incubated dendritic cells were co-cultured with ova-specific $CD8^+$ (OT-I) or $CD4^+$ (OT-II) T cell blasts for 48 h followed by measurement of IL-2 secretion by activated T cells. As shown in Figure 3.14, both CD4+ and CD8+ T cells secreted significantly higher levels of cytokine and the onset of cytokine secretion occurred at lower antigen concentration when antigen was delivered as hydrogel particles than when delivered as soluble antigen. In addition, no cytokine secretion was observed with BSA-containing hydrogel particles suggesting that T cell activation is antigen-specific and cytokine secretion is not a result of phagocytosis of particulate matter.

A. **B.**

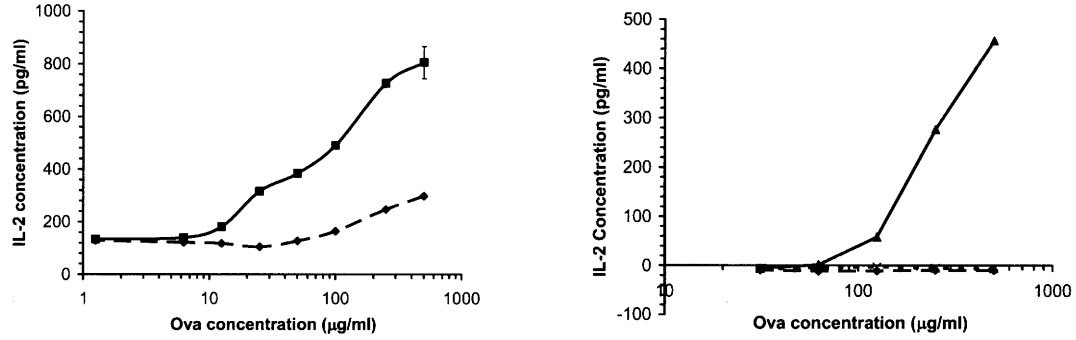

Figure 3.14. IL-2 secretion by primed T cells when incubated for 48 h with bone marrow dendritic cells and unmodified ova-loaded hydrogel particles (■) or soluble ovalbumin (♦) (A) $CD4^+$ T cells (B) $CD8^+$ T cells. CD8+ T cell blasts activation was also studied with BSA-loaded hydrogel particles (x).

3.3.7.2 *In vitro* activation of naïve T cells

Dendritic cells that internalize particulate antigen proteolyze engulfed protein into short peptide fragments, which are intracellularly loaded onto Major Histocompatibility Complex (MHC) molecules and trafficked to the cell surface for presentation to T cells.

T cells expressing the cognate receptor for antigen presented by DCs secrete a battery of cytokines and proliferate after prolonged contact with the antigen-loaded dendritic cell. To measure the efficacy of the endpoint of particle-based antigen delivery to dendritic cells- presentation of antigenic peptides to T cells- we measured the production of IL-2 (a critical cytokine for T cell proliferation produced in an autocrine manner by activated T cells) by T cells incubated with gel particle-pulsed or control dendritic cells. For these experiments, DCs were 'pulsed' for 4 hrs by incubation with different doses of ova protein (mixed with soluble CpG to drive DC activation) or CpG-modified ova gel particles. The cells were washed to remove uninternalized protein/particles and then co-cultured with naïve $CD8^+$ or $CD4^+$ ova-specific T cells for 72 hrs. Finally, IL-2 present in the supernatant was measured by ELISA to quantify T cell activation. $CD8^+$ ova-specific T cells incubated with soluble ova-pulsed DCs secreted IL-2 only in response to high soluble ova pulse concentrations, with negligible activation for pulse concentrations less than 50 μg/mL. However, when ovalbumin was delivered in gel particles, T cells were activated at ~10-fold lower doses of antigen (Figure 3.15A). This is likely due to the enhanced internalization of antigen in a particulate form relative to soluble protein, as well as CpG-enhanced uptake of ova-loaded particles via DC cell surface DNA receptors. A similar trend was observed for the activation of $CD4^+$ ova-specific T cells (Figure 3.15B); IL-2 production reached higher levels and was induced at ~10-fold lower total ova doses when delivered in the gel particle form. When CFSE-labeled naïve T cells were co-cultured with dendritic cells incubated with hydrogel particles, T cells were observed to proliferate as determined by CFSE-dilution; soluble ova did not induce detectable proliferation of naïve T cells (Figure 3.15C and 3.15D). Altogether, these results indicate that the ova-loaded hydrogel particles efficiently deliver antigen into both the MHC class I and MHC class II antigen presentation pathways, and provide DCs with the ability to activate naïve $CD8^+$ and $CD4^+$ T cells, as required for robust T cell-mediated immune responses *in vivo*.

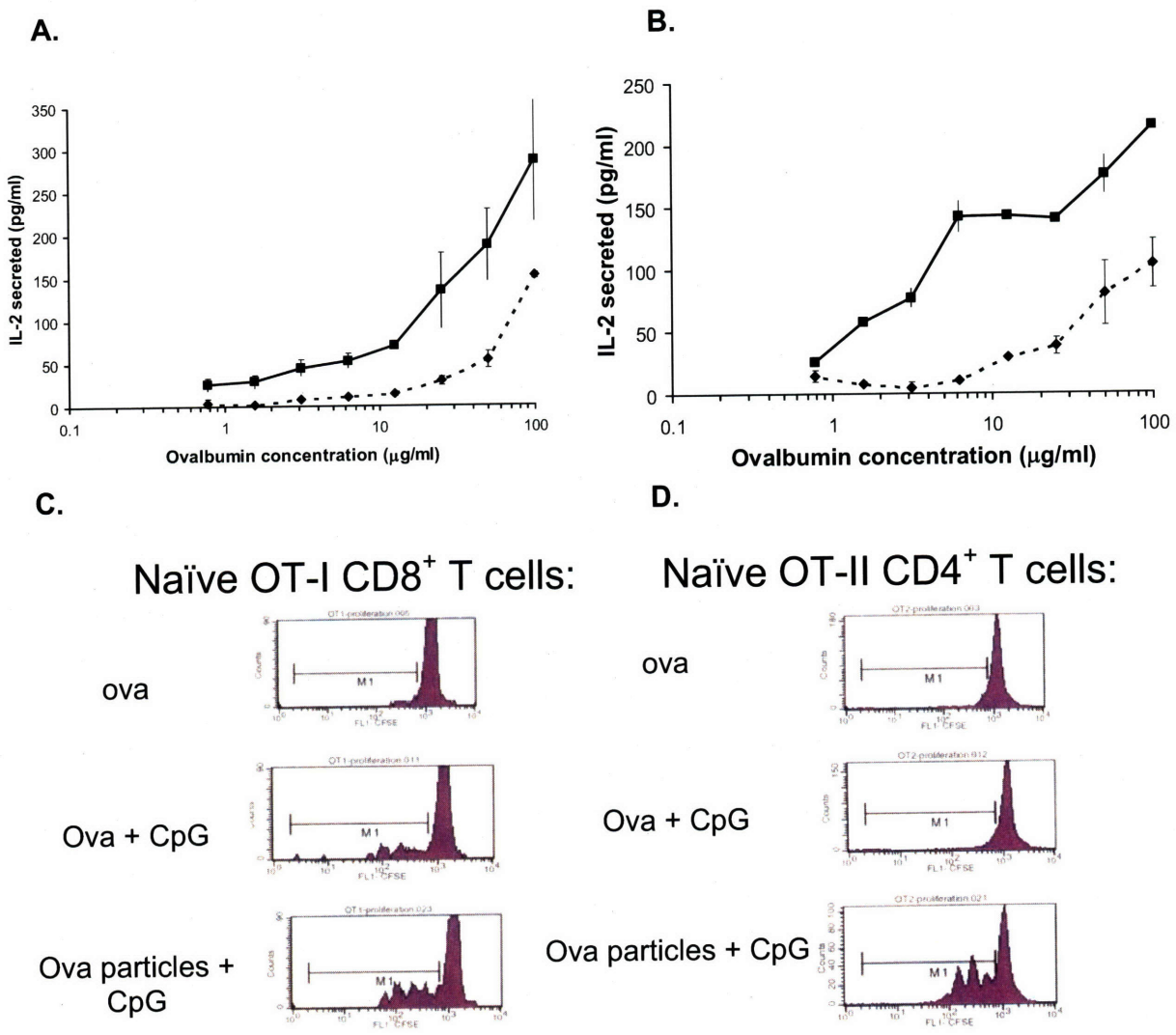

Figure 3.15. Naïve T cell activation by dendritic cells incubated with hydrogel particles. (A,B) IL-2 secretion by activated T cells after 72 h of co-culture with dendritic cells. Solid line represents hydrogel particles and dotted line is soluble ovalbumin. (C,D) Naïve T cell proliferation after 60 h when co-cultured with dendritic cells in presence of antigen in different forms. The CFSE fluorescence intensity of the labeled T cells is halved by each cell division that occurs. (A,C) $CD8^+$ (OT-I) T cells, (B,D) $CD4^+$ (OT-II) T cells.

3.3.8 *In vivo* activation of lymphocytes by hydrogel particles

3.3.8.1 Activation of B cell and generation of anti-ova IgG antibodies in immunized mice

To determine the effect of antigen-loaded hydrogel particles on B cell activation *in vivo*, C57Bl/6 mice were immunized with soluble ovalbumin in the presence or absence of soluble CpG oligonucleotide, ova-loaded hydrogel particles, or CpG-coated hydrogel particles, and anti-ova IgG titers in serum were traced over 7 weeks; mice immunized with PBS or ovalbumin mixed in CFA were used as negative and positive controls, respectively (Figure 3.16). In these experiments, the total quantity of antigen (100 μg) and CpG (8 μg) were fixed for each mode of delivery. Mice immunized with soluble ovalbumin had IgG titers < 100 for the duration of the experiments, and the addition of soluble CpG had no effect on the soluble ova response. By contrast, ova nanoparticles, CpG-modified particles, and ova emulsified in CFA all elicited significant IgG titers by 7 weeks. CpG coating of the nanoparticles significantly enhanced the kinetics of antibody titer development but the final levels of IgG obtained after 7 weeks were not significantly higher for CpG-modified particles ($p = 0.07$). The slightly higher total IgG titers elicited by ova in CFA at 7 weeks relative to CpG-coated hydrogel particles was statistically significant ($p = 0.015$). Antibody titers elicited by CpG-coated particles showed a marginal increase compared to soluble CpG mixed with CpG-free hydrogel particles at 7 weeks but the increase was not statistically significant ($p = 0.42$). Thus, CpG-coated hydrogel particles activate B cells effectively within one week of immunization resulting in high antigen-specific antibodies in the sera of immunized mice and the antibody titers increase rapidly to reach comparable levels as ova in CFA without any apparent toxicity associated with the nanoparticles.

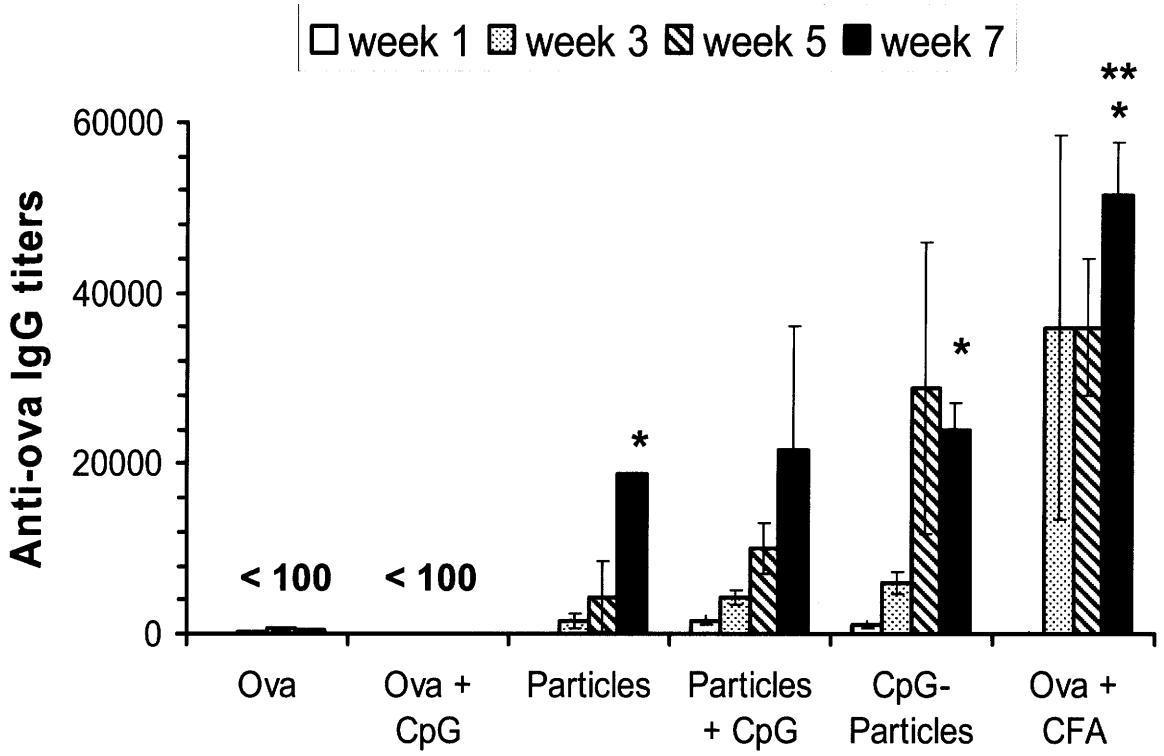

Figure 3.16. Anti-ovalbumin total IgG titers in the serum of C57Bl/6 mice 1, 3, 5, and 7 weeks after s.c. immunization with 100 µg ovalbumin in different forms: soluble ova, soluble ova mixed with 8.5 µg CpG, hydrogel nanoparticles, nanoparticles coated with 8.5 µg CpG, or ova emulsified in CFA. Antibody titers were calculated by endpoint dilution assay. Asterisks denote 7 week data statistically different from ova + soluble CpG ($p < 0.01$); **, statistically different from CpG-particles at 7 weeks ($p < 0.05$). Data shown from one representative of two independent experiments.

3.3.8.2 Immunization with CpG-nanoparticles triggers $CD4^+$ and $CD8^+$ T cell responses comparable to antigen in CFA

Activated dendritic cells loaded with antigen can trigger naïve T cells to proliferate and differentiate into effectors capable of secreting characteristic cytokines such as interferon-γ (IFN-γ) [196,197]. To assess T cell responses, C57Bl/6 mice were immunized with soluble ova, ova nanoparticles, CpG-coated nanoparticles, or ova

emulsified in CFA, as described above for assessing B cell responses. When lymphocytes were isolated from draining lymph nodes and spleens of immunized mice 7 d after a single immunization and restimulated *ex vivo* with MHC class I or class II ova peptides, cells from soluble ova-immunized mice (with or without added soluble CpG) showed no statistically significant IFN-γ secretion compared to cells from sham-immunized mice (Figure 3.17A and B). Splenocytes from mice immunized with ova-loaded hydrogel nanoparticles lacking CpG modification also failed to produce IFN-γ except in $CD8^+$ T cells from the draining lymph nodes. However, when antigen and CpG were co-delivered by hydrogel particles, responding $CD4^+$ (Figure 3.17A) and $CD8^+$ (Figure 3.17B) T cells were detected. In comparison, mice immunized with ovalbumin and CFA showed insignificant T cell responses in the spleen. Thus, CpG-coated nanoparticles were able to induce primary systemic responses from both $CD4^+$ and $CD8^+$ T cells detectable after a single immunization, comparable to or greater than the response elicited by CFA, one of the strongest adjuvants known in mice.

In most vaccine strategies, antigen and immunostimulatory factors are physically mixed and delivered by co-injection. To determine whether delivery of CpG bound to the surfaces of nanoparticles would enhance the T cell response compared to mixing the same quantity of soluble CpG with unfunctionalized nanoparticles, mice were immunized with ova in nanoparticles, nanoparticles mixed with soluble CpG, or nanoparticles coated with CpG, and T cell responses were assessed after 7 d. As shown in Figure 3.18A, IFN-γ secretion by splenocytes from mice immunized with ova nanoparticles without CpG or with soluble CpG was low and significantly lower than that induced by splenocytes from mice immunized with CpG conjugated to nanoparticles; $CD8^+$ T cell activation was significantly higher for CpG-particles than for nanoparticles delivered with soluble CpG ($p = 0.03$) . To determine if this functional difference was accompanied with higher effective primary T cell expansion, we stained splenocytes with peptide-MHC class I tetramers (SIINFEKL/H-$2K^b$) to determine the frequency of ova-specific $CD8^+$ T cells (Figure 3.18B and C). Ova nanoparticles without CpG contained ~0.32% of ova-specific $CD8^+$ T cells; this frequency increased to 1.23% with co-delivery of soluble CpG with ova nanoparticles, and further increased to 2.29% when CpG and antigen were co-delivered on a single particle (Figure 3.18C). Thus, CpG-

coated hydrogel nanoparticles activate naïve T cells *in vivo* effectively resulting in proliferation of $CD8^+$ antigen-specific T cells and elicitation of effector function relative to unmodified nanoparticles and soluble antigen.

A.

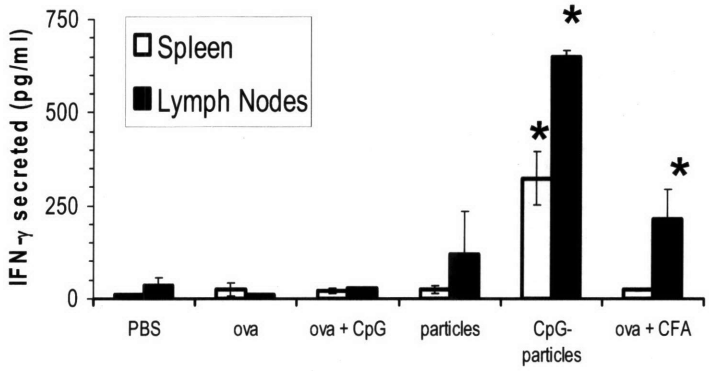

B.

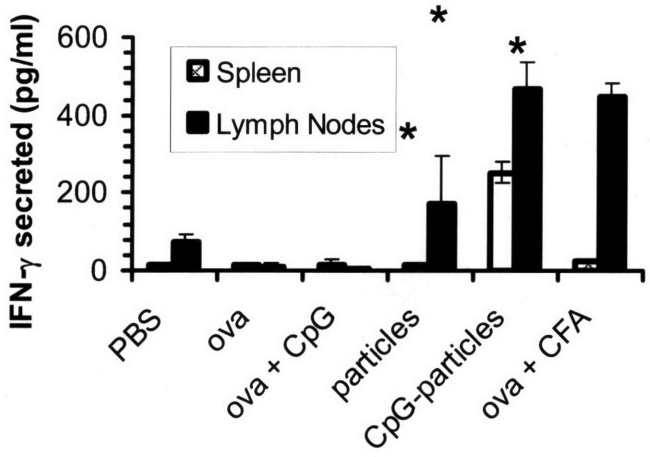

Figure 3.17. C57Bl/6 mice were immunized with antigen in different forms and lymphocytes from the inguinal (draining) lymph nodes (hashed bars) and spleen (solid bars) were restimulated *in vitro* with MHC class II or class I peptides to measure (A) $CD4^+$ and (B) $CD8^+$ T cell responses, respectively. Shown are IFN-γ levels measured in supernatants of restimulated lymphocytes after 48 hrs. Asterisks denote samples statistically different form PBS control ($p < 0.05$). Data shown from one representative of two independent experiments.

A.

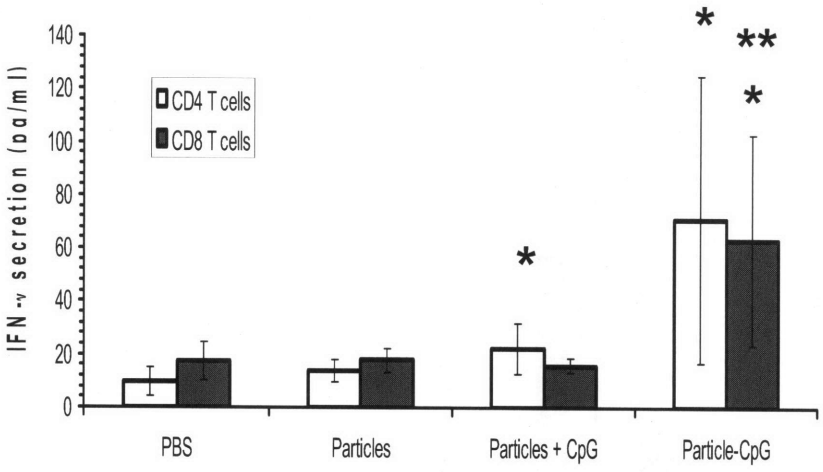
IFN-γ secretion (pg/ml)
140
120
100
80
60
40
20
0
CD4 T cells
CD8 T cells
*
*
**
*
PBS
Particles
Particles + CpG
Particle-CpG

B.

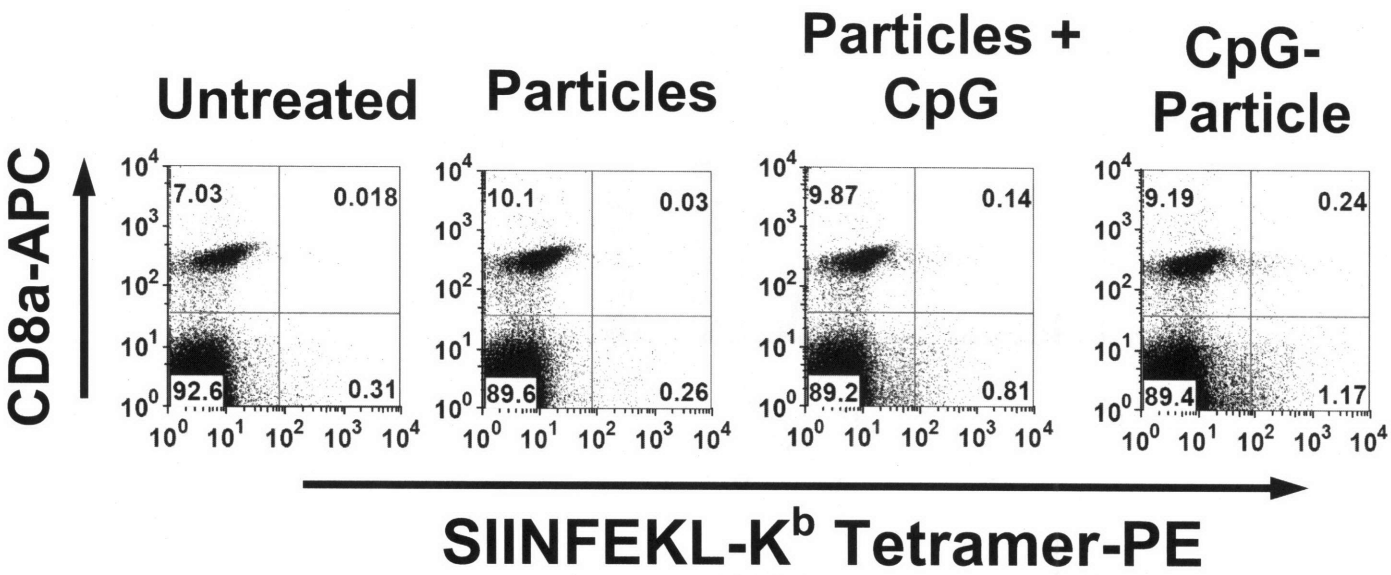
Untreated
Particles
Particles + CpG
CpG-Particle
CD8a-APC
7.03
0.018
92.6
0.31
10.1
0.03
89.6
0.26
9.87
0.14
89.2
0.81
9.19
0.24
89.4
1.17
SIINFEKL-K^b Tetramer-PE

C.

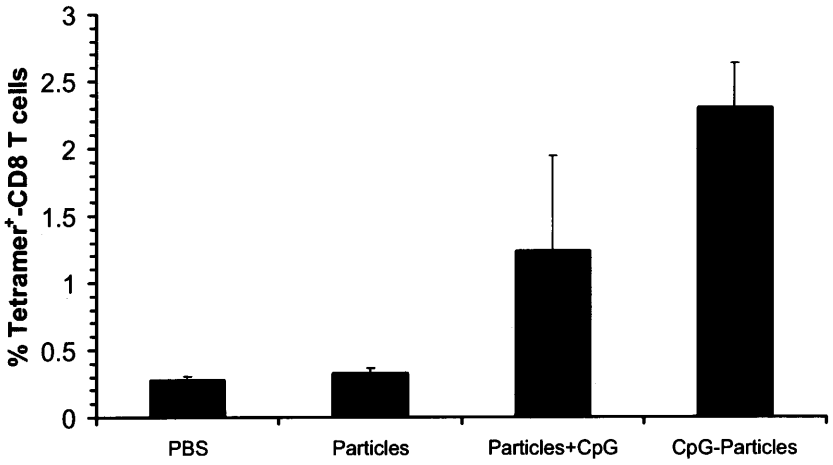

Figure 3.18. (A) C57Bl/6 mice were immunized with ova nanoparticles without CpG, soluble CpG, and particle-bound CpG. Splenocytes were isolated after 1 week and restimulated with MHC class I or class II peptides and IFN-γ levels were measured after 48 hrs as described in Section 3.3.8.2. Asterisks denote samples statistically different from PBS control ($p < 0.05$), and ** denote statistically significant difference from ova nanoparticles delivered along with soluble CpG ($p < 0.05$). (B) Splenocytes from experiment in (A) were stained with anti-CD8α and ova-tetramer, and analyzed by flow cytometry to determine frequency of ova-specific CTLs in immunized mice. Shown are the density plots with $CD8^+$ $tetramer^+$ cells in upper-right quadrant. (C) Mean frequency (n = 4) of ova-specific CTLs for ova nanoparticles delivered without CpG, soluble CpG, or particle-bound CpG.

3.3.8.3 Generation of $CD8^+$ memory T cells in mice immunized with hydrogel particles

Generation of memory T cells and B cells is an important aspect of vaccination in order to protect the host from the pathogen of interest during infection. An effective prophylactic vaccine for viral infections or cancer should elicit a long term $CD8^+$ memory T cell response. To determine whether conjugation of CpG directly to nanoparticles influenced levels of memory T cells induced by vaccination, we measured ova-directed

in vivo cytolytic activity 60 days after immunization of mice with ova nanoparticles, by injecting immunized mice with a mixture of syngeneic ova-pulsed splenocytes and unpulsed splenocytes labeled with high and low levels of CFSE, respectively. Loss of the ova-pulsed splenocytes relative to the unpulsed transferred cells was measured after 24 hrs by flow cytometry. As shown in Figure 3.19, immunization with CpG-coated nanoparticles elicited 35% specific cytolytic activity; ova particles delivered with soluble CpG elicited only 23% specific killing. Thus, co-delivery of antigen and TLR ligands from the hydrogel nanoparticles led to more effective long-term $CD8^+$ T cell memory.

These results indicate that physical co-display of antigen and TLR ligands together on pathogen-sized particles enhances not only the initial T cell responses but also the induction of long term memory relative to soluble co-injection of these same signals.

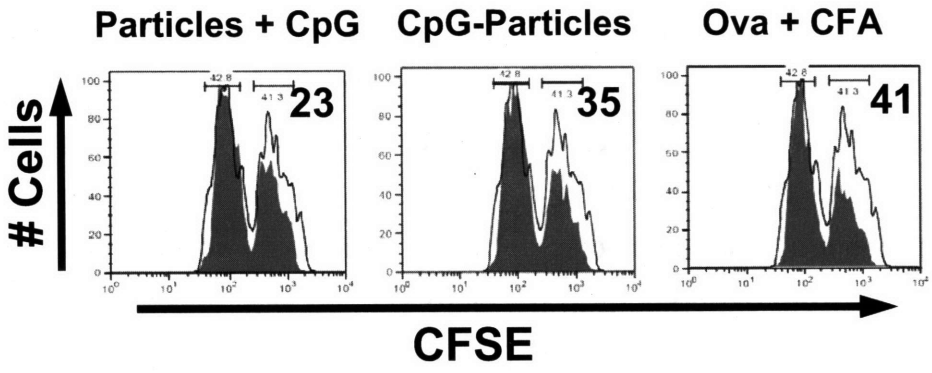

Figure 3.19. Mice were immunized as described in Section 3.3.8.2 followed by intravenous injection of CFSE-labeled syngeneic splenocytes loaded with SIINFEKL peptide after 60 days. Memory response was quantified as % cytolytic activity. Shown are cell populations depicting control ($CFSE^{lo}$) and ova peptide-pulsed target splenocytes ($CFSE^{hi}$). Grey solid histograms represent results from immunized animals and black solid lines are cells recovered from a sham-immunized control. The values shown in the histogram charts are the mean values of cytolytic activity.

3.4 Discussion

Pluronic PEO-PPO-PEO triblock copolymers form micelles in aqueous solutions when present at concentrations above the CMC (critical micellization concentration) and CMT (critical micellization temperature) [198]. At higher temperatures, the poly(ethylene oxide) blocks of pluronics dehydrate, phase-separating into polymer-rich and polymer-poor phases above the cloud point temperature. The PEO-PPO-PEO triblock F-68 is a relatively hydrophilic member of the pluronic family of copolymers, with a cloud point in the pure water of ~105 °C (obtained by extrapolation) [179]. The cloud point of pluronics is strongly influenced by the presence of monovalent salts, which is thought to be due to repulsion between small, weakly polarizable ions and the weakly polarizable PEO blocks [179,199], an effect also observed for PEO homopolymers in salt solutions [200]. For pluronic F-68, Bahadur *et al.* [179] have previously demonstrated that the cloud point can be lowered by 50 °C on addition of 1 M KF to an aqueous F-68 solution. Similarly, we observed that presence of ~5.5 M NaCl lowered the cloud point of pluronic F-68 to 37 °C resulting in phase separation of pluronic as evident by obvious clouding of initially clear solution and an increase in the hydrodynamic diameter of pluronic aggregates from ~35 nm at 32 °C to ~400 nm at 37 °C. In previous work, Drummond and Peppas reported that poly(ethylene glycol) methacrylate (PEGMA) could be successfully polymerized in a suspension polymerization by salting out PEGMA monomers in a saturated sodium chloride solution [201]. This report and the interesting phase behavior of F-68 in aqueous salt solution inspired us to utilize the temperature-induced phase separation of pluronic combined the with well-known salting out behavior of both poly(ethylene glycol) [202] and proteins [203] in high ionic strength solutions to co-localize protein and hydrogel precursor monomers together for polymerization in an organic-solvent free system. Hydrogel particles thus formed were monodisperse with a mean hydrodynamic diameter of 500 nm, and contained up to 80% of the particle dry weight as protein. High protein loading per particle helps in delivering high doses of antigen intracellularly to dendritic cells, which was shown to elicit strong T cell activation.

To elicit a protective T cell response, vaccines must deliver both antigen and an activating danger signal to dendritic cells, which triggers their differentiation from an immature antigen-collecting state to a mature antigen-presenting and T cell-activating

state [5,22]. Likewise, productive naïve B cell responses only occur if B cells contact antigen coincident with danger signals. Hydrogel particles provided negatively-charged groups on their surfaces through the incorporation of methacrylic acid into the gel particles, which were used for adsorption of immunostimulatory CpG oligonucleotides via sequential adsorption of poly(L-arginine) followed by CpG. Poly(L-arginine) was found to be a suitable cationic biopolymer for functionalization of hydrogel particles as it is less cytotoxic than poly(L-lysine) [204,205]. We found that coating the anionic nanoparticles with low molecular weight poly(L-arginine) (~1 kDa) did not result in high loading of CpG oligonucleotides on the particles, whereas high molecular weight poly(L-arginine) (> 70 kDa) caused cytotoxicity in DCs; 10 kDa poly(L-arginine) was however found to be optimal (data not shown). This is in contrast with studies in which Jurkat cells were incubated with poly(arginine) of different lengths and a low molecular weight polymer (~2 kDa) was found to be effective in transporting dye to the interior of cells [206]. We observed that as poly(L-arginine) concentration was increased from 0.5 mg/mL to 5 mg/mL, CpG coupling efficiency increased from 30% to ~100% with a corresponding increase in IL-12p40 secretion from dendritic cells incubated with these CpG-coated hydrogel particles. Thus, poly(L-arginine) coating of hydrogel particles provided functional groups on the particle surface for electrostatic coupling of immunostimulatory CpG oligonucleotides, and these functionalized hydrogel particles delivered CpG to dendritic cells intracellularly at high doses for interaction with their cognate receptor TLR9. In general, this electrostatic adsorption approach should be applicable to a variety of other DC-stimulating ligands to stimulate dendritic cells through different Toll-like receptors.

Professional antigen presenting cells such as dendritic cells are highly efficient phagocytes and rapidly internalize submicron-sized biological or synthetic particles [5,10,115]. We incubated DQ-ovalbumin-loaded hydrogel particles with dendritic cells and antigen uptake was found to be highly efficient when antigen was delivered in particulate form compared to antigen delivery as soluble protein even after 18 h. Efficient delivery of antigen coupled with delivery of high doses of antigen per particle not only induced cross-presentation of antigen but also in efficient processing of antigen and subsequent presentation of antigen on MHC molecules to T cells.

For protein antigens to elicit T cell responses, these biomacromolecules must be delivered to intracellular processing compartments in dendritic cells, where DCs localize a variety of enzymes designed to degrade (digest) proteins into short polypeptides that can be loaded onto class I and class II major histocompatibility complex molecules. Typically, protein carriers are designed to release antigens once the carrier is internalized into the acidic vesicles (phagolysosomes) used by dendritic cells to internalize particles [127]. In recent elegant studies, this release has been engineered to be selectively triggered by the pH change encountered in this intracellular compartment (from pH 7.4 outside the cell to pH 5.5-6.5 in the phagolysosome [207]) [142,208,209]. Such a selective release could clearly be engineered into the hydrogel particle synthesis approach studied here via flexible nature of free-radical polymerization chemistry through incorporation of degradable crosslinkers on the basis of protease-sensitive peptides [210], hydrolysable polyesters [211,212], reducible disulfide-bonded repeat units [213], phosphazene derivatives [214,215], or acid-sensitive cross-linkers [142]. However, when hydrogel particles were incubated with a phagolysosomal protease, cathepsin D, ovalbumin encapsulated in hydrogel particles was digested by the enzyme and fractions were found to be identical to those obtained from cathepsin D digestion of soluble ovalbumin. The peptide fragments were found to range between approximate molecular size of 2 to 30 kDa as reported previously also for ova digestion by cathepsin D [216]. The enzyme tested, cathepsin D, is a ubiquitous protease involved in antigen processing in the endosomes/phagosomes of antigen presenting cells [216,217]. This demonstrates that encapsulated ovalbumin can be processed by phagolysosomal proteases when hydrogel particles are phagocytosed by dendritic cells resulting in generation of peptides that will be loaded onto MHC molecules.

As expected from prior studies of particulate antigen delivery, hydrogel nanoparticles elicited greatly enhanced MHC class I presentation of ova epitopes. As stated above, antigen uptake by DCs via nanoparticles was much faster than soluble ova internalization. However, if DCs were incubated with antigen for 18 hrs, allowing time for soluble ova uptake to occur (nanoparticles afforded only a 1.4-fold greater fraction of DCs positive for antigen uptake relative to soluble ova at this time-point), the amount of ova-derived class I peptide-MHC complexes per cell was still ~4.5-fold

greater for DCs loaded with nanoparticles, suggesting that enhanced class I peptide presentation by DCs encountering particulate antigen is not simply a matter of enhanced antigen uptake alone. Studies of antigen presentation by ova-CpG conjugates have shown that CpG signaling enhances cross presentation of soluble ova protein [188,189,191]. In the case of ova-loaded nanoparticles, CpG-functionalization did not elicit further enhancement of cross-presentation above that obtained with the 'bare' particles, suggesting that in the present case, cross-presentation is already maximally induced by the particulate mode of delivery.

Hydrogel particles delivered high doses of CpG oligonucleotide to dendritic cells resulting in effective interaction between CpG oilgos and their cognate receptor, TLR9 in the phagolysosomes of dendritic cells. CpG-coated hydrogel particles resulted in significantly increased expression of costimulatory molecules such as CD40, CD80, CD86, and MHC class II on the surface of dendritic cells compared to when dendritic cells were incubated with soluble CpG alone. CpG-coated hydrogel particles also induced secretion of pro-inflammatory cytokines such as IL-12, IL-6, and TNF-α by dendritic cells; cytokine secretion could be detected at nearly 10-fold lower CpG concentration when delivered in particulate form than when delivered as soluble oligonucleotide. CpG has a dissociation constant of ~ 200 nM with TLR9 [192], and in agreement with that, soluble CpG induced cytokine secretion at oligo concentration ~ 500 nM. However, hydrogel particles result in a high concentration depot of CpG oligos in the phagolysosomes and cytokine secretion was detectable at an *overall* concentration as low as 50 nM for all cytokines analyzed. This is in contrast with molecular ova-CpG conjugates that resulted in increased antigen uptake through receptor-mediated endocytosis involving nonspecific DNA receptors on dendritic cells surfaces, but reduced cytokine secretion compared to soluble CpG [152].

In vivo, we found that while soluble ova adjuvanted with CpG elicited no antibody response (a result seen by others [102]), a single injection of hydrogel nanoparticles activated B cells and induced levels of anti-ova IgG comparable to ova emulsified with CFA. We showed by staining hydrogel nanoparticles with a monoclonal anti-ova antibody that the particles present ova epitopes on their surfaces [181], and we believe this multivalent presentation of antigen epitopes may be responsible for the enhanced

antibody response seen with the ova-loaded nanoparticles. On the T cell side of the immune response, a single injection of CpG-coated particles, but not uncoated particles or soluble ovalbumin, elicited IFN-γ-producing $CD4^+$ and $CD8^+$ T cells in the spleen and draining lymph nodes to levels comparable to or greater than ova in CFA. Notably, these responses were obtained without overt inflammation visible at the injection site, in contrast to the strong inflammation typical of CFA (data not shown). Furthermore, although conjugation of CpG to nanoparticles did not appear to influence the magnitude of antibody responses, we observed that CpG bound to nanoparticles resulted in a greater frequency of ova-specific $CD8^+$ T cells, higher $CD4^+$ and $CD8^+$ T cell responses in the spleen, and eventually creation of a stronger long term memory $CD8^+$ T cell response compared to soluble CpG mixed with the nanoparticles. These results are consistent with previous studies showing that co-encapsulation of antigen and CpG within synthetic biodegradable particles improves T cell activation significantly relative to antigen encapsulated in particles mixed with soluble CpG [102,149,154]. Development of a strong and long-lasting memory response is necessary for targeting virally infected cells or tumor cells in both therapeutic and prophylactic settings [197,218-220]. Notably, the frequency of antigen-specific CTLs elicited by this nanoparticle-based vaccine (Figures 3.17D and 3.17E) is comparable to that observed with various DNA- and protein-based vaccines that resulted in tumor regression or strong anti-viral response [149,221-223]. The lasting significant specific CTL activity detected in immunized mice suggests the potential for this system to be highly effective in prophylactic applications. Altogether, these results suggest that co-display of antigen epitopes and TLR ligands on the surface of antigen-loaded nanoparticles is an effective strategy for potent B cell and T cell activation *in vivo*.

3.5 Conclusions

Aqueous two-phase systems have long been utilized for protein purification, because the phase-separation process drives aggregation of proteins without denaturation. Pathogen-mimetic hydrogel particles were synthesized by a salting out-based miniemulsion polymerization technique to deliver antigen and CpG oligonucleotide in concert to dendritic cells. By this process, ovalbumin was

encapsulated in poly(ethylene glycol) particles in the absence of organic solvents at near-physiological temperatures. These hydrogel particles were 500 nm in size which is intermediate between the sizes of bacteria and viruses and co-display antigen and TLR ligands at their surfaces mimicking the gross structure of pathogens. Protein antigen was stably encapsulated in the hydrogel particles in the presence of serum but was accessible to antigen-processing enzymes *in vitro* and was processed and potently presented to both $CD4^+$ and $CD8^+$ T cells by dendritic cells that phagocytosed the gels. Delivery of immunostimulatory signals at high dose by hydrogel particles resulted in efficient antigen presentation by dendritic cells and dendritic cell maturation measured as secretion of inflammatory cytokines and upregulation of costimulatory molecules. The activation of B cells and T cells *in vivo* resulted in high anti-ovalbumin antibody titers and naïve T cell activation in draining lymph nodes and spleen, and generation of memory $CD8^+$ T cells detectable at 60 days post-immunization. Thus, co-delivery of antigen and TLR ligands to dendritic cells is highly effective for dendritic cell activation, and as observed in our studies, absence of any signal is unable to induce effective lymphocyte activation *in vivo*. This system may be used as a potent vaccine for diseases that require recruitment of both B and T cells. Moreover, the ability to use multiple dendritic cell modulation factors on the surface of pathogen-mimetic particles could allow the induction of a range of cytokines in dendritic cells tailored to combat specific pathogens.

4. Co-delivery of Chemokine and Antigen/Activation Signals to Dendritic Cells

4.1 Introduction

Dendritic cells are sentinels of the immune system, which scan their environment in search of pathogens. Pathogens are processed by dendritic cells resulting in antigen presentation on MHC molecules and DC maturation [5]. Dendritic cells are thought to be the only antigen presenting cells capable of priming naïve T cells *in vivo* and are superior to other antigen presenting cells (namely, macrophages and B cells) in antigen processing and T cell activation [54]. Therefore, vaccines have been designed to target dendritic cells for delivery of antigen for most effective immune response. However, dendritic cells are rare and therefore targeting strategies need to be highly specific and efficient to locate dendritic cells and deliver antigen to them with high efficiency. Martin-Fontecha *et al.* demonstrated by injection of antigen-loaded dendritic cells that the magnitude of T cell responses correlated with the number of dendritic cells injected into mice [63]. In an attempt to apply this concept directly in the clinic, dendritic cell vaccines involve the *ex vivo* differentiation of monocytes from a patient that are then cultured in presence of antigens and adjuvants to activate the cells effectively. These activated

dendritic cells are injected back into the patient to prime the immune system against the antigen of interest [36,224,225]. Despite promising results obtained with dendritic cell vaccine therapy, various subunit vaccines are sought due to the ease of application of subunit vaccines and their much lower cost. To enhance efficiency of antigen delivery to DCs, subunit vaccines are often based on the principle of using a targeting ligand for intracellular delivery of antigen to dendritic cells along with a maturation signal. Strategies have been designed to target nonspecific DNA receptors through CpG conjugation to antigen [152,153], DEC205 by conjugating anti-DEC205 to antigen or antigen-loaded nanoparticles [24,149,226], Fcγ receptors through use of IgG-conjugated antigens [227], glycolipid globotriacylceramid, by fusing Shiga toxin B to the tumor antigen [228], use of bi-specific antibody to target antigen-encoding adenovirus to dendritic cells via CD40 [229-231], or targeting of antigens conjugated to a TLR2 ligand, S-[2,3-bis(palmitoyloxy)propyl]cysteine [232]. These strategies have shown promising results *in vitro* and *in vivo*.

In contrast to the DC-targeting strategies mentioned above, attraction of dendritic cells and DC precursors to the immunization site by means of a chemoattractant (reverse-targeting) has been studied by some groups to mimic the physiological sequence of events that occur in case of a pathogen infection. In case of an infection, inflammatory signals comprising of chemokines released by epithelial cells [15,16], bacterial fragments [16], and neutrophils [233] form a gradient in the environment by diffusion, which induces DC chemotaxis along the concentration gradient towards the site of infection [49,52,234]. Chemokines targeting dendritic cells such as fMLP [235], CCL20 [42,68,69], MIP-3β [40,41,236], CCL27 [237] have been used *in vitro* and *in vivo* to attract dendritic cells to tumors or sites of immunization where dendritic cells were primed to present antigen to T cells and initiate an immune response [238]. Interestingly, attraction of DCs to tumor sites via constitutive production of chemokine from transfected tumor cells or fibroblasts caused significant tumor regression, while injection of single bolus doses of recombinant chemokines did not elicit anti-tumor immunity [42,67,69]. However, the use of plasmids encoding chemokine may not give control over chemokine gradient and duration of immune response as is with the controlled release systems that release recombinant chemokines [239]. Comparing these systems

that modulate DC trafficking with physiological events, inflammatory signals that attract dendritic cells are present for the duration of the inflammation following which chemokine levels return to basal levels [240]. Taking this into consideration, we developed microparticles that release chemokines for a specific duration to attract dendritic cells followed by delivery of antigen and maturation factor to the attracted cells. This system was designed to mimic a pathogen infection whereby inflammatory signals from individual microparticles mimicked local epithelial cells secreting chemokines into their microenvironment (Figure 1.5).

Our approach was to use alginate microparticles that encapsulated the chemokine CCL20 and the hydrogel nanoparticles described in Chapter 3. We initially sought to co-encapsulate CCL20-loaded PLGA microspheres and hydrogel nanoparticles in the alginate microparticles. However, chemokine release from PLGA microspheres was not effective in sustained attraction of DCs possibly due to low chemokine loading in PLGA microspheres and loss of chemokine as a result of acidic products of PLGA hydrolysis; direct loading of CCL20 in alginate microparticles allowed higher loading of the chemokine in the microspheres with minimal damage to the protein during or after encapsulation process. Alginate is a bacterially-derived or algae-derived polysaccharide-based biopolymer that has been widely studied and used in biotechnology applications. Alginate is formed from blocks of guluronic acid and mannuronic acid monomers that possess a negative charge, which was used for electrostatic coupling of cationic chemokine to the polymer matrix. Multivalent cations such as calcium cross-link guluronic acid between chains causing formation of a cross-linked matrix that was used to encapsulate hydrogel nanoparticles. We observed that controlled release of chemokine from alginate microparticles attracted dendritic cells to the individual microparticles which were then delivered antigen and CpG oligonucleotides. This system resulted in an enhanced and selective delivery of antigen to dendritic cells *in vitro*. The simplicity of the system also enables us to co-deliver various chemokines and other DC modulating factors to dendritic cells and other immune cells for a desired immune response. In addition, ultra-localization of nanoparticles prevents delivery of antigen and maturation signals to non-responding cells, which contributes towards effective use of an antigen to obtain a productive

immune response. Localized drug delivery has been proposed to be useful in inducing a localized effect of the therapeutics, reducing the side effects of the therapy, and in obtaining a more productive response [241]. This was achieved in our system through ultra-localization of hydrogel nanoparticles that were delivered only to the cells that were in the immediate vicinity of the microparticles. In addition, use of controlled release of chemokines to localize cells of interest in a certain location can have applications in design of medical devices, organogenesis, and embryonic development.

4.2 Materials and Methods

4.2.1 Synthesis of alginate microparticles for co-encapsulation of CCL20 and ova-loaded hydrogel nanoparticles

Alginate microparticles were synthesized using a water-in-oil single emulsion technique. Tween 80 (0.5 mL) and Span 80 (1.5 mL) were added to iso-octane (50 mL) with stirring. Addition of Tween 80 turned the solution cloudy, but the cloudiness resolved as Span 80 was added. The surfactant solution was stirred at 8,000 rpm using an Ultra Turrex T-25 homogenizer for 4 min before use. An aqueous phase was prepared by adding 1 μg of CCL20 to 400 μL 1% w/v low viscosity sodium alginate (Sigma, USA), and then dissolving 10 mg low endotoxin BSA (Sigma, USA) in the sodium alginate solution followed by addition of 100 μL of a CpG-coated DQ-ova-containing hydrogel nanoparticles suspension (10 mg/mL). The suspension was well-mixed, added to the iso-octane/ surfactant solution, and homogenized for 3 min at 8,000 rpm. This was followed by addition of 25 μL $CaCl_2$ (5% w/v) to the emulsion to crosslink the alginate, and homogenization for 4 min at 8,000 rpm. The resulting alginate microparticles were pelleted at 4,500 g for 10 min and washed once in iso-octane at the same speed, then resuspended in 1 mL unsupplemented RPMI imaging medium and transferred to an eppendorf tube. The microparticles were pelleted at 10,000 g for 3 min and the aqueous-phase supernatant was collected for estimation of the chemokine encapsulation efficiency. Alginate microparticles were washed 3x in RPMI imaging medium. To remove unencapsulated hydrogel nanoparticles or nanoparticle aggregates,

alginate microparticles were pelleted at 100 g for 30 sec, and the supernatant was gently pipetted off. Alginate microparticles were resuspended in 1 mL RPMI medium and stored at 4 °C until use.

4.2.2 Characterization of alginate microparticles

4.2.2.1 Encapsulation efficiency of chemokine in alginate microparticles

Supernatants were collected during the aqueous washes of the alginate microparticle synthesis for estimation of the chemokine encapsulation efficiency. Suitable dilutions of supernatants were analyzed by ELISA to determine the chemokine concentration and encapsulation efficiency was calculated as:

$$Encapsulation\ Efficiency = \left[1 - \frac{Amount\ of\ CCL20\ in\ supernatant}{Amount\ of\ CCL20\ added}\right] \times 100\% \quad [13]$$

4.2.2.2 Kinetics of chemokine release from alginate microparticles

An alginate microparticle suspension (100 μL) was diluted to 500 μL with complete RPMI medium containing 10% FCS. The microparticles were incubated at 37 °C with shaking, and 500 μL supernatant samples were collected by pelleting the microparticles at 10,000 rpm for 3 min. Supernatant removed was replaced with fresh complete RPMI medium. The supernatants were analyzed using a CCL20 ELISA kit (R&D Systems, USA) to determine the concentration of CCL20 released into the medium.

4.2.2.3 Determination of hydrogel nanoparticle encapsulation efficiency

Supernatants were collected during the aqueous wash of the alginate microparticle synthesis for estimation of the hydrogel particle encapsulation efficiency. Known volumes of supernatants were analyzed by flow cytometry (FACS Scan, Becton Dickinson, USA) to quantify the number of unencapsulated nanoparticles remaining in the supernatants.

4.2.2.4 Determination of alginate microparticle water content

Alginate microparticles were pelleted at 16,000 g for 4 min, and the pellet was blotted on a filter paper to remove excess water. The pellet was transferred to pre-weighed filter paper and the wet mass was measured. The particle pellet was then dried at 70 °C under vacuum overnight followed by measurement of the dry particle mass. The water content of the microparticles was directly determined as the difference of these two measurements.

4.2.2.5 Determination of alginate microparticle density and mean diameter

Alginate microparticle suspension was directly counted for particle density using a hemocytometer. The particle size distribution and mean diameter of alginate spheres was determined using a Vi-Cell Counter (Beckman Coulter).

4.2.3 Analysis of antigen uptake by dendritic cells by flow cytometry

As an *in* vitro model of DC responses to alginate injected subcutaneously, DCs and alginate microspheres were suspended together in collagen gels. Bone marrow dendritic cells (1 x 10^6 cells) were uniformly mixed with 10 μL alginate microparticles with or without chemokine and containing CpG-coated DQ-ova-containing hydrogel nanoparticles (3.2 x10^6 particles/mL), or 1 μL CpG-coated fluorescent DQ-ova-containing hydrogel nanoparticles (5.35 x10^{10} particles/mL) in 1 mL of 1.2 mg/mL bovine collagen (BD Biosciences, USA), and added to 24-well tissue culture treated plates. Collagen was gelled at 37 °C, 5% CO_2 and the cells were incubated for 24 hr within the gels. After 24 hr incubation, 100 μL of 4000 U/mL collagenase D was added to each well, and the collagen matrix was broken down into small fragments by pipetting. The samples were incubated with collagenase D for 1 hr at 37 °C with shaking to digest the collagen. The resulting cell suspensions were transferred to 1.2 mL microtiter tubes, washed 2x in FACS buffer, and stained with anti-CD11c and anti-CD16/CD32 antibodies. The stained cells were analyzed using flow cytometry (FACS Scan, Becton Dickinson, USA) to determine antigen uptake by dendritic cells.

4.2.4 Time-lapse videomicroscopy analysis dendritic cell attraction to alginate microparticles

Bone marrow dendritic cells (1 x 10^6 cells) were uniformly mixed in 1.2 mg/mL bovine collagen with 10 μL/mL alginate microparticles containing CCL20 and CpG-coated DQ-ova-containing hydrogel nanoparticles (3.2 x10^6 particles/mL). The cell/alginate microparticle suspension was added to a 35 mm petridish or 2-well labtek chamber (Nunc) and the collagen was gelled for 30 min at 37 °C, 5% CO_2. The sample was then placed on the environmental stage of a Zeiss Axiovert 200 microscope stage maintained at 37 °C, 5% CO_2 during the course of imaging. Phase contrast and fluorescence images were collected from 9 fields of view every 2 min as described earlier in Chapter 2. Motile cells in the culture were analyzed for determining cell paths and migrated distances using MetaMorph software (Universal Imaging).

4.2.5 Bone marrow-derived macrophage cell culture

Bone marrow-derived macrophages were generated by a procedure similar to that for bone marrow-derived dendritic cells in Appendix 10 [242]. Briefly, bone marrow progenitor cells were plated in 24-well tissue culture treated plates at 1.5 x 10^6 cells/mL/well with 10 ng/mL rmM-CSF in complete RPMI medium. On days 2, 4, and 6, 80% of the medium was replaced with fresh complete medium supplemented with 10 ng/mL rmM-CSF. Cells were used on days 7 and 8.

4.3 Results

4.3.1 Synthesis of alginate microparticles and characterization

Alginate microparticles were synthesized using a water-in-oil single emulsion approach to co-encapsulate hydrogel nanoparticles and chemokine as illustrated in Figure 4.1B. This strategy was modified from Lemoine *et al.* [243] and a similar approach has been used for synthesizing hydrogel nanospheres and microspheres [244,245]. Homogenization of alginate/protein/particle aqueous suspension in iso-octane with 3:1 ratio of Span 80: Tween 80 resulted in a uniform emulsion. Addition of

calcium chloride cross-linked alginate polymer chains within the emulsion droplets to form microparticles that contained both the hydrogel nanoparticles and CCL20.

A.

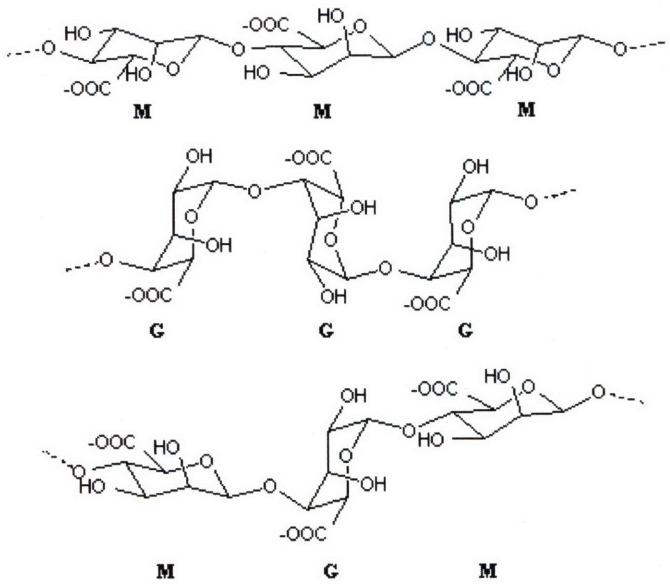

B.

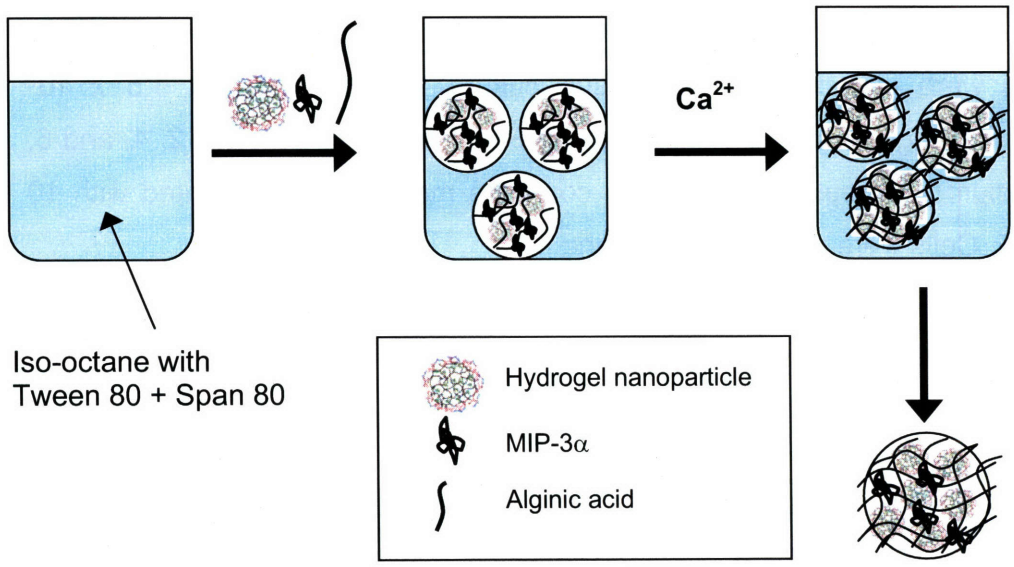

Figure 4.1. (A) Chemical structure of alginate. G = Guluronic Acid and M = Mannuronic Acid. (B) Schematic diagram for encapsulation of hydrogel nanoparticles and chemokine in alginate microparticles.

DQ-ova-containing hydrogel nanoparticles encapsulated in alginate microparticles were observed to be uniformly distributed through the volume of the alginate microparticles by fluorescence microscopy (Figure 4.2A). Similarly, when alexa fluor 594-labeled CCL20 was encapsulated inside the alginate microparticles along with unlabeled hydrogel nanoparticles, fluorescence microscopy revealed that the chemokine was distributed throughout the alginate microparticle and was retained inside the microparticle despite the small size of the protein (Figure 4.2B).

A. **B.**

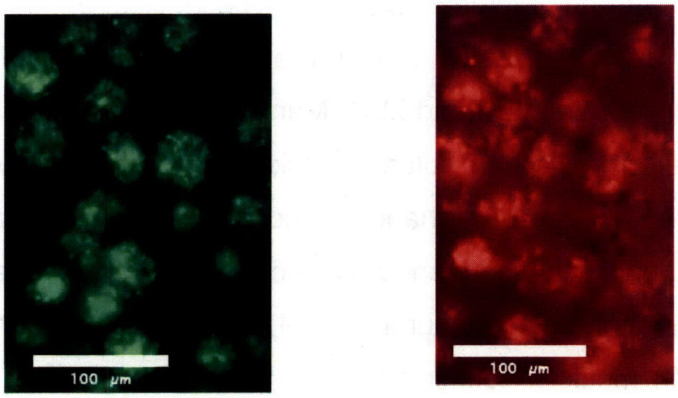

C.

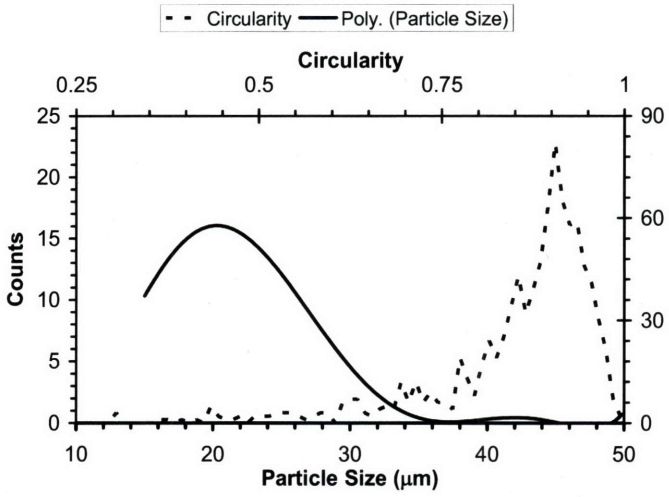

Figure 4.2. Fluorescence micrographs of alginate microparticles containing (A) DQ-ova-containing hydrogel nanoparticles (B) Alexa fluor 594-labeled CCL20. (C) Particle size distribution data and circularity of alginate microspheres obtained by Vi-Cell Counter.

The alginate microparticles had a mean diameter of ~20 μm with a size range from 15 μm to 35 μm (Figure 4.2C). Hydrogel nanoparticles were encapsulated within the alginate microparticles with a high efficiency of ~95%, as determined by analysis of the synthesis supernatant using flow cytometry. Direct counting of the alginate microparticle suspension estimated ~ 3.2 x 10^6 microparticles/mL corresponding to a loading of ~1600 nanoparticles per alginate microparticle. The water content of alginate microparticles was ~95% by weight with the remaining 5% comprising of encapsulated nanoparticles, chemokine, carrier protein, and alginate polymer; this corresponds to a swelling ratio (V_{wet}/V_{dry}) of ~20 for the microparticles. The mesh size of alginate microparticles can be calculated using the theory of Canal and Peppas [180] for an alginate polymer with molecular weight 200 kDa and M/G (Mannuronic/ Guluronic) ratio 1.6 [243]. Alginate crosslinks are formed when guluronic acid from different polymer chains bind the same calcium in an egg-box shaped structure; due to stochastic distribution of the monomers, guluronic acid and mannuronic acid in the polymer chains, the polymer chain comprises of mannuronic-mannuronic (MM), mannuronic- guluronic (MG), or guluronic-guluronic (GG) motifs. Assuming that the polymer chain has GG combination of 20% as observed for most alginate polymers with low G content, we calculated ~100 GG combinations in each alginate polymer chain. Assuming all GG to be placed equally apart, characteristic ratio and monomer size of alginate being same as that of cellulose (Cn ~20 and bond length *l* ~5.5 Å [246]), the mesh size is 19.5 nm. However, due to the statistical distribution of location of guluronic acid and mannuronic acid monomers in the alginate chain, the mesh size will correspondingly be statistically distributed. This mesh size value agreed with our observation that when dendritic cells were incubated with alginate microparticles containing 20 nm FITC-labeled nanoparticles, 80% of the cells in culture were observed to contain nanoparticles after 24 h in contrast with 20% cells containing 500 nm-sized nanoparticles encapsulated in alginate microparticles, indicating that nanoparticles that are as big as the mesh size will be easily taken up by phagocytic cells such as dendritic cells. On the other hand, protein molecules having much smaller dimensions may be released from the alginate microparticles as observed for bovine serum albumin. When FITC-Bovine Serum Albumin (BSA) doses of 1-10 mg per 4 mg sodium alginate were encapsulated in

alginate microparticles, >90% of the BSA protein was released from alginate microparticles during the first aqueous washing step resulting in a net encapsulation efficiency of ~5% for BSA. Previous studies that have reported BSA encapsulation in alginate microspheres used significantly higher amount of calcium chloride followed by dehydration of alginate matrix using isopropanol that resulted in extensive crosslinking of alginate; however, BSA was released from the microparticles very quickly [243]. In contrast, the chemokine, CCL20 was encapsulated with an encapsulation efficiency ranging from 75% when 10 μg CCL20 was encapsulated up to 90% when 10 ng CCL20 was encapsulated. Many chemokines are cationic in nature and CCL20, in particular has a pI of ~10 [247]. We hypothesized that the cationic nature of CCL20 supports electrostatic binding of the protein to the anionic alginate polymer chains, causing the chemokine to be encapsulated inside the polymer matrix with high efficiency. This hypothesis was tested by mixing 1% sodium alginate and different quantities of lysozyme. Like CCL20 and other chemokines, lysozyme is a small protein (14 kDa) protein with a pI of 11 [248]; these properties make lysozyme a good model protein for studying chemokine encapsulation in alginate microparticles. In support of potential ionic interactions between such cationic proteins and alginate, we observed that as lysozyme was added to 400 μL of 1% (wt/vol) sodium alginate in increasing amounts, 100 μg lysozyme precipitated the polysaccharide, as evident from clouding of the polymer solution.

Thought CCL20 was readily encapsulated, it was expected that it should be slowly released from alginate microspheres by slow diffusion through the ionic alginate matrix. We studied the kinetics of CCL20 release from alginate microparticles in complete RPMI medium to incorporate effects of serum proteins and buffer conditions at 37 ^{o}C. Alginate microparticles release the chemokine with a burst release of ~20%; ~50% of the encapsulated chemokine was released after 24 h. Release then continued at a slower rate for several days further (Figure 4.3). After releasing chemokine from alginate microparticles for one week, the release curve plateaued at 80%. This could possibly be due to remaining chemokine being tightly bound to the alginate matrix, preventing its complete release on this timescale.

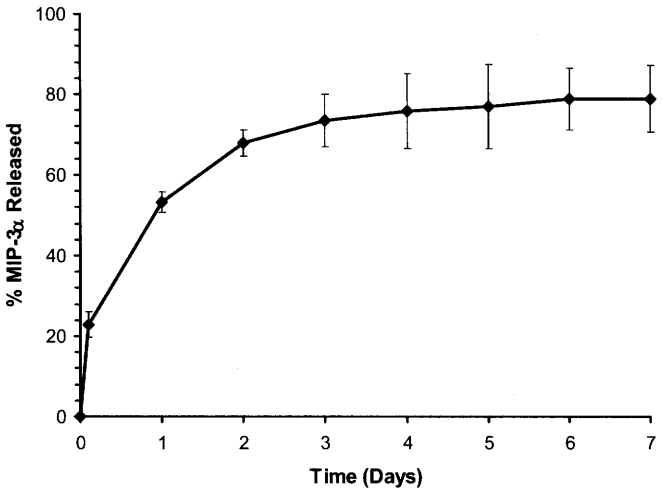

Figure 4.3. Release profile of CCL20 from alginate microparticles in complete RPMI medium at 37 °C.

Dendritic cells are highly phagocytic and avidly take up particulate antigen by phagocytosis. We hypothesized that dendritic cells might extract antigen-loaded hydrogel nanoparticles from alginate microparticles by the process of phagocytosis. In order to study uptake of hydrogel nanoparticles by DCs from the interior of alginate microparticles, we incubated DCs with alginate microparticles loaded with fluorescent DQ-ova-containing nanoparticles, and nanoparticle uptake was visualized using timelapse videomicroscopy. As shown in Figure 4.4, DCs that come into contact with alginate microspheres extended their processes to reach the interior of the microsphere and phagocytose fluorescent nanoparticles.

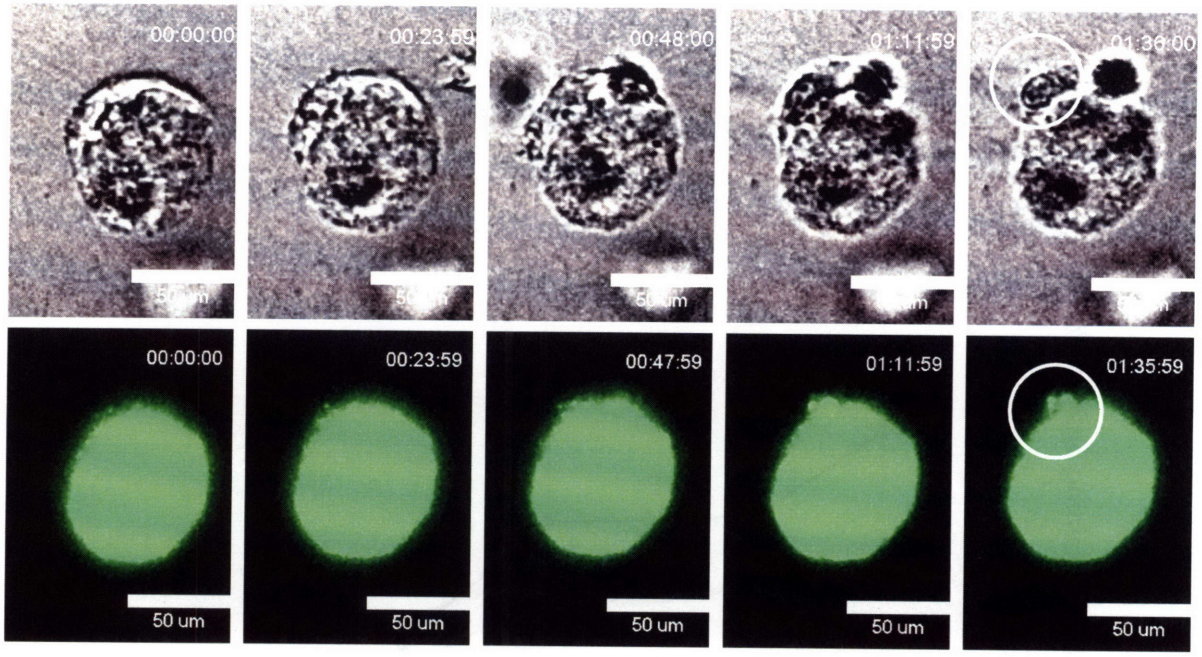

Figure 4.4. Uptake of DQ-ova-containing nanoparticles loaded in alginate microspheres by DCs visualized by timelapse videomicroscopy. Region where DC phagocytoses the nanoparticle is encircled.

To understand uptake of nanoparticles from alginate microspheres, we hypothesized that the access to the nanoparticles will be dependent on the mesh size of alginate carriers, which is a function of the cross-linking density of the alginate polymer chains. We thus studied the effect of the amount of calcium chloride used for cross-linking the alginate chains on the uptake of nanoparticles by dendritic cells. As shown in Figure 4.4, at low calcium chloride amounts (62.5 μg/mg sodium alginate), as many as 70% of maximal uptake of nanoparticles by dendritic cells (measured for DCs incubated in collagen with unencapsulated nanoparticles for the same time period) was observed after 24 h of culture; in addition, the encapsulation efficiency of nanoparticles was low. On the other hand, with 12.5 mg calcium chloride /mg sodium alginate, only 30% of maximal uptake of nanoparticles was observed. In the intermediate range of 0.25-2.5 mg calcium chloride/ mg sodium alginate, 50% of maximal uptake was observed after 24 h of culture. Plateauing of nanoparticle uptake in the calcium chloride amount of 0.25-2.5 mg/ mg sodium alginate is predicted since the RPMI medium used for washing

the microparticles contains ~10 mg/mL of calcium chloride, which results in the cross-linking of alginate polymers attaining equilibrium state. Based on these data, we decided to use 1 mg calcium chloride for microparticle formation.

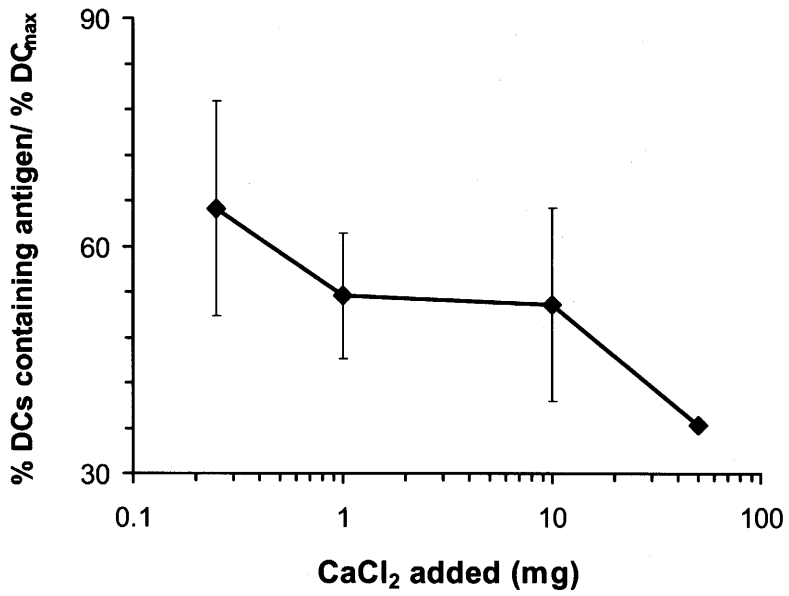

Figure 4.5. Antigen uptake by bone marrow dendritic cells from alginate microparticles synthesized using different amounts of calcium chloride.

4.3.2 Chemoattraction of dendritic cells to alginate microparticles

Immature dendritic cells have a high expression of CCR6 on their surface, which binds CCL20, resulting in migration of DCs in response to concentration gradients of the chemokine [14,88]. Alginate microparticles release CCL20 into their microenvironment, which by diffusion into the medium forms a gradient to chemoattract dendritic cells toward the individual microparticles.

Once a suitable chemokine gradient is formed in the collagen gel, dendritic cells from the surrounding environment of a given alginate microparticle will migrate toward it. However, DCs are known to exhibit a non-monotonic response to the dose of CCL20 [249] in modified Boyden chamber assays (Figure 2.2), with reduced chemotaxis at high chemokine concentrations. To determine the optimal dose of chemokine per microsphere for maximal DC chemoattraction, we used the collagen gel model and

analyzed the uptake of DQ-ova-containing nanoparticles by DCs interacting with alginate microparticles loaded with different quantities of CCL20 ranging from ~2.5 fg/microparticle to ~2.5 pg/microparticle. Bone marrow dendritic cells and alginate microparticles with different CCL20 loadings and fluorescent nanoparticles were suspended in 3D collagen gels as shown in Figure 4.6A, incubated for 24 hrs, followed by digestion of the matrix to recover the cells and analysis of fluorescent nanoparticle uptake by flow cytometry. As shown in Figure 4.6B, nanoparticle uptake by DCs increased as chemokine loading was increased from 2.5 fg/microparticle to 250 fg/microparticle followed by a decrease on further increasing the loading to 2500 fg/microparticle (Figure 4.6B). Thus, 250 fg/microparticle was found to be the optimal CCL20 loading and was used in subsequent experiments.

A.

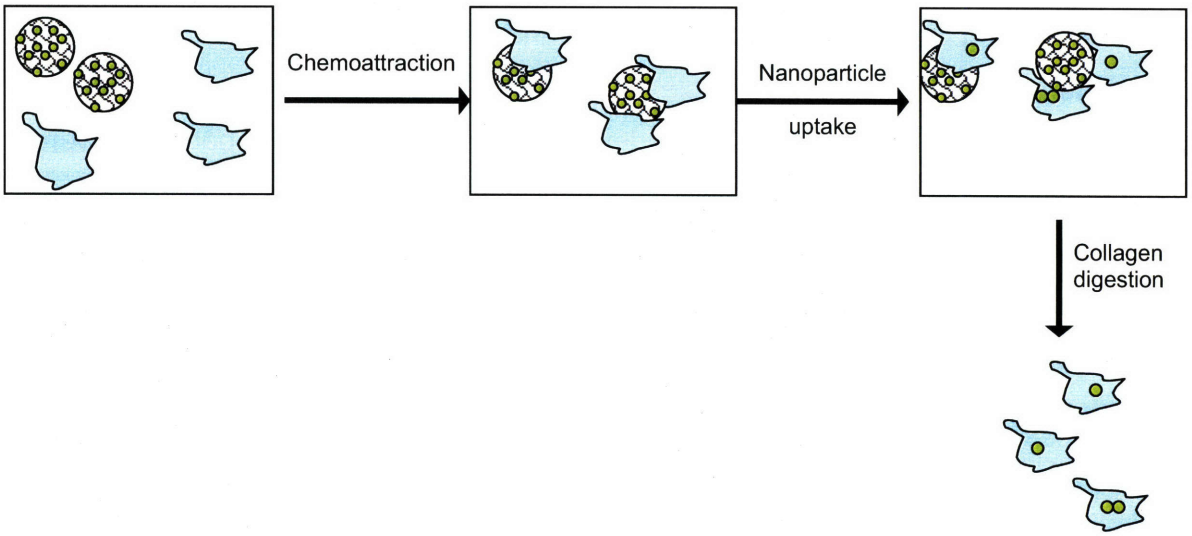

B.

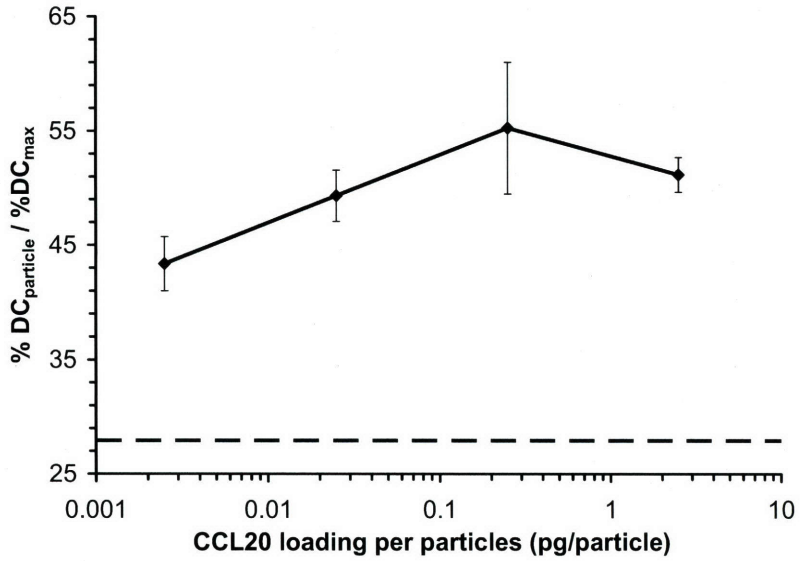

Figure 4.6. (A) Schematic diagram of bone marrow dendritic cell migration to alginate microparticles in 3D collagen gel set up. (B) Nanoparticle uptake by dendritic cells as a function of CCL20 loading per particle. Dashed line represents nanoparticle uptake with alginate microparticles without chemokine.

Using the optimized loading of CCL20 in alginate microparticles, we next visualized migration of bone marrow dendritic cells towards individual alginate microparticles by timelapse videomicroscopy using the same collagen gel assay. As

shown in images obtained from timelapse videomicroscopy (Figure 4.7A), dendritic cells in collagen are chemoattracted to a point source of chemokine. Microscopic examination at low magnification after 24 h of incubation showed formation of cell clusters around individual alginate microparticles throughout the collagen gel (data not shown). Analysis of the paths of motile cells in the vicinity of individual alginate microparticle revealed that dendritic cells within 200 μm of an alginate microsphere were concentrated at a single location due to chemoattraction (Figure 4.7B). In contrast, when control microparticles were used that contained the BSA carrier protein but no chemokine, dendritic cells migrated randomly in the vicinity of microspheres. Some dendritic cells that encountered alginate microparticles through random migration, however, stayed next to the microparticle for short durations compared to that with CCL20-loaded alginate microparticles. Further, dendritic cells migrated a mean distance of ~ 150 μm towards the alginate microparticles in response to the chemokine gradient, suggesting that dendritic cells can be attracted over significant distances (Figure 4.7C).

A.

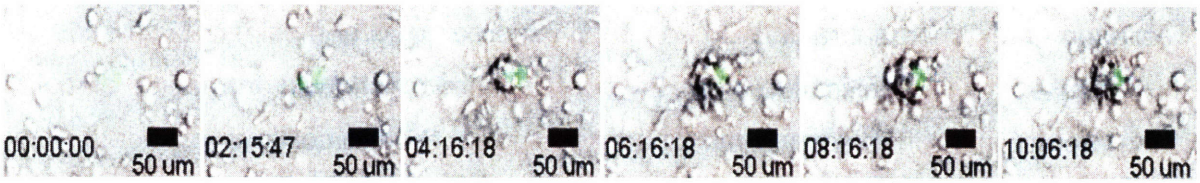

B.

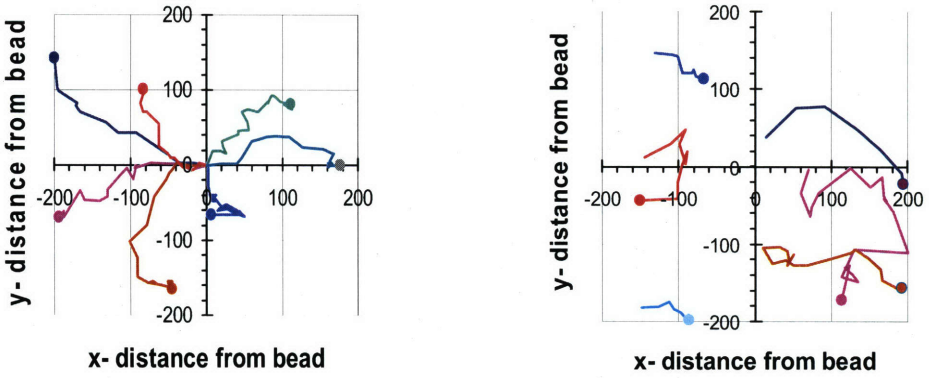

C.

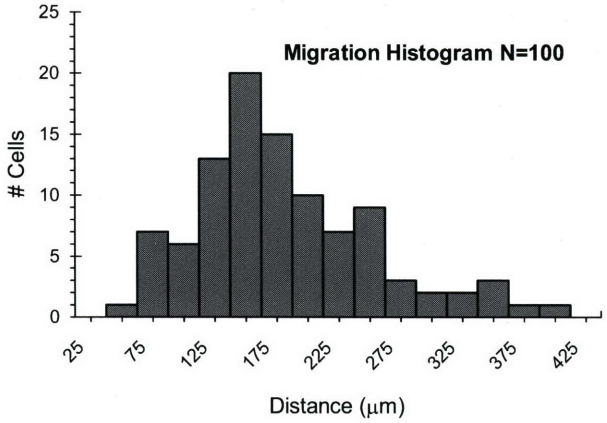

Figure 4.7. (A) Images from timelapse videomicroscopy of bone marrow dendritic cell migration to alginate microparticle in 3D collagen gel. Green fluorescence in the overlay derives from fluorescent ova-labeled nanoparticles in the alginate carriers. This example shows two alginate microcarriers near the center of the image. (B) Cell paths for migration in response to CCL20-loaded alginate microparticles (left) or control alginate microparticle (right) (C) Distribution of distances migrated by BMDCs in response to CCL20 gradients created by alginate microparticles in 3D collagen.

4.3.3 Enhanced antigen delivery to dendritic cells by 'reverse-targeting'

Concentration of dendritic cells around individual alginate microparticles increases the number of dendritic cells that have access to nanoparticles. This should result in increased antigen delivery to dendritic cells and also an increase in the number of dendritic cells receiving antigen. To test if that indeed was the case with alginate microparticles, we digested collagen gels after 24 h incubation, stained dendritic cells with anti-CD11c antibody, and analyzed uptake of DQ-ova-containing nanoparticles by flow cytometry. As shown in Figure 4.8A, alginate microparticles containing nanoparticles but no chemokine localized and retained nanoparticles very efficiently with only ~50% of dendritic cells in the culture containing antigen. However, when CCL20 was co-encapsulated inside the alginate microparticles, more than 70% of all cells in culture were observed to contain antigen resulting in ~200% increase in dendritic cell targeting due to reverse-targeting. In addition, dendritic cells were observed to contain 5-fold higher quantity of antigen per cell due to reverse-targeting of DCs than when chemokine was absent (Figure 4.8B). In comparison to these, when nanoparticles were suspended uniformly in collagen gel making them accessible to all cells in culture, ~75% cells contained nanoparticles. This confirms our hypothesis that 'reverse-targeting' of dendritic cells by co-delivering CCL20 and antigen-loaded nanoparticles could enhance antigen delivery to dendritic cells.

A.

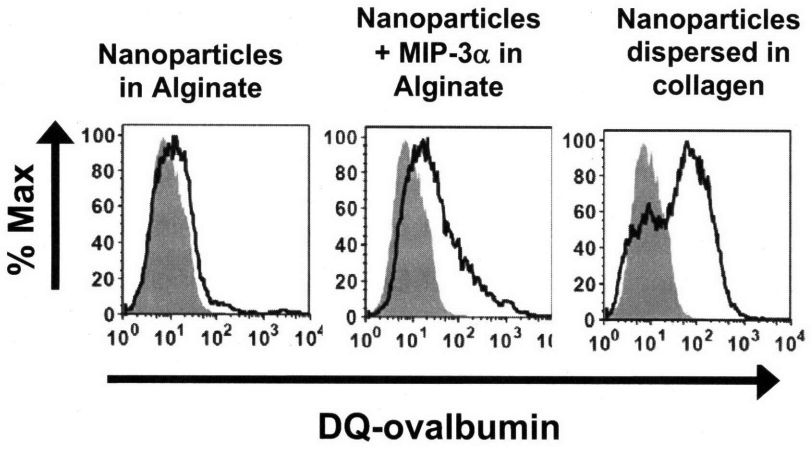

B.

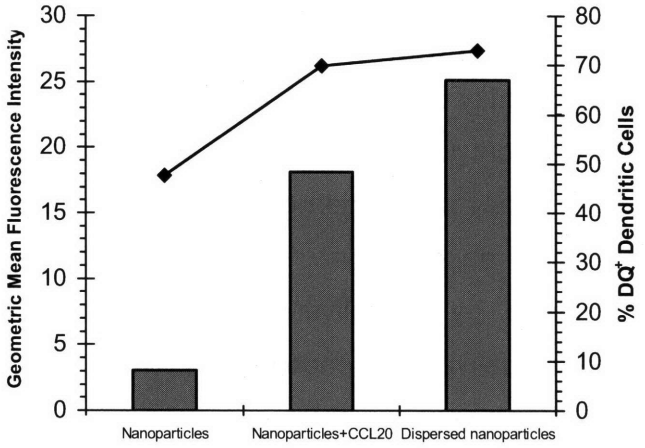

Figure 4.8. (A) Nanoparticle uptake by CD11c$^+$-BMDCs in collagen after 24 h culture when incubated with alginate microparticles containing DQ-ova-containing nanoparticles with or without CCL20. (B) Mean Fluorescence Intensity of BMDCs (histograms) and percentage of CD11c$^+$ BMDCs containing antigen (line).

Next, we looked at enhanced delivery of antigen when microparticle: cell ratio was varied to study if similar enhancement is observed for a range of microparticle doses. As shown in Figure 4.9A, antigen delivery to dendritic cells was significantly higher in case of CCL20-loaded alginate microparticles compared to the alginate

microparticles that did not contain the chemokine. We looked at CD86 expression of cells containing CpG-coated nanoparticles to see if increased uptake of nanoparticles results in effective maturation of dendritic cells. As nanoparticle dose was increased, the percentage of dendritic cells containing high levels of DQ-ova-containing nanoparticles and high CD86 expression increased and was consistently significantly higher for CCL20-loaded alginate microparticles than for control microparticles (Figure 4.9B). As expected, at high alginate carrier: DC ratios, chemoattraction had little effect on the frequency of DCs internalizing nanoparticles. Alginate microparticles containing CCL20 and BSA only did not cause any CD86 upregulation indicating that alginate polymer or chemokines did not mature the DCs.

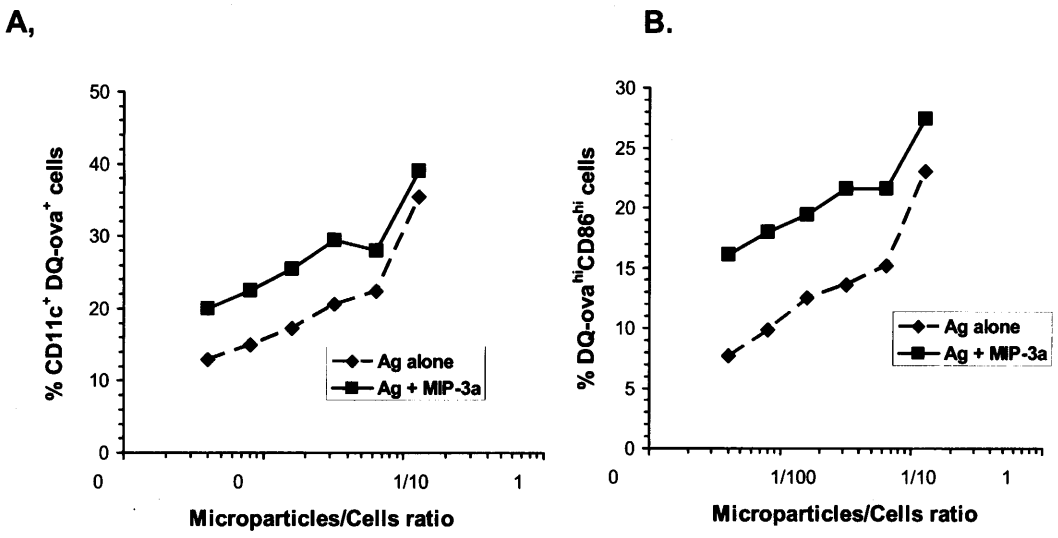

Figure 4.9. Flow cytometry analysis of dendritic cells after 24 h culture in collagen gel with different doses of alginate microparticles with or without CCL20 for (A) antigen uptake and (B) DC maturation.

4.3.4 Selective delivery of antigen to dendritic cells by 'reverse-targeting'

Dendritic cells are the only antigen presenting cells known to activate naïve T cells [5,54]. Therefore, it is desired that in clinical application, most antigen is delivered to the dendritic cells while minimizing antigen uptake by other phagocytic cells present in tissues such as macrophages and neutrophils. Reverse-targeting of dendritic cells was hypothesized to attract dendritic cells preferentially towards alginate microparticles

and in the process increase the antigen delivery selectively to dendritic cells. To demonstrate this concept, we co-cultured equal numbers of bone marrow-derived macrophages (0.5 $x10^5$ cells/mL) and BMDCs (0.5 $x10^5$ cells/mL) in collagen gel with alginate microparticles and analyzed nanoparticle uptake by each cells type by timelapse videomicroscopy. BMDCs were labeled with 0.5 μM CFSE and BMDMs with 5 μg/mL Fura-2 dye, and were mixed 1:1 in collagen gel along with Alexa fluor 647-ova-containing hydrogel nanoparticles-loaded alginate microparticles. As shown in images obtained from timelapse videomicroscopy during the first 3 h (Figure 4.10A), dendritic cells were preferentially attracted towards alginate microparticles and macrophages due to random migration did not get access to alginate microparticles during the course of experiment. During 3 h, as many as 8 BMDCs were observed to be localized around single alginate microparticles compared to only 2 BMDMs in the same period of time, as also shown in cell paths plots for BMDCs and BMDMs migrating in response to alginate microparticles loaded with CCL20 (Figure 4.10B). This observation suggests that by combining controlled release of chemokine with delivery of antigen by means of nanoparticles, we were not only able to achieve enhanced delivery of antigen to dendritic cells but selective delivery as well. This selectivity will be of significant importance in physiological situation where dendritic cells being rare may not be able to compete with other phagocytes, but reverse-targeting of dendritic cells can increase the delivery of antigen to the dendritic cells relative to other non-responding cells.

A.

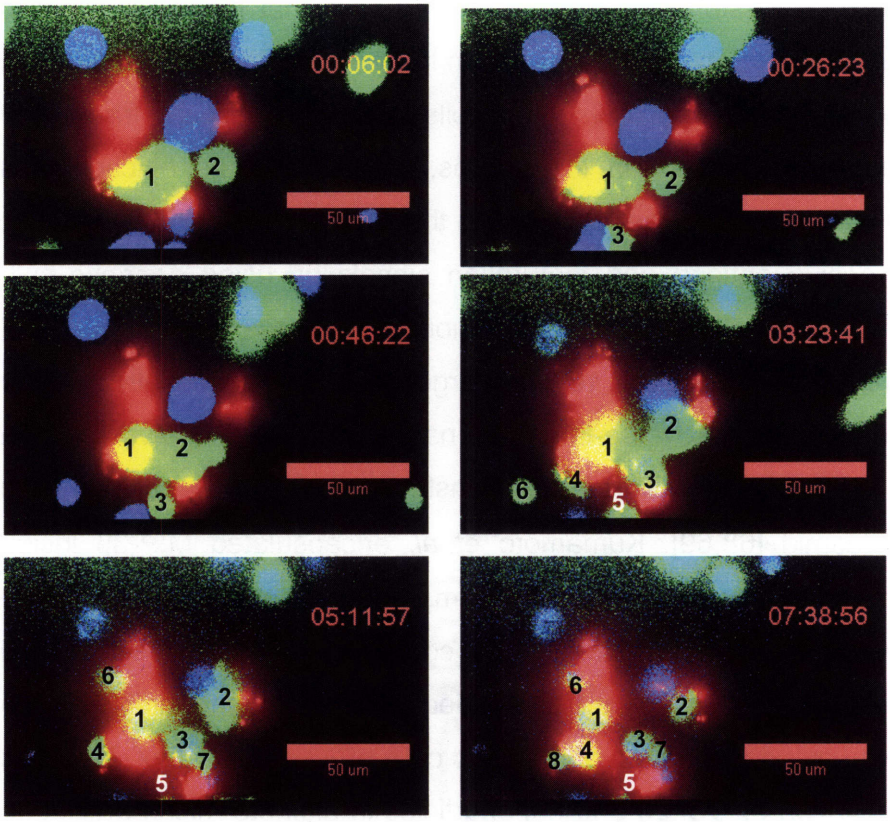

B.

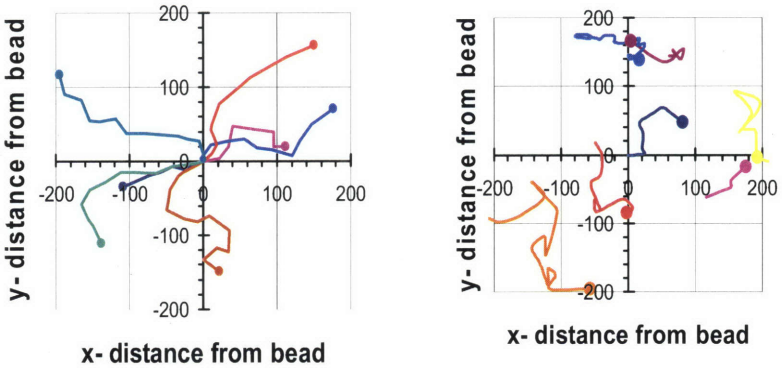

Figure 4.10. (A) Images from timelapse videomicroscopy for migration of dendritic cells towards alginate microparticles (red) by CCL20 in a co-culture of macrophages (blue) and dendritic cells (green). (B) Cell paths of BMDCs (left) and BMDMs (right) in response to CCL20-containing alginate microparticle placed at origin.

4.4 Discussion

Dendritic cells are professional antigen presenting cells that play a key role in immune system activation during an infection [5,54]. In homeostatic state, dendritic cells are present at a low frequency of < 1% of all cells, with a significant fraction of macrophages and neutrophils present in the tissues. To improve the efficacy of a vaccine, it is therefore necessary to target vaccines to the dendritic cells [250]. Dendritic cells can selectively receive antigen and maturation signals by using dendritic cell-specific targeting ligand such as DEC205-ova, as demonstrated in the past [24,149,226]. However, we explored the ability of reverse-targeting to preferentially deliver nanoparticles to dendritic cells. Reverse-targeting has been used *in* vivo through intratumoral injection [42] of chemokine and transfection of tumor cells with a chemokine-encoding plasmid [68,69]. Kumamoto *et al.* encapsulated MIP-3β inside poly(thylene-*co*-vinyl) acetate rods and implanted them in mice to chemoattract mature dendritic cells that were then loaded with antigen contained in another similar rod [40,41]. In order to reverse-target DCs, we first needed to localize nanoparticles in an injectable matrix followed by concentration of dendritic cells around the matrix. This was achieved by co-encapsulation of CCL20 and nanoparticles in alginate microparticles to reduce access of cells distributed in the tissue to nanoparticles, and then provide access to cells in immediate vicinity of microparticles, which were primarily dendritic cells through the process of reverse-targeting.

In order to specifically target dendritic cells and to deliver antigen to these cells, we developed microparticles using a polysaccharide, alginate to co-deliver a chemokine specific to immature dendritic cells, CCL20 and antigen-loaded nanoparticles. Alginate is produced by various algae and certain bacteria that use this biopolymer to form a capsule and protect the cells from unfavorable environmental conditions [251,252]. Alginate has also been proposed to be the cause of resistance to drugs and immune response to a pathogen since it helps bacteria attach to basement membranes and also hides the pathogen's antigens and surface molecules [253]. Alginate has been used for various tissue engineering and biotechnology applications such as for encapsulation of cells [254,255] and proteins in alginate matrices [243,251]. Alginate is a biodegradable and biocompatible polymer with few side effects. Alginate has also been proposed to

modulate immune response and has been shown to act as adjuvant in some studies. Alginate polymer chains containing high mannuronic content cause activation of macrophages resulting in secretion of inflammatory cytokines [256,257] though use of alginate films was shown not to cause any DC maturation [258]. Similarly, alginate polymer obtained from bacterial sources should be tested for endotoxin content due to possibility of endotoxin presence in the alginate sample. Alginate is generally available in a water-soluble form of sodium alginate; on addition of calcium to the alginate solution, sodium is displaced and guluronic acid monomers cross-link between alginate polymer chains to form an egg-box shape resulting in phase separation of calcium alginate [255]. Alginate particles are usually formed by dropping sodium alginate solution into an aqueous calcium chloride bath resulting in particles in the size range of 0.5-2 mm [251]. However, for making our vaccine injectable, we designed a water-in-oil strategy modified from a previously reported protocol [243] to form microparticles. Alginate microparticles thus formed were ~20 μm mean diameter and encapsulated nanoparticles and chemokine with high efficiency. We observed that microparticle size could be easily modulated by changing the surfactant content or by changing the homogenization speed during microparticle synthesis. The encapsulated nanoparticles were well-retained and were not observed to be released in complete RPMI medium at 37 ^{o}C for a week. In contrast, CCL20 was released at a controlled rate for 4-5 days, which would be sufficient for targeting significant number of dendritic cells based on previous studies.

We studied dendritic cell responses to alginate microparticles by culturing DCs with alginate microparticles in collagen. The density of nanoparticles per alginate microparticle was chosen for all our experiments as cell: microparticle ratio of 30: 1; based on encapsulation of nanoparticles in alginate microparticles, this cell: microparticle density corresponds to each dendritic cell getting an average of 50 nanoparticles assuming all dendritic cells receive antigen. It has been shown in the past that dendritic cells when incubated with ~1 μm-sized particles can internalize up to ~100 particles/cell [115], and using the density used in our experiments, we can provide maximal quantities of antigen to each dendritic cell. We observed dendritic cell migration towards alginate microparticles using timelapse videomicroscopy. Microscopic

examination of DC migration revealed that dendritic cells migrated to the microparticles from distances ranging from 50 μm to 400 μm with a mean distance migrated of 150 μm. Dendtitic cells were observed to start migrating within 1 h of setting up collagen gels and migration continued for up to 5-6 h; DC migration after 6 h was markedly reduced thereafter. Reduced migration at later time could be due to chemokine gradients from neighboring particles beginning to overlap thereby confusing the DCs in the process or due to internalization of surface chemokine receptors are reduced response of cells to chemokine gradients. Dendritic cells that migrated to the microparticles stayed attached to the microparticle surface with few cells observed to extract nanoparticles from the inside of alginate microparticle. During the course of microscopy, few cells were also observed to leave the microparticle surface and migrate away from the particle. This was possibly a result of CpG-induced maturation of dendritic cells upon uptake of CpG-coated nanoparticles, resulting in downregulation of the immature dendritic cell chemokine receptor, CCR6 [54]. In the culture, nearly 50% of cells were immotile or less motile whereas the more motile cells were mostly observed to migrate to the alginate microparticles. This is not unexpected as BMDC cultures contain contaminating granulocytes, neutrophils, and macrophages that do not respond to CCL20. Based on CD11c staining of cells, these cells form ~30% of the population in the culture after 7 days of culturing bone marrow progenitor cells, which possibly formed the immotile or less motile cell population observed by microscopy. Cell clusters formed around CCL20-loaded alginate microparticles varied in size ranging from 3-10 cells per cluster. In contrast, fewer dendritic cells (~1-5 cells/cluster) were observed localized around alginate microparticles lacking chemokine.

An increased presence of dendritic cells around alginate microparticles resulted in an enhanced delivery of nanoparticles to the DCs. DCs could be brought directly to the surface of microparticles from where they could extract the nanoparticles containing antigen and CpG oligonucleotides. An increase in number of dendritic cells containing antigen by ~150% was observed in our experiments, and a significant fraction of cells contained 2-3 times more antigen when CCL20-loaded microparticles were used compared to control microparticles. Nanoparticles delivered antigen that was processed and presented on DC surface and CpG oligonucleotides caused activation of DCs.

Together, alginate microparticles increased the number of effectively activated DCs for a strong subsequent T cell activation. When dendritic cells and macrophages were co-cultured with CCL20-loaded alginate microparticles, macrophages were observed to migrate randomly in collagen whereas dendritic cells migrated selectively towards alginate microparticles thereby increasing the fraction of DCs in the immediate microenvironment of alginate microparticles. By analyzing uptake of uniformly dispersed hydrogel nanoparticles in collagen, we found that dendritic cells and macrophages are nearly equally phagocytic; however, concentration of dendritic cells at the surface of microparticles can help deliver antigen and maturation signals to dendritic cells selectively and at higher doses.

Alginate microparticles can also be used to mimic and study dendritic cell responses to a pathogen *in vitro* and *in vivo*. Chemokine release from microparticles mimics inflammatory signals at site of infection, and sub-micron sized nanoparticles closely mimic a pathogen by means of surface-displaying antigenic epitopes and Toll like receptor ligands. Co-encapsulation of different chemokines can be used to modulate dendritic cell trafficking and control the kinetics of immune response suitably. Further, alginate being mucoadhesive [259] has a potential as a vaccine carrier for various modes of delivery, and has been tested for oral [260,261] and nasal vaccination [259,262] in some previous studies.

Cellular organization is an important aspect of organogenesis and tissue engineering. Various morphogens have been proposed to form concentration gradients and control differentiation and cell organization in three dimensions [263,264]. Controlled release of chemokine using microparticles can be used to study cell differentiation and tissue organization, and can thus be used for various tissue engineering applications.

4.5 Conclusions

Alginate microparticles were synthesized by using a single emulsion technique to co-encapsulate CCL20 and hydrogel nanoparticles containing antigen and DC maturation signal with very high encapsulation efficiency. Co-encapsulation created a point source for chemokine and antigen; dendritic cells were chemoattracted to the

alginate microparticles and then were delivered nanoparticles to deliver and antigen and maturation signal in concert. Reverse-targeting of dendritic cells resulted in concentration of dendritic cells around alginate microparticles, which enhanced the delivery of antigen to dendritic cells by 2-3 fold and selectively delivered antigen to dendritic cells. Reverse-targeting not only provides an ultra-localized strategy for targeting dendritic cells in contrast to searching for dendritic cells for targeted delivery of antigen in a larger volume of a tissue but can also be used in tissue engineering for organogenesis and cell differentiation.

5. Summary and Future Work

5.1 Summary of results

Vaccines – therapeutic and prophylactic – are sought for a variety of diseases such as HIV, influenza, and tuberculosis that require recruitment of both humoral and cellular arms of the immune system. Currently, most commercially-available vaccines are based on live or attenuated bacteria or viruses, which have been successful in cases of certain infections, but are often associated with the risk of pathogenicity. Multi-subunit vaccines are therefore believed to address the toxicity/pathogenicity issue with the current vaccines while priming the immune system against the antigens of interest effectively. The immune system has evolved over time to mount a strong response against pathogens by means of cellular intermediates such as dendritic cells. These cells phagocytose pathogens avidly, process the pathogen-associated antigens, and receive maturation signals in the form of pathogen-associated molecular patterns. We developed a pathogen-mimetic multi-subunit vaccine to take advantage of the efficiency of the immune system to act against bacteria. Alginate-based carrier microparticles were synthesized to encapsulate the immature dendritic cell-specific chemokine CCL20 and antigen-containing hydrogel nanoparticles. The microspheres were ~20 μm mean diameter whereas nanoparticles were ~500 nm in size. The gross structure of this

system closely represents the physiological state during an infection; chemokine release from alginate microspheres represented inflammatory signals in response to a pathogen, whereas nanoparticles mimicked a pathogen through co-display of antigen epitopes and TLR ligands on surface. Because this system is designed to elicit a cascade of responses mimicking early events following infection, the system might be used as an *in vitro* model to study dendritic cell responses during infection. We demonstrated *in vitro* that through controlled release of CCL20, dendritic cells could be chemoattracted specifically up to the point of contact with alginate microspheres, where DCs extracted antigen-loaded nanoparticles from the interior of microspheres. Chemoattraction of dendritic cells not only increased the number of dendritic cells receiving antigen and TLR ligands on nanoparticles, but also increased the antigen dose received by each DC. DCs upon phagocytosis of hydrogel nanoparticles process the encapsulated antigen in their endosomal compartments and present the antigen on MHC class II molecules for presentation to $CD4^+$ T cells. Nanoparticles were observed to also induce effective cross-presentation of dendritic cells and consequently MHC class I presentation of antigen for $CD8^+$ T cell priming. Co-display of antigen and TLR 9 ligand on the surface of nanoparticles resulted in strong maturation of DCs causing secretion of pro-inflammatory cytokines and upregulation of MHC and co-stimulatory molecules. *In vivo*, CpG-coated nanoparticles activated B cells, and IgG could be detected as early as 1 week post-immunization of wild-type mice. The anti-ovalbumin IgG titers rose quickly during the duration of the experiment (7 weeks) reaching levels comparable to that with ova in CFA. CpG-coated nanoparticles were shown to activate $CD4^+$ and $CD8^+$ naïve T cells in draining lymph nodes and spleen, and a significantly higher ova-specific CTL frequency in splenocyte population of the immunized mice. In addition to short term immunity, we also tested for a long term memory $CD8^+$ T cell response, which was observed to be comparable to that with ova in CFA and higher than that when nanoparticles were co-delivered with soluble CpG.

Based on these studies, we conclude that particulate system for delivery of antigen and TLR ligands is significantly more effective than delivery of antigen and TLR ligands in soluble form. However, we studied only CpG in these studies which acts in the endosomes of dendritic cells, and therefore, it remains an interesting open question

whether immunostimulatory ligands targeting surface-expressed TLR receptors (e.g., TLR4) would elicit different responses. We also found that co-display of antigen and TLR ligands on the surface of nanoparticles was significantly more effective in activation of T cells *in* vivo than delivery of antigen as nanoparticles along with soluble CpG. Current vaccination strategies involve co-injection of antigen and adjuvants in soluble form; we propose, that co-delivery of antigen and an adjuvant on a single particle can boost immune responses several fold. Dendritic cells are the only cells capable of priming naïve T cells and DCs are significantly superior to other APCs in antigen processing and presentation. It is therefore desired to target antigen to DCs for a stronger immune response. To achieve this objective, recent studies by other groups have shown that by use of antigen conjugated to a targeting ligand such as CpG or DEC205, antigen delivery to dendritic cells and resulting *in vivo* responses can be enhanced manifold [24,149,152,153,226]. In parallel, other studies have demonstrated complete tumor regression by employing chemoattraction of dendritic cells to the tumors by means of using chemokine-encoding plasmid-transfected tumor cells [42,67] or controlled release of mature dendritic cell-specific chemokine [40,41]. We created a system that chemoattracted dendritic cells to the individual microparticles where the DCs received antigen- and TLR9 ligand-containing nanoparticles. Selective and enhanced antigen delivery to DCs is expected to enhance the immune responses to antigen of interest compared to delivery of antigen alone.

The system developed in this work may be used for several applications ranging from the study of DC trafficking to improved vaccines and tissue engineering. Labeled nanoparticles can be used for studying DC trafficking and the kinetics of B cell and T cell activation in vivo. Intravital imaging is used for studying processes occurring inside lymph nodes, and the same technique may be employed for studying the processes that occur at the site of infection. Chemokine delivery may be used for modulating DC trafficking and control DC attraction of emigration, and understanding the role of different chemokines at different stages of immune response. Chemokines have been found to be involved in a variety of processes such as organogenesis, inflammation, angiogenesis, metastasis, and autoimmune diseases. The system described here, which allows modulation of chemokine gradients, can be used to unravel a wealth of

information regarding how certain cells respond differently and may be controlled for clinical applications. As described earlier, this system can be used as an effective vaccine especially in cases of diseases where no characteristic epitope is currently known. For example, we propose that tumor lysates may be encapsulated in hydrogel nanoparticles and these nanoparticles coated with TLR ligands such as CpG or poly(I:C) for priming the immune system to tumor-associated antigens. Conversely, self-antigens may be delivered in conjunction with immunosuppressive signals to induce a tolerance to the specific antigens or cell lysates to treat autoimmune diseases. In order to enhance the 'clinicability' of our vaccine, a biocompatible and biodegradable vaccine is highly desired. Presently, all the components of our vaccine are biocompatible and did not show acute toxicity *in vitro* or *in vivo*. However, hydrogel nanoparticles are nondegradable but can be made biodegradable using several strategies proposed in the literature and as mentioned in Chapter 3.

This system also has several applications beyond the realm of immunology. Concentration gradients of ligands play roles in tissue engineering [265], embryonic development [263], and organogenesis [266]. Modulation of these gradients can not only help understand these systems in great detail but also form basis for various therapies. Such a system may also be used for arranging cells of interest in a specific pattern by surface-patterning the chemokine-releasing microspheres. The all-aqueous synthesis of protein-encapsulating nanoparticles can also have applications in delivery of sensitive proteins and other biologics. Hormones, cytokines, growth factors, siRNA, and peptides are some of the therapeutics that may be delivered without risking loss of activity using the nanoparticles. Such a system for ultra-localized delivery of encapsulated molecules along with chemoattraction of cells of interest may be applied to medical devices as well. An example in this regard is a drug-eluting stent. Restenosis is often caused by faster infiltration and proliferation of smooth muscle cells (SMC) compared to endothelial cells. Current stent designs inhibit SMC proliferation but these drugs have their associated side-effects. Instead, chemoattraction of endothelial cells to the site of implantation may accelerate the process of healing with reduced restenosis rates.

Thus, the hydrogel-based system proposed here is highly applicable in a variety of biological subsystems, and may be advantageous due to the biomimickry it brings in to therapy designed with the system. The vaccine may be further improved for better efficacy by making it biodegradable and by studying the effect of combination of chemoattractants encapsulated in the alginate microparticles.

5.2 List of Research Publications and Conference Presentations

5.2.1 Research Publications

1. Jain, S., Navot, B., Wang, Y.Y. and Irvine, D.J., Ultra-localized delivery of antigen by reverse-targeting of dendritic cells using hydrogel microparticles (in preparation, 2006).
2. Jain, S., Navot, B., Yap, W.T., Horrigan, E.M., Statile, J.K. and Irvine, D.J., Mimicking pathogen structure by surface-displayed TLR ligands and protein antigen epitopes on antigen-carrying hydrogel nanoparticles (in preparation, 2006).
3. Jain, S., Yap, W.T. and Irvine, D.J., Synthesis of protein-loaded hydrogel particles in an aqueous two-phase system for coincident antigen and CpG oligonucleotide delivery to antigen-presenting cells, *Biomacromolecules*, **6**, 2590-2600 (2005).
4. Zhao, X.J.*, Jain, S.*, Larman, H., Gonzalez, S. and Irvine, D.J., Directed migration of monocytes and dendritic cells via chemoattractants released from degradable microspheres, *Biomaterials*, **26**, 5048-5063 (2005).
5. Irvine, D.J., Stachowiak, A. and Jain, S., Engineering materials for control of immune functions, *Mat. Res. Forum*, **426-432**, 3213-3218 (2003)

5.2.2 Conference Presentations

1. Jain, S., Yap, W.T. and Irvine, D.J., Synthesis of hydrogel based vaccine to mimic dendritic cell responses to a viral infection, *Material Res. Soc.* (Nov 2005).
2. Jain, S. Yap, W.T., Gonzalez, S. and Irvine, D.J., Rational design of a vaccine for chemoattraction and 'programming' of dendritic cells, *MEDI2005 Conference on Medical Technologies* (Oct 2005).

3. Jain, S., Irvine, D.J., Yap, W.T. and Huang, Y.-C., Colloidal micelles as multisubunit vaccines, *230th National ACS Meeting* (Aug 2005).
4. Jain, S., Zhao, X.J., Yap, W.T., Gonzalez, S. and Irvine, D.J., Micro- and nano-particle-based composite delivery of chemokine, antigen, and maturation factors as a tool to modulate dendritic cell trafficking and function, *Keystone Symposium on "Leukocyte Trafficking: Cellular and Molecular Mechanism"* (Feb 2005).
5. Jain, S., Zhao, X.J., Yap, W.T., Gonzalez, S. and Irvine, D.J., Rational design of a vaccine for chemoattraction and 'programming' of dendritic cells, *Conference on Experimental Biology, FASEB* (Apr 2004).
6. Jain, S. and Irvine, D.J., Design of hydrogel-based antigen delivery particles for dendritic cell activation, *Material Res. Soc.* (Dec 2003).
7. Jain, S. and Irvine, D.J., Design of a novel vaccine via spatial and temporal control of dendritic cell activation, *Soc. for Biomaterials* (May 2003).

6. References

1 Abbas, A.K., Lichtman, A.H. & Pober, J.S. *Cellular and molecular immunology*, W.B. Saunders, Philadelphia, 2000. vii, 553 p.

2 Abbas, A.K. & Lichtman, A.H. *Basic immunology : functions and disorders of the immune system*, W.B. Saunders, Philadelphia, 2004. ix, 322 p.

3 Roitt, I.M., Brostoff, J. & Male, D.K. *Immunology*, Mosby, Edinburgh ; New York, 2001. 480 p.

4 http://www.uta.fi/imt/ramet/figure1.html.

5 Banchereau, J. & Steinman, R.M. Dendritic cells and the control of immunity. Nature 1998; 392(6673): 245-252.

6 Santambrogio, L., Pakaski, M., Wong, M.L. *et al.* Antigen presenting capacity of brain microvasculature in altered peptide ligand modulation of experimental allergic encephalomyelitis. Journal of Neuroimmunology 1999; 93(1-2): 81-91.

7 Santambrogio, L., Sato, A.K., Carven, G.J., Dorf, M.E., Strominger, J.L. & Stern, L.J. Extracellular antigen processing and presentation by dendritic cells. Journal of Investigative Dermatology 2000; 114(1): 214-214.

8 Heath, W.R. & Carbone, F.R. Cross-presentation, dendrttic cells, tolerance and immunity. Annual Review of Immunology 2001; 19 47-64.

9 Rodriguez, A., Regnault, A., Kleijmeer, M., Ricciardi-Castagnoli, P. & Amigorena, S. Selective transport of internalized antigens to the cytosol for MHC class I presentation in dendritic cells. Nature Cell Biology 1999; 1(6): 362-368.

10 Shen, Z.H., Reznikoff, G., Dranoff, G. & Rock, K.L. Cloned dendritic cells can present exogenous antigens on both MHC class I and class II molecules. Journal of Immunology 1997; 158(6): 2723-2730.

11 Guermonprez, P., Saveanu, L., Kleijmeer, M., Davoust, J., van Endert, P. & Amigorena, S. ER-phagosome fusion defines an MHC class I cross-presentation compartment in dendritic cells. Nature 2003; 425(6956): 397-402.

12 http://www.mc.vanderbilt.edu/microbio/vankaer/mhc.html.

13 Immunology, G. & University, N. http://www.karpuslab.northwestern.edu/GraduateImmunology2003ChemokineLecture.ppt.

14 Perez-Canadillas, J.M., Zaballos, A., Gutierrez, J. *et al.* NMR solution structure of murine CCL20/MIP-3 alpha, a chemokine that specifically chemoattracts immature dendritic cells and lymphocytes through its highly specific interaction with the beta-chemokine receptor CCR6. Journal of Biological Chemistry 2001; 276(30): 28372-28379.

15 Yang, D., Chertov, O., Bykovskaia, N. *et al.* beta-defensins: Linking innate and adaptive immunity through dendritic and T cell CCR6. Science 1999; 286(5439): 525-528.

16 Sozzani, S., Sallusto, F., Luini, W. *et al.* Migration of Dendritic Cells in Response to Formyl Peptides, C5a, and a Distinct Set of Chemokines. Journal of Immunology 1995; 155(7): 3292-3295.

17 Le, Y.Y., Yang, Y.M., Cui, Y.H. *et al.* Receptors for chemotactic formyl peptides as pharmacological targets. International Immunopharmacology 2002; 2(1): 1-13.

18 Yang, D., Chen, Q., Stoll, S., Chen, X., Howard, O.M.Z. & Oppenheim, J.J. Differential regulation of responsiveness to fMLP and C5a upon dendritic cell maturation: Correlation with receptor expression. Journal of Immunology 2000; 165(5): 2694-2702.

19 Forster, R., Schubel, A., Breitfeld, D. *et al.* CCR7 coordinates the primary immune response by establishing functional microenvironments in secondary lymphoid organs. Cell 1999; 99(1): 23-33.

20 Kirschning, C.J. & Bauer, S. Toll-like receptors: cellular signal transducers for exogenous molecular patterns causing immune responses. International Journal of Medical Microbiology 2001; 291(4): 251-260.

21 Lenz, P., Day, P., Pang, Y., Lowy, D. & Schiller, J. Papillomavirus-like particles cause dendritic cell maturation and induce a potent in vitro primary immune response. Journal of Investigative Dermatology 2001; 117(2): 450-450.

22 Pulendran, B. Modulating vaccine responses with dendritic cells and Toll-like receptors. Immunological Reviews 2004; 199(1): 227-250.

23 Marshak-Rothstein, A., Busconi, L., Rifkin, I.R. & Viglianti, G.A. The stimulation of Toll-like receptors by nuclear antigens: a link between apoptosis and autoimmunity. Rheumatic Disease Clinics of North America 2004; 30(3): 559-+.

24 Bonifaz, L., Bonnyay, D., Mahnke, K., Rivera, M., Nussenzweig, M.C. & Steinman, R.M. Efficient targeting of protein antigen to the dendritic cell receptor DEC-205 in the steady state leads to antigen presentation on major histocompatibility complex class I products and peripheral CD8(+) T cell tolerance. Journal of Experimental Medicine 2002; 196(12): 1627-1638.

25 Burton, D.R. Antibodies, viruses and vaccines. Nature Reviews Immunology 2002; 2(9): 706-713.

26 Burton, D.R. & Parren, P.W.H.I. Vaccines and the induction of functional antibodies: Time to look beyond the molecules of natural infection? Nature Medicine 2000; 6(2): 123-125.

27 Letvin, N.L. Strategies for an HIV vaccine. Journal of Clinical Investigation 2002; 110(1): 15-20.

28 Letvin, N.L., Bloom, B.R. & Hoffman, S.L. Prospects for vaccines to protect against AIDS, tuberculosis, and malaria. Jama-Journal of the American Medical Association 2001; 285(5): 606-611.

29 Baba, T.W., Jeong, Y.S., Penninck, D., Bronson, R., Greene, M.F. & Ruprecht, R.M. Pathogenicity of Live, Attenuated Siv after Mucosal Infection of Neonatal Macaques. Science 1995; 267(5205): 1820-1825.

30 Murpheycorb, M., Martin, L.N., Davisonfairburn, B. *et al.* A Formalin-Inactivated Whole Siv Vaccine Confers Protection in Macaques. Science 1989; 246(4935): 1293-1297.

31 Stott, E.J., Kitchin, P.A., Page, M. *et al.* Anti-Cell Antibody in Macaques. Nature 1991; 353(6343): 393-393.

32 Moore, A., McGuirk, P., Adams, S. *et al.* Immunization with a soluble recombinant HIV protein entrapped in biodegradable microparticles induces HIV-specific CD8(+) cytotoxic T lymphocytes and CD4(+) Th1 cells. Vaccine 1995; 13(18): 1741-1749.

33 Berman, P.W., Gregory, T.J., Riddle, L. *et al.* Protection of Chimpanzees from Infection by Hiv-1 after Vaccination with Recombinant Glycoprotein Gp120 but Not Gp160. Nature 1990; 345(6276): 622-625.
34 Egan, M.A., Charini, W.A., Kuroda, M.J. *et al.* Simian immunodeficiency virus (SIV) gag DNA-vaccinated rhesus monkeys develop secondary cytotoxic T-lymphocyte responses and control viral replication after pathogenic SIV infection. Journal of Virology 2000; 74(16): 7485-7495.
35 Penichet, M.L. & Morrison, S.L. Antibody-cytokine fusion proteins for the therapy of cancer. Journal of Immunological Methods 2001; 248(1-2): 91-101.
36 Fukao, T. Dendritic-cell-based anticancer vaccination: has it matured? Trends Immunol 2002; 23(5): 231-232.
37 Crooke, S.T. Molecular mechanisms of action of antisense drugs. Biochimica Et Biophysica Acta-Gene Structure and Expression 1999; 1489(1): 31-44.
38 Riddell, S.R. & Greenberg, P.D. Principles for Adoptive T-Cell Therapy of Human Viral Diseases. Annual Review of Immunology 1995; 13 545-586.
39 Polyak, S., Chen, H.C., Hirsch, D., George, I., Hershberg, R. & Sperber, K. Impaired class II expression and antigen uptake in monocytic cells after HIV-1 infection. Journal of Immunology 1997; 159(5): 2177-2188.
40 Kumamoto, T., Huang, E.K., Valentini, R.F. & Takashima, A. Entrapment and antigen loading of Langerhans cells in situ by an artificial chemokine gradient. Journal of Investigative Dermatology 2001; 117(4): 1017-1017.
41 Kumamoto, T., Huang, E.K., Paek, H.J. *et al.* Induction of tumor-specific protective immunity by in situ Langerhans cell vaccine. Nature Biotechnology 2002; 20(1): 64-69.
42 Furumoto, K., Soares, L., Engleman, E.G. & Merad, M. Induction of potent antitumor immunity by in situ targeting of intraturnoral DCs. Journal of Clinical Investigation 2004; 113(5): 774-783.
43 Sumida, S.M., McKay, P.F., Truitt, D.M. *et al.* Recruitment and expansion of dendritic cells in vivo potentiate the immunogenicity of plasmid DNA vaccines. Journal of Clinical Investigation 2004; 114(9): 1334-1342.
44 Westermann, J., Ehlers, E.M., Exton, M.S., Kaiser, M. & Bode, U. Migration of naive, effector and memory T cells: implications for the regulation of immune responses. Immunological Reviews 2001; 184 20-37.
45 Young, A.J. The physiology of lymphocyte migration through the single lymph node in vivo. Seminars in Immunology 1999; 11(2): 73-83.
46 Cyster, J.G. Chemokines - Chemokines and cell migration in secondary lymphoid organs. Science 1999; 286(5447): 2098-2102.
47 Sozzani, S., Allavena, P., Vecchi, A. & Mantovani, A. Chemokines and dendritic cell traffic. Journal of Clinical Immunology 2000; 20(3): 151-160.
48 Gerard, C. & Rollins, B.J. Chemokines and disease. Nature Immunology 2001; 2(2): 108-115.
49 Campbell, D.J., Kim, C.H. & Butcher, E.C. Chemokines in the systemic organization of immunity. Immunological Reviews 2003; 195 58-71.
50 Cyster, J.G., Ansel, K.M., Reif, K. *et al.* Follicular stromal cells and lymphocyte homing to follicles. Immunological Reviews 2000; 176 181-193.

51 Ansel, K.M., Ngo, V.N., Hyman, P.L. *et al.* A chemokine-driven positive feedback loop organizes lymphoid follicles. Nature 2000; 406(6793): 309-314.
52 Dieu-Nosjean, M.C., Massacrier, C., Homey, B. *et al.* Macrophage inflammatory protein 3 alpha is expressed at inflamed epithelial surfaces and is the most potent chemokine known in attracting Langerhans cell precursors. Journal of Experimental Medicine 2000; 192(5): 705-717.
53 Cyster, J.G. Chemokines and the homing of dendritic cells to the T cell areas of lymphoid organs. Journal of Experimental Medicine 1999; 189(3): 447-450.
54 Banchereau, J., Briere, F., Caux, C. *et al.* Immunobiology of dendritic cells. Annual Review of Immunology 2000; 18 767-+.
55 McColl, S.R. Chemokines and dendritic cells: A crucial alliance. Immunology and Cell Biology 2002; 80(5): 489-496.
56 Dieu, M.C., Vanbervliet, B., Vicari, A. *et al.* Selective recruitment of immature and mature dendritic cells by distinct chemokines expressed in different anatomic sites. Journal of Experimental Medicine 1998; 188(2): 373-386.
57 Fillion, I., Ouellet, N., Simard, M., Bergeron, Y., Sato, S. & Bergeron, M.G. Role of chemokines and formyl peptides in pneumococcal pneumonia-induced monocyte/macrophage recruitment. Journal of Immunology 2001; 166(12): 7353-7361.
58 Xu, L.L., Warren, M.K., Rose, W.L., Gong, W.H. & Wang, J.M. Human recombinant monocyte chemotactic protein and other c-c chemokines bind and induce directional migration of dendritic cells in vitro. Journal of Leukocyte Biology 1996; 60(3): 365-371.
59 Dunzendorfer, S., Kaser, A., Meierhofer, C., Tilg, H. & Wiedermann, C.J. Dendritic cell migration in different micropore filter assays. Immunology Letters 2000; 71(1): 5-11.
60 Sozzani, S., Allavena, P., D'Amico, G. *et al.* Cutting edge: Differential regulation of chemokine receptors during dendritic cell maturation: A model for their trafficking properties. Journal of Immunology 1998; 161(3): 1083-1086.
61 Odoherty, U., Steinman, R.M., Peng, M. *et al.* Dendritic Cells Freshly Isolated from Human Blood Express Cd4 and Mature into Typical Immunostimulatory Dendritic Cells after Culture in Monocyte-Conditioned Medium. Journal of Experimental Medicine 1993; 178(3): 1067-1078.
62 Hart, D.N.J. Dendritic cells: Unique leukocyte populations which control the primary immune response. Blood 1997; 90(9): 3245-3287.
63 Martin-Fontecha, A., Sebastiani, S., Hopken, U.E. *et al.* Regulation of dendritic cell migration to the draining lymph node: Impact on T lymphocyte traffic and priming. Journal of Experimental Medicine 2003; 198(4): 615-621.
64 Song, R.J. & Leong, K.W. The effects of MIP-1 alpha, MIP-3 alpha, and MIP-3 beta on the induction of gag-specific immunity with DNA vaccines. Molecular Therapy 2003; 7(5): S257-S257.
65 Haddad, D., Ramprakash, J., Sedegah, M. *et al.* Plasmid vaccine expressing granulocyte-macrophage colony-stimulating factor attracts infiltrates including immature dendritic cells into injected muscles. Journal of Immunology 2000; 165(7): 3772-3781.

66 Mwangi, W., Brown, W.C., Lewin, H.A. *et al.* DNA-encoded fetal liver tyrosine kinase 3 ligand and granulocyte macrophage-colony-stimulating factor increase dendritic cell recruitment to the inoculation site and enhance antigen-specific CD4(+) T cell responses induced by DNA vaccination of Outbred animals. Journal of Immunology 2002; 169(7): 3837-3846.
67 Fushimi, T., Kojima, A., Moore, M.A.S. & Crystal, R.G. Macrophage inflammatory protein 3 alpha transgene attracts dendritic cells to established murine tumors and suppresses tumor growth. Journal of Clinical Investigation 2000; 105(10): 1383-1393.
68 Barouch, D.H., McKay, P.F., Sumida, S.M. *et al.* Plasmid chemokines and colony-stimulating factors enhance the immunogenicity of DNA priming-viral vector boosting human immunodeficiency virus type 1 vaccines. Journal of Virology 2003; 77(16): 8729-8735.
69 McKay, P.F., Barouch, D.H., Santra, S. *et al.* Recruitment of different subsets of antigen-presenting cells selectively modulates DNA vaccine-elicited CD4(+) and CD8(+) T lymphocyte responses. European Journal of Immunology 2004; 34(4): 1011-1020.
70 Lackie, J.M., Wilkinson, P.C. & Society for Experimental Biology (Great Britain). *Biology of the chemotactic response*, Cambridge University Press, Cambridge ; New York, 1981. xiii, 177 p.
71 Schutyser, E., Struyf, S. & Van Damme, J. The CC chemokine CCL20 and its receptor CCR6. Cytokine & Growth Factor Reviews 2003; 14(5): 409-426.
72 Baba, M., Imai, T., Nishimura, M. *et al.* Identification of CCR6, the specific receptor for a novel lymphocyte-directed CC chemokine LARC. Journal of Biological Chemistry 1997; 272(23): 14893-14898.
73 Varona, R., Zaballos, A., Gutierrez, J. *et al.* Molecular cloning, functional characterization and mRNA expression analysis of the murine chemokine receptor CCR6 and its specific ligand MIP-3 alpha. Febs Letters 1998; 440(1-2): 188-194.
74 Islam, L.N., Mckay, I.C. & Wilkinson, P.C. The Use of Collagen or Fibrin Gels for the Assay of Human Neutrophil Chemotaxis. Journal of Immunological Methods 1985; 85(1): 137-151.
75 Haddox, J.L., Pfister, R.R. & Sommers, C.I. A Visual Assay for Quantitating Neutrophil Chemotaxis in a Collagen Gel Matrix - a Novel Chemotactic Chamber. Journal of Immunological Methods 1991; 141(1): 41-52.
76 Moghe, P.V., Nelson, R.D. & Tranquillo, R.T. Cytokine-Stimulated Chemotaxis of Human Neutrophils in a 3-D Conjoined Fibrin Gel Assay. Journal of Immunological Methods 1995; 180(2): 193-211.
77 Knapp, D.M., Helou, E.F. & Tranquillo, R.T. A fibrin or collagen gel assay for tissue cell chemotaxis: Assessment of fibroblast chemotaxis to GRGDSP. Experimental Cell Research 1999; 247(2): 543-553.
78 Kim, T.K. & Burgess, D.J. Pharmacokinetic characterization C-14-vascular endothelial growth factor controlled release microspheres using a rat model. Journal of Pharmacy and Pharmacology 2002; 54(7): 897-905.
79 Castellanos, I.J., Carrasquillo, K.G., Lopez, J.D., Alvarez, M. & Griebenow, K. Encapsulation of bovine serum albumin in poly(lactide-co-glycolide)

microspheres by the solid-in-oil-in-water technique. Journal of Pharmacy and Pharmacology 2001; 53(2): 167-178.
80 Sallusto, F. & Lanzavecchia, A. Efficient Presentation of Soluble-Antigen by Cultured Human Dendritic Cells Is Maintained by Granulocyte-Macrophage Colony-Stimulating Factor Plus Interleukin-4 and Down-Regulated by Tumor-Necrosis-Factor-Alpha. Journal of Experimental Medicine 1994; 179(4): 1109-1118.
81 McCutcheon, M. Chemotaxis in leukocytes. Physiological Reviews 1946; 26(3): 319-336.
82 Lauffenburger, D.A. & Zigmond, S.H. Chemotactic Factor Concentration Gradients in Chemotaxis Assay Systems. Journal of Immunological Methods 1981; 40(1): 45-60.
83 Zigmond, S.H. Ability of Polymorphonuclear Leukocytes to Orient in Gradients of Chemotactic Factors. Journal of Cell Biology 1977; 75(2): 606-616.
84 Nagano, C., Azuma, A., Ishiyama, H., Sekiguchi, K., Imagawa, K. & Kikuchi, M. Rebamipide suppresses formyl-methionyl-leucyl-phenylalanine (fMLP)-induced superoxide production by inhibiting fMLP-receptor binding in human neutrophils. Journal of Pharmacology and Experimental Therapeutics 2001; 297(1): 388-394.
85 Okada, H., Yamamoto, M., Heya, T. *et al.* Drug-Delivery Using Biodegradable Microspheres. Journal of Controlled Release 1994; 28(1-3): 121-129.
86 Thomazzi, S.M., Moreira, J., Marcondes, S., De Nueci, G. & Antunes, E. Role of cyclic GMP on inhibition by nitric oxide donors of human eosinophil chemotaxis in vitro. British Journal of Pharmacology 2004; 141(4): 653-660.
87 Karsten, V., Tritschler, S., Mandes, K., Belcourt, A., Pinget, M. & Kessler, L. Chemotaxis activation of peritoneal murine macrophages induced by the transplantation of free and encapsulated pancreatic rat islets. Cell Transplantation 2000; 9(1): 39-43.
88 Greaves, D.R., Wang, W., Dairaghi, D.J. *et al.* CCR6, a CC chemokine receptor that interacts with macrophage inflammatory protein 3 alpha and is highly expressed in human dendritic cells. Journal of Experimental Medicine 1997; 186(6): 837-844.
89 Kucharzik, T., Hudson, J.T., Waikel, R.L., Martin, W.D. & Williams, I.R. CCR6 expression distinguishes mouse myeloid and lymphoid dendritic cell subsets: demonstration using a CCR6 EGFP knock-in mouse. European Journal of Immunology 2002; 32(1): 104-112.
90 Bousso, P. & Robey, E. Dynamics of CD8(+) T cell priming by dendritic cells in intact lymph nodes. Nature Immunology 2003; 4(6): 579-585.
91 Mempel, T.R., Henrickson, S.E. & von Andrian, U.H. T-cell priming by dendritic cells in lymph nodes occurs in three distinct phases. Nature 2004; 427(6970): 154-159.
92 Dormann, D. & Weijer, C.J. Chemotactic cell movement during development. Current Opinion in Genetics & Development 2003; 13(4): 358-364.
93 Gotte, M. Syndecans in inflammation. Faseb Journal 2003; 17(6): 575-591.
94 English, D., Brindley, D.N., Spiegel, S. & Garcia, J.G.N. Lipid mediators of angiogenesis and the signalling pathways they initiate. Biochimica Et Biophysica Acta-Molecular and Cell Biology of Lipids 2002; 1582(1-3): 228-239.

95 Zlotnik, A. Chemokines in neoplastic progression. Seminars in Cancer Biology 2004; 14(3): 181-185.
96 Payne, A.S. & Cornelius, L.A. The role of chemokines in melanoma tumor growth and metastasis. Journal of Investigative Dermatology 2002; 118(6): 915-922.
97 Rot, A. & von Andrian, U.H. Chemokines in innate and adaptive host defense: Basic chemokinese grammar for immune cells. Annual Review of Immunology 2004; 22 891-928.
98 Thanarajasingam, U., Crittenden, M.R., Thompson, J.M., Gough, M.J. & Vile, R.G. Duration of chemokine expression and release of tumor antigen influences efficacy of immune control of tumors. Faseb Journal 2004; 18(4): A64-A64.
99 Nixon, D.F., Hioe, C., Chen, P.D. *et al.* Synthetic peptides entrapped in microparticles can elicit cytotoxic T cell activity. Vaccine 1996; 14(16): 1523-1530.
100 Eyles, J.E., Spiers, I.D., Williamson, E.D. & Alpar, H.O. Analysis of local and systemic immunological responses after intra-tracheal, intra-nasal and intra-muscular administration of microsphere co-encapsulated Yersinia pestis sub-unit vaccines. Vaccine 1998; 16(20): 2000-2009.
101 Eyles, J.E., Bramwell, V.W., Singh, J., Williamson, E.D. & Alpar, H.O. Stimulation of spleen cells in vitro by nanospheric particles containing antigen. Journal of Controlled Release 2003; 86(1): 25-32.
102 Diwan, M., Tafaghodi, M. & Samuel, J. Enhancement of immune responses by co-delivery of a CpG oligodeoxynucleotide and tetanus toxoid in biodegradable nanospheres. Journal of Controlled Release 2002; 85(1-3): 247-262.
103 Marx, P.A., Compans, R.W., Gettie, A. *et al.* Protection against Vaginal Siv Transmission with Microencapsulated Vaccine. Science 1993; 260(5112): 1323-1327.
104 Hilbert, A.K., Fritzsche, U. & Kissel, T. Biodegradable microspheres containing influenza A vaccine: Immune response in mice. Vaccine 1999; 17(9-10): 1065-1073.
105 Hedley, M.L., Curley, J. & Urban, R. Microspheres containing plasmid-encoded antigens elicit cytotoxic T-cell responses. Nature Medicine 1998; 4(3): 365-368.
106 Singh, M., Ott, G., Kazzaz, J. *et al.* Cationic microparticles are an effective delivery system for immune stimulatory CpG DNA. Pharmaceutical Research 2001; 18(10): 1476-1479.
107 Sharpe, S., Hanke, T., Tinsley-Bown, A. *et al.* Mucosal immunization with PLGA-microencapsulated DNA primes a SIV-specific CTL response revealed by boosting with cognate recombinant modified vaccinia virus Ankara. Virology 2003; 313(1): 13-21.
108 Levine, M.M. & Sztein, M.B. Vaccine development strategies for improving immunization: the role of modern immunology. Nature Immunology 2004; 5(5): 460-464.
109 Jeon, N.L., Baskaran, H., Dertinger, S.K.W., Whitesides, G.M., Van de Water, L. & Toner, M. Neutrophil chemotaxis in linear and complex gradients of interleukin-8 formed in a microfabricated device. Nature Biotechnology 2002; 20(8): 826-830.
110 Radomsky, M.L., Whaley, K.J., Cone, R.A. & Saltzman, W.M. Macromolecules Released from Polymers - Diffusion into Unstirred Fluids. Biomaterials 1990; 11(9): 619-624.

111 Patel, D.D., Koopmann, W., Imai, T., Whichard, L.P., Yoshie, O. & Krangel, M.S. Chemokines have diverse abilities to form solid phase gradients. Clinical Immunology 2001; 99(1): 43-52.
112 Pelletier, A.J., van der Laan, L.J.W., Hildbrand, P. *et al.* Presentation of chemokine SDF-1 alpha by fibronectin mediates directed migration of T cells. Blood 2000; 96(8): 2682-2690.
113 Proudfoot, A.E.I., Handel, T.M., Johnson, Z. *et al.* Glycosaminoglycan binding and oligomerization are essential for the in vivo activity of certain chemokines. Proceedings of the National Academy of Sciences of the United States of America 2003; 100(4): 1885-1890.
114 Tabata, Y. & Ikada, Y. Protein Precoating of Polylactide Microspheres Containing a Lipophilic Immunopotentiator for Enhancement of Macrophage Phagocytosis and Activation. Pharmaceutical Research 1989; 6(4): 296-301.
115 Thiele, L., Rothen-Rutishauser, B., Jilek, S., Wunderli-Allenspach, H., Merkle, H.P. & Walter, E. Evaluation of particle uptake in human blood monocyte-derived cells in vitro. Does phagocytosis activity of dendritic cells measure up with macrophages? Journal of Controlled Release 2001; 76(1-2): 59-71.
116 Randolph, G.J., Inaba, K., Robbiani, D.F., Steinman, R.M. & Muller, W.A. Differentiation of phagocytic monocytes into lymph node dendritic cells in vivo. Immunity 1999; 11(6): 753-761.
117 Waeckerle-Men, Y., Scandella, E., Allmen, E.U. *et al.* Phenotype and functional analysis of human monocyte-derived dendritic cells loaded with biodegradable poly(lactide-co-glycolide) microspheres for immunotherapy. Journal of Immunological Methods 2004; 287(1-2): 109-124.
118 Lacasse, F.X., Filion, M.C., Phillips, N.C., Escher, E., McMullen, J.N. & Hildgen, P. Influence of surface properties at biodegradable microsphere surfaces: Effects on plasma protein adsorption and phagocytosis. Pharmaceutical Research 1998; 15(2): 312-317.
119 Inaba, K., Inaba, M., Naito, M. & Steinman, R.M. Dendritic Cell Progenitors Phagocytose Particulates, Including Bacillus-Calmette-Guerin Organisms, and Sensitize Mice to Mycobacterial Antigens in-Vivo. Journal of Experimental Medicine 1993; 178(2): 479-488.
120 Yeh, M.K., Coombes, A.G.A., Jenkins, P.G. & Davis, S.S. A Novel Emulsification-Solvent Extraction Technique for Production of Protein Loaded Biodegradable Microparticles for Vaccine and Drug-Delivery. Journal of Controlled Release 1995; 33(3): 437-445.
121 Jeffery, H., Davis, S.S. & Ohagan, D.T. The Preparation and Characterization of Poly(Lactide-Co-Glycolide) Microparticles .1. Oil-in-Water Emulsion Solvent Evaporation. International Journal of Pharmaceutics 1991; 77(2-3): 169-175.
122 Ada, G. Advances in immunology - Vaccines and vaccination. New England Journal of Medicine 2001; 345(14): 1042-1053.
123 Raychaudhuri, S. & Rock, K.L. Fully mobilizing host defense: Building better vaccines. Nature Biotechnology 1998; 16(11): 1025-1031.
124 Pardoll, D.M. Tumor reactive T cells get a boost. Nature Biotechnology 2002; 20(12): 1207-1208.

125 O'Hagan, D.T. & Valiante, N.M. Recent advances in the discovery and delivery of vaccine adjuvants. Nature Reviews Drug Discovery 2003; 2(9): 727-735.
126 Pulendran, B. Variegation of the immune response with dendritic cells and pathogen recognition receptors. Journal of Immunology 2005; 174(5): 2457-2465.
127 O'Hagan, D.T., MacKichan, M.L. & Singh, M. Recent developments in adjuvants for vaccines against infectious diseases. Biomolecular Engineering 2001; 18(3): 69-85.
128 Klenerman, P., Lechner, F., Kantzanou, M., Ciurea, A., Hengartner, H. & Zinkernagel, R. Viral escape and the failure of cellular immune responses. Science 2000; 289(5487): 2003.
129 Zinkernagel, R.M. & Hengartner, H. Regulation of the immune response by antigen. Science 2001; 293(5528): 251-253.
130 Bachmann, M.F., Rohrer, U.H., Kundig, T.M., Burki, K., Hengartner, H. & Zinkernagel, R.M. The influence of antigen organization on B cell responsiveness. Science 1993; 262(5138): 1448-1451.
131 Turley, S.J., Inaba, K., Garrett, W.S. *et al.* Transport of peptide-MHC class II complexes in developing dendritic cells. Science 2000; 288(5465): 522-527.
132 Kovacsovicsbankowski, M., Clark, K., Benacerraf, B. & Rock, K.L. Efficient Major Histocompatibility Complex Class-I Presentation of Exogenous Antigen Upon Phagocytosis by Macrophages. Proceedings of the National Academy of Sciences of the United States of America 1993; 90(11): 4942-4946.
133 Sousa, C.R.E. & Germain, R.N. Major Histocompatibility Complex Class-I Presentation of Peptides Derived from Soluble Exogenous Antigen by a Subset of Cells Engaged in Phagocytosis. Journal of Experimental Medicine 1995; 182(3): 841-851.
134 Huang, Q., Liu, D.Y., Majewski, P. *et al.* The plasticity of dendritic cell responses to pathogens and their components. Science 2001; 294(5543): 870-875.
135 Samuel, J., Elamanchili, P., Chong, C. *et al.* Biodegradable nanoparticles for targeted delivery of therapeutic vaccines to dendritic cells. Faseb Journal 2003; 17(7): C332-C332.
136 Keegan, M.E., Whittum-Hudson, J.A. & Saltzman, W.M. Biomimetic design in microparticulate vaccines. Biomaterials 2003; 24(24): 4435-4443.
137 Singh, M. & O'Hagan, D. The preparation and characterization of polymeric antigen delivery systems for oral administration. Advanced Drug Delivery Reviews 1998; 34(2-3): 285-304.
138 Thomasin, C., Ho, N.T., Merkle, H.P. & Gander, B. Drug microencapsulation by PLA/PLGA coacervation in the light of thermodynamics. 1. Overview and theoretical considerations. Journal of Pharmaceutical Sciences 1998; 87(3): 259-268.
139 Mestecky, J., Moldoveanu, Z., Novak, M. *et al.* Biodegradable Microspheres for the Delivery of Oral Vaccines. Journal of Controlled Release 1994; 28(1-3): 131-141.
140 Men, Y., Audran, R., Thomasin, C. *et al.* MHC class I- and class II-restricted processing and presentation of microencapsulated antigens. Vaccine 1999; 17(9-10): 1047-1056.

141 Jung, T., Kamm, W., Breitenbach, A., Hungerer, K.D., Hundt, E. & Kissel, T. Tetanus toroid loaded nanoparticles from sulfobutylated poly(vinyl alcohol)-graft-poly(lactide-co-glycolide): Evaluation of antibody response after oral and nasal application in mice. Pharmaceutical Research 2001; 18(3): 352-360.
142 Murthy, N., Xu, M.C., Schuck, S., Kunisawa, J., Shastri, N. & Frechet, J.M.J. A macromolecular delivery vehicle for protein-based vaccines: Acid-degradable protein-loaded microgels. Proceedings of the National Academy of Sciences of the United States of America 2003; 100(9): 4995-5000.
143 Machluf, M., Apte, R.N., Regev, O. & Cohen, S. Enhancing the immunogenicity of liposomal hepatitis B surface antigen (HBsAg) by controlling its delivery from polymeric microspheres. J Pharm Sci 2000; 89(12): 1550-1557.
144 Miyata, T., Asami, N. & Uragami, T. A reversibly antigen-responsive hydrogel. Nature 1999; 399(6738): 766-769.
145 Cohen, S., Alonso, M.J. & Langer, R. Novel approaches to controlled-release antigen delivery. Int J Technol Assess Health Care 1994; 10(1): 121-130.
146 Kempf, M., Mandal, B., Jilek, S. *et al.* Improved stimulation of human dendritic cells by receptor engagement with surface-modified microparticles. Journal of Drug Targeting 2003; 11(1): 11-18.
147 Hawiger, D., Inaba, K., Dorsett, Y. *et al.* Dendritic cells induce peripheral T cell unresponsiveness under steady state conditions in vivo. Journal of Experimental Medicine 2001; 194(6): 769-779.
148 Fifis, T., Gamvrellis, A., Crimeen-Irwin, B. *et al.* Size-dependent immunogenicity: Therapeutic and protective properties of nano-vaccines against tumors. Journal of Immunology 2004; 173(5): 3148-3154.
149 Bonifaz, L.C., Bonnyay, D.P., Charalambous, A. *et al.* In vivo targeting of antigens to maturing dendritic cells via the DEC-205 receptor improves T cell vaccination. Journal of Experimental Medicine 2004; 199(6): 815-824.
150 Sasaki, S., Inamura, K. & Okuda, K. Genes that induce immunity - DNA vaccines. Microbiology and Immunology 1999; 43(3): 191-200.
151 Sasaki, S., Takeshita, F., Xin, K.Q., Ishii, N. & Okuda, K. Adjuvant formulations and delivery systems for DNA vaccines. Methods 2003; 31(3): 243-254.
152 Maurer, T., Heit, A., Hochrein, H. *et al.* CpG-DNA aided cross-presentation of soluble antigens by dendritic cells. European Journal of Immunology 2002; 32(8): 2356-2364.
153 Cho, H.J., Takabayashi, K., Cheng, P.M. *et al.* Immunostimulatory DNA-based vaccines induce cytotoxic lymphocyte activity by a T-helper cell-independent mechanism. Nature Biotechnology 2000; 18(5): 509-514.
154 Diwan, M., Elamanchili, P., Lane, H., Gainer, A. & Samuel, J. Biodegradable nanoparticle mediated antigen delivery to human cord blood derived dendritic cells for induction of primary T cell responses. Journal of Drug Targeting 2004; 11(8-10): 495-507.
155 Gursel, I., Gursel, M., Ishii, K.J. & Klinman, D.M. Sterically stabilized cationic liposomes improve the uptake and immunostimulatory activity of CpG oligonucleotides. Journal of Immunology 2001; 167(6): 3324-3328.

156 Chong, C.S.W., Cao, M., Wong, W.W. *et al.* Enhancement of T helper type 1 immune responses against hepatitis B virus core antigen by PLGA nanoparticle vaccine delivery. Journal of Controlled Release 2005; 102(1): 85-99.
157 Crum, C.P. & Rivera, M.N. Vaccines for cervical cancer. Cancer Journal 2003; 9(5): 368-376.
158 Daemen, T., de Mare, A., Bungener, L., de Jonge, J., Huckriede, A. & Wilschut, J. Virosomes for antigen and DNA delivery. Advanced Drug Delivery Reviews 2005; 57(3): 451-463.
159 Bungener, L., Huckriede, A., de Mare, A., de Vries-Idema, J., Wilschut, J. & Daemen, T. Virosome-mediated delivery of protein antigens in vivo: efficient induction of class I MHC-restricted cytotoxic T lymphocyte activity. Vaccine 2005; 23(10): 1232-1241.
160 Kim, H.K. & Park, T.G. Microencapsulation of human growth hormone within biodegradable polyester microspheres: Protein aggregation stability and incomplete release mechanism. Biotechnology and Bioengineering 1999; 65(6): 659-667.
161 Fu, K., Klibanov, A.M. & Langer, R. Protein stability in controlled-release systems. Nature Biotechnology 2000; 18(1): 24-25.
162 Ertel, W., Morrison, M.H., Ayala, A. & Chaudry, I.H. Insights into the Mechanisms of Defective Antigen Presentation after Hemorrhage. Surgery 1991; 110(2): 440-447.
163 Schirmbeck, R., Bohm, W. & Reimann, J. Injection of Detergent-Denatured Ovalbumin Primes Murine Class I-Restricted Cytotoxic T-Cells in-Vivo. European Journal of Immunology 1994; 24(9): 2068-2072.
164 Creusot, R.J., Thomsen, L.L., van Wely, C.A., Topley, P., Tite, J.P. & Chain, B.M. Early commitment of adoptively transferred CD4(+) T cells following particle-mediated DNA vaccination: implications for the study of immunomodulation. Vaccine 2001; 19(13-14): 1678-1687.
165 Yang, Y.W., Wu, C.A. & Morrow, W.J.W. Cell death induced by vaccine adjuvants containing surfactants. Vaccine 2004; 22(11-12): 1524-1536.
166 Singh, M., Kazzaz, J., Chesko, J. *et al.* Anionic microparticles are a potent delivery system for recombinant antigens from Neisseria meningitidis serotype B. Journal of Pharmaceutical Sciences 2004; 93(2): 273-282.
167 Singh, M., Kazzaz, J., Ugozzoli, M., Chesko, J. & O'Hagan, D.T. Charged polylactide co-glycolide microparticles as antigen delivery systems. Expert Opinion on Biological Therapy 2004; 4(4): 483-491.
168 Venkataprasad, N., Coombes, A.G.A., Singh, M. *et al.* Induction of cellular immunity to a mycobacterial antigen adsorbed on lamellar particles of lactide polymers. Vaccine 1999; 17(15-16): 1814-1819.
169 Jiao, X.M., Wang, R.Y.H., Qiu, Q., Alter, H.J. & Shih, J.W.K. Enhanced hepatitis C virus NS3 specific Th1 immune responses induced by co-delivery of protein antigen and CpG with cationic liposomes. Journal of General Virology 2004; 85 1545-1553.
170 Saurwein-Teissl, M., Zisterer, K., Schmitt, T.L., Gluck, R., Cryz, S. & Grubeck-Loebenstein, B. Whole virus influenza vaccine activates dendritic cells (DC) and stimulates cytokine production by peripheral blood mononuclear cells (PBMC)

while subunit vaccines support T cell proliferation. Clinical and Experimental Immunology 1998; 114(2): 271-276.
171 Diminsky, D., Schirmbeck, R., Reimann, J. & Barenholz, Y. Comparison between hepatitis B surface antigen (HBsAg) particles derived from mammalian cells (CHO) and yeast cells (Hansenula polymorpha): Composition, structure and immunogenicity. Vaccine 1997; 15(6-7): 637-647.
172 Stober, D., Trobonjaca, Z., Reimann, J. & Schirmbeck, R. Dendritic cells pulsed with exogenous hepatitis B surface antigen particles efficiently present epitopes to MHC class I-restricted cytotoxic T cells. European Journal of Immunology 2002; 32(4): 1099-1108.
173 Elamanchili, P., Diwan, M., Cao, M. & Samuel, J. Characterization of poly(D,L-lactic-co-glycolic acid) based nanoparticulate system for enhanced delivery of antigens to dendritic cells. Vaccine 2004; 22(19): 2406-2412.
174 Kazzaz, J., Singh, M., Ugozzoli, M., Chesko, J., Soenawan, E. & O'Hagan, D.T. Encapsulation of the immune potentiators MPL and RC529 in PLG microparticles enhances their potency. Journal of Controlled Release 2006; 110(3): 566-573.
175 Heikenwalder, M., Polymenidou, M., Junt, T. *et al.* Lymphoid follicle destruction and immunosuppression after repeated CpG oligodeoxynucleotide administration. Nature Medicine 2004; 10(2): 187-192.
176 Landfester, K. Recent developments in miniemulsions - Formation and stability mechanisms. Macromolecular Symposia 2000; 150 171-178.
177 Landfester, K., Bechthold, N., Tiarks, F. & Antonietti, M. Miniemulsion polymerization with cationic and nonionic surfactants: A very efficient use of surfactants for heterophase polymerization. Macromolecules 1999; 32(8): 2679-2683.
178 Porgador, A., Yewdell, J.W., Deng, Y.P., Bennink, J.R. & Germain, R.N. Localization, quantitation, and in situ detection of specific peptide MHC class I complexes using a monoclonal antibody. Immunity 1997; 6(6): 715-726.
179 Bahadur, P., Li, P.Y., Almgren, M. & Brown, W. Effect of Potassium Fluoride on the Micellar Behavior of Pluronic F-68 in Aqueous-Solution. Langmuir 1992; 8(8): 1903-1907.
180 Canal, T. & Peppas, N.A. Correlation between Mesh Size and Equilibrium Degree of Swelling of Polymeric Networks. Journal of Biomedical Materials Research 1989; 23(10): 1183-1193.
181 Jain, S., Yap, W.T. & Irvine, D.J. Synthesis of protein-loaded hydrogel particles in an aqueous two-phase system for coincident antigen and CpG oligonucleotide delivery to antigen-presenting cells. Biomacromolecules 2005; 6(5): 2590-2600.
182 Reece, J.C., Vardaxis, N.J., Marshall, J.A., Crowe, S.M. & Cameron, P.U. Uptake of HIV and latex particles by fresh and cultured dendritic cells and monocytes. Immunology and Cell Biology 2001; 79(3): 255-263.
183 Newman, K.D., Elamanchili, P., Kwon, G.S. & Samuel, J. Uptake of poly(D,L-lactic-co-glycolic acid) microspheres by antigen-presenting cells in vivo. Journal of Biomedical Materials Research 2002; 60(3): 480-486.
184 Arttamangkul, S., Alvarez-Maubecin, V., Thomas, G., Williams, J.T. & Grandy, D.K. Binding and internalization of fluorescent opioid peptide conjugates in living cells. Molecular Pharmacology 2000; 58(6): 1570-1580.

185 Becker, P.D. & Guzman, C.A. Rational design of vaccination strategies to promote antigen entry into the MHC class I-restricted presentation pathway. Transfusion Medicine and Hemotherapy 2004; 31(6): 398-411.
186 Porgador, A. & Germain, R.N. Monoclonal antibody detection of specific cell-bound peptide-MHC class I complexes with a sensitivity approaching CD8+ T cells. Journal of Allergy and Clinical Immunology 1997; 99(1): 472-472.
187 Mareeva, T., Lebedeva, T., Anikeeva, N., Manser, T. & Sykulev, Y. Antibody specific for the peptide center dot major histocompatibility complex - Is it T cell receptor-like? Journal of Biological Chemistry 2004; 279(43): 44243-44249.
188 Datta, S.K. & Raz, E. Induction of antigen cross-presentation by Toll-like receptors. Springer Seminars in Immunopathology 2005; 26(3): 247-255.
189 Datta, S.K., Redecke, V., Prilliman, K.R. *et al.* A subset of toll-like receptor ligands induces cross-presentation by bone marrow-derived dendritic cells. Journal of Immunology 2003; 170(8): 4102-4110.
190 Bevaart, L., Van Ojik, H.H., Sun, A.W. *et al.* CpG oligodeoxynucleotides enhance Fc gamma RI-mediated cross presentation by dendritic cells. International Immunology 2004; 16(8): 1091-1098.
191 Kuchtey, J., Chefalo, P.J., Gray, R.C., Ramachandra, L. & Harding, C.V. Enhancement of dendritic cell antigen cross-presentation by CpG DNA involves type IIFN and stabilization of class I MHC mRNA. Journal of Immunology 2005; 175(4): 2244-2251.
192 Rutz, M., Metzger, J., Gellert, T. *et al.* Toll-like receptor 9 binds single-stranded CpG-DNA in a sequence- and pH-dependent manner. European Journal of Immunology 2004; 34(9): 2541-2550.
193 Latz, E., Schoenemeyer, A., Visintin, A. *et al.* TLR9 signals after translocating from the ER to CpG DNA in the lysosome. Nature Immunology 2004; 5(2): 190-198.
194 Jakob, T., Walker, P.S., Krieg, A.M., Udey, M.C. & Vogel, J. Activation of cutaneous dendritic cells by bacterial DNA and CpG-oligodeoxynucleotides: Implications for the induction of Th1 responses by immunostimulatory DNA. Journal of Leukocyte Biology 1998; 36-36.
195 Jakob, T., Walker, P.S., Krieg, A.M., von Stebut, E., Udey, M.C. & Vogel, J.C. Bacterial DNA and CpG-containing oligodeoxynucleotides activate cutaneous dendritic cells and induce IL-12 production: Implications for the augmentation of Th1 responses. International Archives of Allergy and Immunology 1999; 118(2-4): 457-461.
196 Bongrand, P. & Malissen, B. Quantitative aspects of T-cell recognition: from within the antigen-presenting cell to within the T cell. Bioessays 1998; 20(5): 412-422.
197 Robinson, H.L. & Amara, R.R. T cell vaccines for microbial infections. Nature Medicine 2005; 11(4): S25-S32.
198 Nace, V.M. *Nonionic surfactants : polyoxyalkylene block copolymers*, M. Dekker, New York, 1996. x, 266 p.
199 Jain, N.J., Aswal, V.K., Goyal, P.S. & Bahadur, P. Salt induced micellization and micelle structures of PEO/PPO/PEO block copolymers in aqueous solution.

Colloids and Surfaces a-Physicochemical and Engineering Aspects 2000; 173(1-3): 85-94.
200 Florin, E., Kjellander, R. & Eriksson, J.C. Salt Effects on the Cloud Point of the Poly(Ethylene Oxide) + Water-System. Journal of the Chemical Society-Faraday Transactions I 1984; 80 2889-2910.
201 Drummond, R.K., Klier, J., Alameda, J.A. & Peppas, N.A. Preparation of Poly(Methacrylic Acid-G-Ethylene Oxide) Microspheres. Macromolecules 1989; 22(9): 3816-3818.
202 Guermant, C., Brygier, J., Baeyensvolant, D. *et al.* Quantitative-Determination of Polyethylene-Glycol Based Upon Its Salting-out and Partitioning of a Dye into the Resulting Aqueous 2-Phase System. Analytical Biochemistry 1995; 230(2): 254-258.
203 Shih, Y.C., Prausnitz, J.M. & Blanch, H.W. Some Characteristics of Protein Precipitation by Salts. Biotechnology and Bioengineering 1992; 40(10): 1155-1164.
204 Morgan, D.M., Larvin, V.L. & Pearson, J.D. Biochemical characterisation of polycation-induced cytotoxicity to human vascular endothelial cells. J Cell Sci 1989; 94 (Pt 3) 553-559.
205 Fischer, D., Li, Y.X., Ahlemeyer, B., Krieglstein, J. & Kissel, T. In vitro cytotoxicity testing of polycations: influence of polymer structure on cell viability and hemolysis. Biomaterials 2003; 24(7): 1121-1131.
206 Mitchell, D.J., Kim, D.T., Steinman, L., Fathman, C.G. & Rothbard, J.B. Polyarginine enters cells more efficiently than other polycationic homopolymers. Journal of Peptide Research 2000; 56(5): 318-325.
207 Clague, M.J. Molecular aspects of the endocytic pathway. Biochemical Journal 1998; 336 271-282.
208 Kyriakides, T.R., Cheung, C.Y., Murthy, N., Bornstein, P., Stayton, P.S. & Hoffman, A.S. pH-sensitive polymers that enhance intracellular drug delivery in vivo. Journal of Controlled Release 2002; 78(1-3): 295-303.
209 Little, S.R., Lynn, D.M., Ge, Q. *et al.* Poly-beta amino ester-containing microparticles enhance the activity of nonviral genetic vaccines. Proceedings of the National Academy of Sciences of the United States of America 2004; 101(26): 9534-9539.
210 Mann, B.K., Gobin, A.S., Tsai, A.T., Schmedlen, R.H. & West, J.L. Smooth muscle cell growth in photopolymerized hydrogels with cell adhesive and proteolytically degradable domains: synthetic ECM analogs for tissue engineering. Biomaterials 2001; 22(22): 3045-3051.
211 Elbert, D.L., Pratt, A.B., Lutolf, M.P., Halstenberg, S. & Hubbell, J.A. Protein delivery from materials formed by self-selective conjugate addition reactions. Journal of Controlled Release 2001; 76(1-2): 11-25.
212 Sawhney, A.S., Pathak, C.P., Vanrensburg, J.J., Dunn, R.C. & Hubbell, J.A. Optimization of Photopolymerized Bioerodible Hydrogel Properties for Adhesion Prevention. Journal of Biomedical Materials Research 1994; 28(7): 831-838.
213 Oupicky, D., Parker, A.L. & Seymour, L.W. Laterally stabilized complexes of DNA with linear reducible polycations: Strategy for triggered intracellular activation of

DNA delivery vectors. Journal of the American Chemical Society 2002; 124(1): 8-9.
214 Oh, J.S., Kim, J.M., Lee, K.J. & Bae, Y.C. Swelling behavior of N-isopropylacrylamide gel particles with degradable crosslinker. European Polymer Journal 1999; 35(4): 621-630.
215 GrosseSommer, A. & Prudhomme, R.K. Degradable phosphazene-crosslinked hydrogels. Journal of Controlled Release 1996; 40(3): 261-267.
216 Rodriguez, G.M. & Diment, S. Role of Cathepsin-D in Antigen Presentation of Ovalbumin. Journal of Immunology 1992; 149(9): 2894-2898.
217 Diment, S. Different Roles for Thiol and Aspartyl Proteases in Antigen Presentation of Ovalbumin. Journal of Immunology 1990; 145(2): 417-422.
218 Bathe, O.F., Dalyot-Herman, N. & Malek, T.R. Therapeutic limitations in tumor-specific CD8+ memory T cell engraftment. Bmc Cancer 2003; 3 -.
219 Chouquet, C., Autran, B., Gomard, E. *et al.* Correlation between breadth of memory HIV-specific cytotoxic T cells, viral load and disease progression in HIV infection. Aids 2002; 16(18): 2399-2407.
220 Seaman, M.S., Peyerl, F.W., Jackson, S.S. *et al.* Subsets of memory cytotoxic T lymphocytes elicited by vaccination influence the efficiency of secondary expansion in vivo. Journal of Virology 2004; 78(1): 206-215.
221 Thumann, P., Moc, I., Humrich, J. *et al.* Antigen loading of dendritic cells with whole tumor cell preparations. Journal of Immunological Methods 2003; 277(1-2): 1-16.
222 Wakita, D., Chamoto, K., Narita, Y. *et al.* An indispensable role of type-1 IFNs for inducing CTL-mediated complete eradication of established tumor tissue by CpG-liposome co-encapsulated with model tumor antigen. International Immunology 2006; 18(3): 425-434.
223 Greenland, J.R., Liu, H.N., Berry, D. *et al.* beta-amino ester polymers facilitate in vivo DNA transfection and adjuvant plasmid DNA immunization. Molecular Therapy 2005; 12(1): 164-170.
224 Palucka, A.K., Dhodapkar, M.V., Paczesny, S. *et al.* Single injection of CD34+ progenitor-derived dendritic cell vaccine can lead to induction of T-cell immunity in patients with stage IV melanoma. Journal of Immunotherapy 2003; 26(5): 432-439.
225 Banchereau, J., Palucka, A.K., Dhodapkar, M. *et al.* Immune and clinical responses in patients with metastatic melanoma to CD34(+) progenitor-derived dendritic cell vaccine. Cancer Research 2001; 61(17): 6451-6458.
226 Kwon, Y.J., James, E., Shastri, N. & Frechet, J.M.J. In vivo targeting of dendritic cells for activation of cellular immunity using vaccine carriers based on pH-responsive microparticles. Proceedings of the National Academy of Sciences of the United States of America 2005; 102(51): 18264-18268.
227 Bot, A.I., Smith, D.J., Bot, S. *et al.* Receptor-mediated targeting of spray-dried lipid particles coformulated with immunoglobulin and loaded with a prototype vaccine. Pharmaceutical Research 2001; 18(7): 971-979.
228 Haicheur, N., Bismuth, E., Bosset, S. *et al.* The B subunit of shiga toxin fused to a tumor antigen elicits CTL and targets dendritic cells to allow MHC class I-

restricted presentation of peptides derived from exogenous antigens. Journal of Immunology 2000; 165(6): 3301-3308.
229 Tillman, B.W., Hayes, T.L., deGruijl, T.D., Douglas, J.T. & Curiel, D.T. Adenoviral vectors targeted to CD40 enhance the efficacy of dendritic cell-based vaccination against human papillomavirus 16-induced tumor cells in a murine model. Cancer Research 2000; 60(19): 5456-5463.
230 Tillman, B.W., de Gruijl, T.D., Luykx-De Bakker, S.A. *et al.* Maturation of dendritic cells accompanies high-efficiency gene transfer by a CD40-targeted adenoviral vector. Journal of Immunology 1999; 162(11): 6378-6383.
231 Tillman, B., de Gruijl, T., Luykx, S. *et al.* Dendritic cells are transduced with high efficiency by a CD40-targeted Adenovirus that also induces dendritic cell maturation. Journal of Leukocyte Biology 1998; 45-45.
232 Jackson, D.C., Lau, Y.F., Le, T. *et al.* A totally synthetic vaccine of generic structure that targets Toll-like receptor 2 on dendritic cells and promotes antibody or cytotoxic T cell responses. Proceedings of the National Academy of Sciences of the United States of America 2004; 101(43): 15440-15445.
233 Scapini, P., Laudanna, C., Pinardi, C. *et al.* Neutrophils produce biologically active macrophage inflammatory protein-3 alpha (MIP-3 alpha)/CCL20 and MIP-3 beta/CCL19. European Journal of Immunology 2001; 31(7): 1981-1988.
234 Devalaraja, M.N. & Richmond, A. Multiple chemotactic factors: fine control or redundancy? Trends in Pharmacological Sciences 1999; 20(4): 151-156.
235 Onyia, K.A. Invivo Chemotaxis of Rat Leukocytes to N-Formyl-L-Methionyl-L-Leucyl-L-Phenylalanine (Fmlp). Comparative Immunology Microbiology and Infectious Diseases 1987; 10(1): 33-39.
236 Krautwald, S., Ziegler, E., Forster, R., Ohl, L., Amann, K. & Kunzendorf, U. Ectopic expression of CCL19 impairs alloimmune response in mice. Immunology 2004; 112(2): 301-309.
237 Okada, N., Gao, J.Q., Sasaki, A. *et al.* Anti-tumor activity of chemokine is affected by both kinds of tumors and the activation state of the host's immune system: implications for chemokine-based cancer immunotherapy. Biochemical and Biophysical Research Communications 2004; 317(1): 68-76.
238 Coscia, M. & Biragyn, A. Cancer immunotherapy with chemoattractant peptides. Seminars in Cancer Biology 2004; 14(3): 209-218.
239 Zhao, X., Jain, S., Benjamin Larman, H., Gonzalez, S. & Irvine, D.J. Directed cell migration via chemoattractants released from degradable microspheres. Biomaterials 2005; 26(24): 5048-5063.
240 Belay, T., Eko, F.O., Ananaba, G.A. *et al.* Chemokine and chemokine receptor dynamics during genital chlamydial infection. Infection and Immunity 2002; 70(2): 844-850.
241 Westendorf, A.M., Gunzer, F., Deppenmeier, S. *et al.* Intestinal immunity of Escherichia coli NISSLE 1917: a safe carrier for therapeutic molecules. Fems Immunology and Medical Microbiology 2005; 43(3): 373-384.
242 Oliveira, M.A.P., Lima, G.M.A.C., Shio, M.T., Leenen, P.J.M. & Abrahamsohn, I.A. Immature macrophages derived from mouse bone marrow produce large amounts of IL-12p40 after LPS stimulation. Journal of Leukocyte Biology 2003; 74(5): 857-867.

243 Lemoine, D., Wauters, F., Bouchend'homme, S. & Preat, V. Preparation and characterization of alginate microspheres containing a model antigen. International Journal of Pharmaceutics 1998; 176(1): 9-19.
244 Podual, K., Doyle, F.J. & Peppas, N.A. Preparation and dynamic response of cationic copolymer hydrogels containing glucose oxidase. Polymer 2000; 41(11): 3975-3983.
245 Kriwet, B., Walter, E. & Kissel, T. Synthesis of bioadhesive poly(acrylic acid) nano- and microparticles using an inverse emulsion polymerization method for the entrapment of hydrophilic drug candidates. Journal of Controlled Release 1998; 56(1-3): 149-158.
246 KroonBatenburg, L.M.J., Kruiskamp, P.H., Vliegenthart, J.F.G. & Kroon, J. Estimation of the persistence length of polymers by MD simulations on small fragments in solution. Application to cellulose. Journal of Physical Chemistry B 1997; 101(42): 8454-8459.
247 Yang, D., Chen, Y., Hoover, D.M. *et al.* Many chemokines including CCL20/MIP-3 alpha, display in vitro antimicrobial activity. Faseb Journal 2003; 17(7): C116-C116.
248 Tani, H., Suzuki, Y., Matsuda, A. & Kamidate, T. Enhancement of the excluded-volume effect in protein extraction using triblock copolymer-based aqueous micellar two-phase systems. Analytica Chimica Acta 2001; 429(2): 301-309.
249 Charbonnier, A.S., Kohrgruber, N., Kriehuber, E., Stingl, G., Rot, A. & Maurer, D. Macrophage inflammatory protein 3 alpha is involved in the constitutive trafficking of epidermal Langerhans cells. Journal of Experimental Medicine 1999; 190(12): 1755-1767.
250 Foged, C., Sundblad, A. & Hovgaard, L. Targeting vaccines to dendritic cells. Pharmaceutical Research 2002; 19(3): 229-238.
251 Gombotz, W.R. & Wee, S.F. Protein release from alginate matrices. Advanced Drug Delivery Reviews 1998; 31(3): 267-285.
252 Draget, K.I., SkjakBraek, G. & Smidsrod, O. Alginate based new materials. International Journal of Biological Macromolecules 1997; 21(1-2): 47-55.
253 Leid, J.G., Willson, C.J., Shirtliff, M.E., Hassett, D.J., Parsek, M.R. & Jeffers, A.K. The exopolysaccharide alginate protects Pseudomonas aeruginosa biofilm bacteria from IFN-gamma-mediated macrophage killing. Journal of Immunology 2005; 175(11): 7512-7518.
254 Stabler, C., Wilks, K., Sambanis, A. & Constantinidis, I. The effects of alginate composition on encapsulated beta TC3 cells. Biomaterials 2001; 22(11): 1301-1310.
255 Simpson, N.E., Stabler, C.L., Simpson, C.P., Sambanis, A. & Constantinidis, L. The role of the CaCl2-guluronic acid interaction on alginate encapsulated beta TC3 cells. Biomaterials 2004; 25(13): 2603-2610.
256 Flo, T.H., Ryan, L., Latz, E. *et al.* Involvement of Toll-like receptor (TLR) 2 and TLR4 in cell activation by mannuronic acid polymers. Journal of Biological Chemistry 2002; 277(38): 35489-35495.
257 Kulseng, B., Skjak-Braek, G., Ryan, L. *et al.* Transplantation of alginate microcapsules - Generation of antibodies against alginates and encapsulated porcine islet-like cell clusters. Transplantation 1999; 67(7): 978-984.

258 Babensee, J.E. & Paranjpe, A. Differential levels of dendritic cell maturation on different biomaterials used in combination products. Journal of Biomedical Materials Research Part A 2005; 74A(4): 503-510.
259 Gavini, E., Rassu, G., Sanna, V., Cossu, M. & Giunchedi, P. Mucoadhesive microspheres for nasal administration of an antiemetic drug, metoclopramide: in-vitro/ex-vivo studies. Journal of Pharmacy and Pharmacology 2005; 57(3): 287-294.
260 Takka, S. & Acarturk, F. Calcium alginate microparticles for oral administration: I: effect of sodium alginate type on drug release and drug entrapment efficiency. Journal of Microencapsulation 1999; 16(3): 275-290.
261 Acarturk, F. & Takka, S. Calcium alginate microparticles for oral administration: II effect of formulation factors on drug release and drug entrapment efficiency. Journal of Microencapsulation 1999; 16(3): 291-301.
262 Rajinikanth, P.S., Sankar, C. & Mishra, B. Sodium alginate microspheres of metoprolol tartrate for intranasal systemic delivery: Development and evaluation. Drug Delivery 2003; 10(1): 21-28.
263 Okada, Y., Nonaka, S., Tanaka, Y., Saijoh, Y., Hamada, H. & Hirokawa, N. Abnormal nodal flow precedes situs inversus in iv and inv mice. Molecular Cell 1999; 4(4): 459-468.
264 Nonaka, S., Tanaka, Y., Okada, Y. *et al.* Randomization of left-right asymmetry due to loss of nodal cilia generating leftward flow of extraembryonic fluid in mice lacking KIF3B motor protein (vol 95, pg 829, 95). Cell 1999; 99(1): -.
265 Francis, K. & Palsson, B.O. Effective intercellular communication distances are determined by the relative time constants for cyto/chemokine secretion and diffusion. Proceedings of the National Academy of Sciences of the United States of America 1997; 94(23): 12258-12262.
266 Treier, M., Gleiberman, A.S., O'Connell, S.M. *et al.* Multistep signaling requirements for pituitary organogenesis in vivo. Genes & Development 1998; 12(11): 1691-1704.
267 Inaba, K., Inaba, M., Romani, N. *et al.* Generation of Large Numbers of Dendritic Cells from Mouse Bone-Marrow Cultures Supplemented with Granulocyte Macrophage Colony-Stimulating Factor. Journal of Experimental Medicine 1992; 176(6): 1693-1702.

APPENDIX 1 – CelII Culture Medium and Buffers

1.1 Complete RPMI Medium

1. Aseptically remove 70 mL of medium from 500 mL of sterile RPMI 1640 medium (Invitrogen) containing sodium bicarbonate and 2 mM L-Glutamine,
2. Add 5 mL of 100X sodium pyruvate and 5 mL of 100X Non-essential amino acids solution.
3. Add 10 mL of penicillin and streptomycin solution.
4. Add 500 μl of gentamicin antibiotic solution.
5. Thaw fetal calf serum at 37 °C and add 50 mL of FCS to the above medium.
6. Gently rock the medium to mix the components, cover with aluminum foil, and store at 4 °C.
7. Keep the medium sterile and use only in sterile laminar hood.

1.2 Magnetic-Assisted Cell Sorting (MACS) Buffer

1. Prepare 1 l phosphate-buffered saline pH 7.2 using a PBS tablet in 1 l milliQ water.
2. Add 5 g bovine serum albumin (BSA) to PBS and 1 g sodium azide.
3. Add 2 mM EDTA to prevent cell clumping or attachment to column.
4. Filter the buffer using 0.2 μm bottle-top sterile membrane filter.
5. Store buffer at 4 °C and degas using vacuum before use. Always use cold buffer.

1.3 Flow-Assisted Cell Sorting (FACS) Buffer

1. Prepare 1 l phosphate-buffered saline pH 7.2 using a PBS tablet in 1 l milliQ water.
2. Add 10 g bovine serum albumin (BSA) and 50 g sucrose to PBS.
3. Add 500 mg sodium azide to above solution.
4. Filter the buffer using a 0.2 μm bottle-top Teflon filter.
5. Store the buffer at 4 °C.

1.4 ELISA Buffers

1.4.1 Block Buffer

1. Prepare 1 l phosphate-buffered saline pH 7.2 using a PBS tablet in 1 l milliQ water.
2. Add 10 g bovine serum albumin (BSA) and 50 g sucrose to PBS.
3. Add 500 mg sodium azide to above solution.
4. Filter the buffer using a 0.2 μm bottle-top Teflon filter.
5. Store the buffer at 4 °C.

1.4.2 Reagent Diluent

1. Prepare 1 l phosphate-buffered saline pH 7.2 using a PBS tablet in 1 l milliQ water.
2. Add 10 g bovine serum albumin (BSA) to PBS.
3. Filter the buffer using a 0.2 μm bottle-top Teflon filter.
4. Store the buffer at 4 °C.

1.4.3 Wash Buffer

1. Prepare 1 l PBS using a PBS tablet in 1 l milliQ water
2. Add 500 μl tween 20 to PBS.
3. Mix well and use as wash buffer for ELISA.

1.5 10x RPMI Medium for Collagen Gels

1. Dissolve 5.2 g RPMI medium in 20 mL milliQ water in a 50 mL conical tube
2. Add 1.25 g sodium bicarbonate to the above solution
3. Add 2 g Hepes acid to the above solution
4. Add 5 mL 100x sodium pyruvate and 5 mL of 100x nonessential amino acids
5. Add 10 mL penicillin/streptomycin solution and 500 μl of gentamicin solution.
6. Mix well and make up the volume to 50 mL with milliQ water
7. Sterile filter the solution using 0.2 μm membrane filter
8. Store at 4 °C and keep sterile.

APPENDIX 2 – Murine bone marrow-derived dendritic cell culture

Bone marrow-derived dendritic cells were cultured using the protocol of Inaba *et al.* [267]. The details of the protocol are as follows:

1. Euthanize a C57Bl/6 mouse (6-10 weeks old) using CO_2 asphyxiation
2. Pin down the mouse by laying the mouse on its back while stretching the limbs
3. Make a cut in the abdomen and continue cutting the skin to the ankles
4. Cut out the tendons that are attached to the bones, and remove femur and tibia from both legs
5. Immediately put the legs in complete RPMI medium
6. Cut open the ends of each bone, and flush the bones thoroughly with complete RPMI medium using a 26 ¾ gauge needle attached to 1 mL syringe
7. Collect the bone marrow in a 50 mL sterile centrifuge tube and break the cell aggregates with pipette to form single cell suspension
8. Pellet down cells at 1400 rpm for 6 min
9. Aspirate supernatant and loosen the pellet using small amount of medium
10. Add 5 mL Tris acetate-ammonium chloride (TAC) buffer (0.02 M Tris-HCl adjusted to pH 7.2, 0.14 M NH_4Cl, sterile-filtered) for hemolysis and incubate for 3 min at room temperature
11. Neutralize ionic strength using 20 mL of serum-free RPMI medium
12. Remove cell debris using 40 μm cell strainer
13. Pellet cells at 1400 rpm for 6 min
14. Resuspend cells at 1.5 x 10^6 cells/mL in complete RPMI medium and add 10 ng/mL rmGM-CSF
15. Plate cells in a 24-well tissue culture treated plate at 1.5 x 10^6 cells/mL/well and incubate at 37 °C, 5% CO_2
16. Pipette out 800 μl medium on days 2, 4, and 6 from each well and replace with fresh complete RPMI medium supplemented with 10 ng/mL rmGM-CSF
17. Bone marrow-derived dendritic cells are loosely adherent cells and can be extracted by pipeting; cells were used between days 6 and 8.

APPENDIX 3 – Preparation of collagen gel for migration studie

1. Keep acidic collagen solution, 10x RPMI medium, and 0.1 N NaOH on ice
2. Cool down the eppendorfs and conical tubes on ice used to handling collagen
3. Mix 800 μl of acidic collagen solution, 100 μl of 0.1 N NaOH, and 100 μl 10x RPMI medium in this order in cool eppendorf tube to prepare 1 mL of 2.4 mg/mL collagen gel
4. To prepare a mould for creating chemokine source well, take a clean razor blade and cut out at the wide-end of 200 μl pipette tip, and place the wide-end part at the center of a 35-mm or 2-well labtek chamber.
5. Mix 1 mL of collagen (2.4 mg/mL) and 1 mL cell suspension at desired cell density (e.g., 2 x 10^6 cell/mL for final density 1 x 10^6 cells/mL) and pipette collagen-cell suspension into the petridish or labtek chamber without disturbing the mould
6. Gel the collagen-cell suspension at 37 °C for 30 min, and observe migration using microscope
7. For migration studies involving two-wells (cell well and chemokine source well), attach two identical moulds to the cover of the petridish, pour collagen (1.2 mg/mL) into the lower part of petridish and close the cover to create two wells. For migration studies involving no well, pipette collagen-cell suspension into petridish or labtek chamber and gel.

APPENDIX 4 – Magnetic-Assisted Cell Sorting for T cell purification

4.1 Negative selection for $CD4^+$ T cell isolation

1. Splenocytes were isolated from mouse spleen and hemolysed. Cell were pelleted at 1400 rpm for 6 min and washed once with cold MACS buffer
2. Splenocytes were resuspended in 200 μl MACS buffer for all splenocytes
3. Add 50 μl antibody cocktail solution
4. Mix well and incubate for 15 min on ice
5. Add 150 μl of medium and 100 μl of Streptavidin-conjugated microbeads
6. Mix well and incubate on ice for 20 min
7. Add 10 mL of MACS buffer and pellet cells at 1400 rpm for 6 min
8. Aspirate supernatant completely and resuspend cells in 500 μl MACS buffer
9. Install MiniMACS column on magnet and add 0.5 mL cold MACS buffer
10. Add cell suspension followed by addition of 500 μl MACS buffer in three steps
11. Collect eluted cells, pellet them at 1400 rpm for 6 min, and wash cells in serum-free RPMI medium 2x. Resuspend cells finally at desired cell density in complete RPMI medium

4.2 Positive selection for $CD8^+$ T cell isolation

1. Splenocytes were isolated from mouse spleen and hemolysed. Cells were pelleted at 1400 rpm for 6 min and washed once with cold MACS buffer
2. Resuspend splenocytes in 400 µl MACS buffer
3. Add 50 µl CD8a (Ly-2) microbeads to cell suspension
4. Mix well and incubate on ice for 20 min
5. Add 10 mL MACS buffer and wash cells 1x
6. Resuspend cells in 500 µl MACS buffer
7. Install MiniMACS column on magnet and add 500 µl MACS buffer
8. Add cell suspension to column followed by addition of 500 µl MACS buffer in three steps
9. Add 1 mL MACS buffer and push trapped cells using plunger into a tube
10. Pellet cells at 1400 rpm for 6 min, and wash cells in serum-free RPMI medium 2x. Resuspend cells finally at desired cell density in complete RPMI medium

APPENDIX 5 – Enzyme Linked Immunosorbant Assay (ELISA)

5.1 ELISA for cytokine/chemokine detection

1. Pipette 100 μl capture antibody solution in PBS to each well of MaxiSorp ELISA plate and incubate the plate at room temperature overnight for antibody adsorption. Seal the plate with plate sealant or parafilm to prevent evaporation
2. Wash plate with 400 μl/well wash buffer 4x
3. Add 300 μl block buffer and incubate plate at room temperature for 1 h
4. Wash plate with 400 μl/well wash buffer 4x
5. Prepare 7-8 standard dilutions in reagent diluent and suitable dilutions of samples also in reagent diluent
6. Add 100 μl/well of standard dilution or sample dilution. Incubate the plate for 2 h at room temperature
7. Wash plate with 400 μl/well wash buffer 4x
8. Add 100 μl/well detection antibody solution in reagent diluent and incubate the plate for 2 h at room temperature
9. Wash plate with 400 μl/well wash buffer 4x
10. Add 100 μl/well of 200x-diluted streptavidin-horse radish peroxidase, and incubate for 20 min at room temperature in dark
11. Wash plate with 400 μl/well wash buffer 4x
12. Add 100 μl/well of substrate reagent containing 1:1 Solution A: Solution B and incubate at room temperature in dark for 20 min
13. Add 50 μl/well of 2 N H_2SO_4 to quench the color development
14. Read the absorbance of the plate at 450 nm and 540 nm using a plate reader and compute $A_{450} - A_{540}$. Plot the standard curve and use it to determine the concentration of cytokine/chemokine in samples

5.2 ELISA for determination of antibody titers in mouse sera

1. Pipette 100 μl/well of 5 μg/mL ovalbumin solution in PBS. Cover the plate with parafilm to avoid evaporation and incubate at room temperature overnight.
2. Wash plate with 400 μl/well wash buffer 4x
3. Centrifuge mouse blood samples in serum separator tubes at 10,000 rpm for 3 min.
4. Prepare 100x, 1000x, 10000x, and 100000x dilutions of all sera samples in reagent diluent and add 100 μl/well. Incubate the plate at room temperature for 1.5 h
5. Wash plate with 400 μl/well wash buffer 4x
6. Add 100 μl/well of 5000x diluted HRP-conjugated goat anti-mouse IgG antibody in reagent diluent and incubate plate for 1.5 h
7. Wash plate with 400 μl/well wash buffer 4x
8. Add 100 μl/well TMB substrate and incubate plate in dark for 10 min
9. Quench color development by adding 50 μl/well of 2 N H_2SO_4
10. Measure absorbance at 450 nm, and calculate A_{450}
11. Antibody titer was calculated by endpoint dilution as sample dilution at which A_{450} is twice of A_{450} for PBS control

APPENDIX 6 – Cell labeling with fluorescent dyes

6.1 Labeling with CFSE dye

1. Pipette cells in a sterile conical tube and pellet the cells at 1400 rpm for 6 min
2. Resuspend cells in serum-free medium at 10 x 10^6 cells/mL
3. Add suitable dilution of carboxyfluorescein succinimidyl ester (CFSE) dye to obtain desired final concentration
4. Incubate cells at 37 °C, 5% CO_2 for 20 min
5. Quench free dye with excess volume of complete RPMI medium
6. Pellet cells at 1400 rpm for 6 min and wash in complete RPMI medium 2x
7. Resuspend cells to desired cell density in complete RPMI medium

6.2 Labeling with Fura-2 AM dye

1. Pipette cells in a sterile conical tube and pellet cells at 1400 rpm for 6 min
2. Resuspend cells in 200 μl serum-free medium and add 5 g/mL fura-2 AM dye
3. Incubate cells for 20 min at 37 °C, 5% CO_2
4. Quench free dye with excess volume of complete RPMI medium and wash cells 2x in complete RPMI medium
5. Resuspend cells to desired cell density in complete RPMI medium

APPENDIX 7 – Protein/peptide modification: Labeling with a fluorescent dye or PEGylation/ acrylation

1. Prepare suitable dilution of protein of interest in PBS or 50 μM sodium carbonate buffer pH 8.5
2. Add 5x by molar ratio of fluorescent dye-succinimidyl ester, and incubate the protein-dye solution at 37 °C for 2 h
3. Dialyze out the free dye using a 5000 MW cut-off dialysis membrane against PBS overnight at 4 °C changing buffer at least once
4. Run size exclusion chromatography on the labeled protein to determine the ratio of labeled: unlabeled protein measuring the absorbance at 280 nm.
5. Concentrate the labeled protein using Centricon protein concentrators, protein lyophilization followed by reconstitution, or using Spectra/Gel absorbent
6. For PEGylation of protein, incubate the protein/peptide solution with PEG-NHS as described above for protein labeling with fluorescent dye
7. For protein acrylation, incubate the protein or peptide solution with NHS-acrylic acid for 2 h at 37 °C as described above

APPENDIX 8 – Cell staining and Flow-Assisted Cell Sorting (FACS)

8.1 Cell staining with antibodies

1. Pipette up to 1 x 10^6 cells into a microtiter tube and pellet them at 16,000 g for 15 sec
2. Remove the supernatant and resuspend cells in 200 μl FACS buffer
3. Pellet cells again at 16,000 g for 15 sec
4. Resuspend cells in 100 μl FACS buffer containing 100x dilution of anti-CD16.CD32 antibody
5. Incubate cells over ice for 30 min
6. Pellet cells at 16,000 g for 15 sec, and wash them 1x in 200 μl FACS buffer
7. Resuspend cells in 100 μl FACS buffer containing 100x dilution of primary antibodies (antibodies of interest or corresponding isotype controls)
8. Incubate cells over ice for 30 min
9. Pellet cells at 16,000 g for 15 sec, and wash cells 2x in 200 μl FACS buffer
10. Resuspend cells in 100 μl FACS buffer containing 100x dilution of fluorophore-conjugated streptavidin, if applicable
11. Incubate cells over ice for 30 min
12. Pellet cells at 16,000 g for 15 sec, and wash cells 2x in 200 μl FACS buffer
13. Resuspend cells in 200 μl FACS buffer and keep on ice until flow cytometry
14. If cells need to be stored for long period of time, they may be fixed by addition of 100 μl 4% paraformaldehyde to the cell suspension. Tubes must be covered well with Saran wrap to prevent evaporation and with aluminum foil to prevent photobleaching, and stored at 4 oC until analyzed

8.2 Flow cytometry

1. Turn on the flow cytometer and restart computer. Flow cytometer must always be turned on before computer
2. Start the CellQuest program and connect to the cytometer
3. Set up the plots and the gates, and set up the file names and folders for saving data under *Parameter Description* menu
4. Enter the number of events to be counted in each cycle under *Acquisition and Storage* menu
5. Select the compensation and voltage settings from a previous experiment with similar antibodies and same cells. If this is the first time with cells being studied or different fluorophore, run the unstained, single stained, and multiple stained samples to set up the compensation
6. Run the isotype control samples and adjust the scatter plot gate position to exclude cell debris. Keep the fluorescence of isotype samples under 10^1 intensity units by adjusting the voltages
7. Run the samples and save the data for analysis later
8. At the end of data collection, run bleach through the system for 5 min followed by water for 5 min
9. Turn the system to standby mode, and then shut down the flow cytometer

APPENDIX 9 – Epifluorescence microscopy

1. Turn on Xenon lamp followed by other components. Xenon lamp is needed for fluorescence imaging but not for phase contrast. If only phase contrast images are being taken, do not turn on xenon lamp
2. If environment needs to be controlled for cell culture, set up the chamber and turn on the temperature and CO_2 controllers
3. Start the program, MetaMorph on computer
4. Choose the objective lens appropriate for imaging and put a drop of immersion oil on 40x and 100x objective lenses but not on 10x objective lens
5. Place your sample in sample placeholder and by direct observation, bring the sample in focus
6. Using *'Show Live'* option under *Acquire* menu, fine adjust the focus to get the best quality image on the screen.
7. For fluorescence, select the exposure time and click the fluorescence tab to take the image
8. Move to another plane of view in $x - y$ plane using joystick
9. For running timelapse, set up a journal to move the stage by appropriate distance and take images at every position, and finally home after taking the images
10. From *Acquire Timelapse* menu, select the frequency of images and total period of timelapse, and journal to be used, and collect images
11. For Z-stack imaging, select the distance to be covered in each Z-stack, number of planes in the Z-stack, exposure time, and click the tab for fluorescence Z-stack imaging.
12. At the end of imaging, save the data on the computer hard disk or portable hard drive, and close the MetaMorph program
13. Shut down all the components of microscope with Xenon lamp being the last component to be turned off

APPENDIX 10 – Synthesis of end-acrylated triblock copolymer for hydrogel synthesis

10.1 Synthesis of PLGA-PEG-PLGA triblock copolymer

1. Dissolve 15 g of glycolide in 50 mL ethyl acetate (dried over molecular sieves) at 70°C with continuous stirring. Precipitate glycolide in 300 mL Petroleum ether cooled to 4°C. If required, precipitate in diethyl ether as well
2. Repeat step 1 for *D,L*-lactide also
3. Dissolve 30 mg PEG in 50 mL acetone at 60°C and precipitate in 300 mL Petroleum ether/ diethyl ether
4. Dry all the three comonomers in the vacuum oven overnight
5. Take out dried two-necked 100 mL round bottom flask and Dean-Stark apparatus from the oven
6. Assemble the set-up and seal it as soon as possible
7. Purge it with N_2 for 5 min. Attach water connections
8. Add 100 mL of anhydrous toluene to the round bottom flask. Place the set-up in silicon oil at 130°C. Stir the solution at 300 rpm
9. Add 16 g PEG and 2 g each of lactide and glycolide (for PLGA:PEG = 20:80) to the round bottom flask
10. Dissolve the contents and purge N_2 till ~10 ml of toluene is collected in the trap
11. Add 100 μL of 100 mM stannous diethyl hexanoate (162 μL stannous octoate in 5 mL toluene) to the reaction mixture drop wise
12. Keep purging nitrogen and periodically add more toluene to make up for any lost toluene (due to purging)
13. Let the reaction go on for ~18 hours
14. Cool down the reaction mixture after 18 hours and in the process, remove some toluene to reduce the volume to half
15. Precipitate the polymer in 300 mL diethyl ether at 4°C. Decant the ether and vacuum dry the polymer. Dissolve the polymer in DCM and repeat precipitation few times (usually three times in total with diethyl ether) if the polymer is colored (e.g., yellow)

16. Dissolve the polymer in DCM and precipitate in 300 mL cooled Petroleum ether
17. Vacuum dry the polymer at 70°C

10.2 Acrylation of triblock copolymer

1. Dissolve 3 g of triblock copolymer in 30 mL DCM in a round bottom flask (which has been taken out of oven and purged with N_2).
2. Cool the reaction mixture to 4°C.
3. Add 0.2 mL triethylamine and purge N_2 for 5 min.
4. Cool the reaction mixture to 4°C.
5. Add 0.2 mL acryloyl chloride/ methacryloyl chloride drop wise.
6. Stir the reaction at 4°C for 12 hours.
7. After 12 hours at 4°C, let the reaction continue at room temperature for another 12 hours.
8. Filter the reaction mixture using a Whatmann/ membrane filter to remove the TEA.HCl salt.
9. Precipitate the polymer in cooled diethyl ether.
10. Dissolve in DCM and precipitate in Petroleum ether.
11. Vacuum dry the polymer.

APPENDIX 11- T cell blasts from ova-specific $CD4^+$ and $CD8^+$ transgenic mice

1. Euthanize an OT-I or OT-II mouse for preparing $CD8^+$ or $CD4^+$ T cell blasts, respectively
2. Isolate spleen and mince using frosted cover slips to obtain single cell suspension
3. Hemolyse the erythrocytes, wash cells, and resuspend at 3 x 10^6 cells/mL in complete RPMI medium
4. Plate T cells at 3 x 10^6 cells/mL/well in a 24-well tissue culture-treated plate along with 100 μg/mL ovalbumin in case of OT-II cells or 250 μg/mL ovalbumin in case of OT-I cells
5. Incubate cells at 37 °C, 5% CO_2
6. After 48 h, split cells 1:3 and add 5 ng/mL rmIL-2 to the cell suspension
7. Incubate cells at 37 °C, 5% CO_2 for 3-5 days after which they are ready to be used as T cell blasts (> 98% purity as measured by CD4 expression)
8. To obtain high viability cells for experiments, ficoll the cells to remove dead cells
9. In a 15 mL sterile centrifuge tube, take 2 mL of ficoll reagent followed by addition of 3 mL of cell suspension gently without disturbing the interface
10. Centrifuge cells at 1400 rpm for 10 min
11. Gently pipette off the top layer and the interface that are rich in viable cells
12. Transfer to another sterile centrifuge tube, add excess serum-free RPMI medium, and wash cells 2x
13. Resuspend cells at desired density in complete RPMI medium

Note:- OT-I cells must be used on day 5 as cell viability decreases substantially between days 5 and 7.